DYNAMICS OF HYDROTHERMAL OXIDATION

Kenji KOIDO
Department of Aerospace Engineering
Nagoya University

A thesis submitted for the degree of Doctor of Philosophy
at the Nagoya University
Nagoya, Japan

January 2011

I would like to dedicate this thesis to my parents.

Acknowledgements

This research project would not have been possible without the support of a number of individuals. First and foremost, I would like to express my gratitude to my supervisor, Prof. Dr. Tatsuya HASEGAWA who was abundantly helpful and offered invaluable assistance, support and guidance. Deepest gratitude is also expressed to the members of the supervisory committee, Prof. Dr. Akira UMEMURA, Dr. Norihiko YOSHIKAWA and Dr. Yoshinori ITAYA, without whose knowledge and assistance the research would not have seen its completion.

I would also sincerely thank Prof. Dr. Kozo MATSUMOTO, Dr. Yasuyuki ISHIDA, Dr. Takashi KUBO and Dr. Kazuhiro KUMABE for invaluable assistance to carry out research with the hydrothermal process research group at Nagoya University.

The enthusiastic support and inspiration from Dr. Kazuya TSUBOI, Dr. Masahiro UCHIDA, Dr. Kazuma HIROSAKA, had a strong impact on this research. And I would like to acknowledge Dr. Yajun TIAN, Dr. Nora Alam BHUIYAN and Dr. Ram CHANDRA for supporting and encouraging my research life.

Special thanks also to all my laboratory mates in the group, especially group members: Kazuhiro ORYOJI, Masato FUKAYAMA, Yousuke YURIKUSA and Takeshi MIYAKITA. My sincere thanks also go to Maria R.H. TAKEUCHI and Naomi OYAMATSU for giving care to me and the laboratory mates.

The author would also like to convey thanks to the Ministry and Faculty for providing the financial means and laboratory facilities.

Last but not the least, I would like to express my gratitude to my families for their understanding through the duration of the studies.

Abstract

Wet biowastes are not suitable for incineration, for its moisture content. The hydrothermal processes are useful energy conversion technologies for the wet biowaste via hot-compressed water near or above the critical point (p = 22.1 MPa and T = 374 °C) with no drying process. For design of hot-water boiler processes via hydrothermal oxidation, the numerical experiments were performed. To develop the simulator, the reaction rates and the reaction pathway were obtained for hydrothermal oxidation.

Numerical experiments: Behaviours of ethanol oxidation under sub-/super critical conditions were numerically simulated. Effects of preheat temperature, heat loss and flow velocity were examined by simulation. The differences of preheat temperatures led to the differences of temperature increase, ΔT, around critical point because of the specific heat peak at the critical point. Larger flow velocity caused slower increase of ethanol conversion and temperature increase. Changes of reaction rate for different flow velocities showed that larger flow velocity caused thicker reaction zone and higher reaction peak than that for smaller one because of the fluid advection. From the calculation with different heat losses (different heat transfer rate coefficients, α), two-step temperature decrease appeared for larger heat loss ($\alpha = 2.5\times10^{4}$ $W\cdot m^{-2}\cdot K^{-1}$) while monotonous temperature decrease appeared for smaller heat loss ($\alpha = 2.5\times10^{3}$ $W\cdot m^{-2}\cdot K^{-1}$).

Oxidation rates for hot-compressed water: Ethanol oxidation in subcritical water was examined at 25 MPa in the temperature range of 260–350 °C with equivalence ratio of 0.6. With oxygen as the oxidiser, the overall first-order decomposition reaction parameters were determined to be $10^{2.9\pm0.4}$ s^{-1} for the pre-exponential factor and 53.8 ± 4.6 $kJ\cdot mol^{-1}$ for the activation energy. The products obtained by the hydrothermal oxidation of ethanol were acetaldehyde, acetic acid, carbon monoxide and carbon dioxide. First-order kinetics was enough to capture the main characteristics of species concentration profiles. Consecutive reaction network: $C_2H_5OH \rightarrow CH_3CHO \rightarrow CH_3COOH \rightarrow CO \rightarrow CO_2$ well described the behaviour of components obtained from wet oxidation of ethanol.

Oxidation rates for steam: Ethanol oxidation rate in high pressure steam at the pressure of 10 MPa in the temperature ranging from 430 to 490 °C was studied with the fuel

equivalence ratio of 0.4. On the assumption that the reaction order is first order, the reaction rate parameters obtained in the experiments are $10^{11.6 \pm 0.4}$ s^{-1} for the pre-exponential factor and 166.5 ± 6.1 $kJ \cdot mol^{-1}$ for the activation energy. This ethanol oxidation rate in high-pressure steam was equivalent to that in supercritical water oxidation of ethanol. Liquid products were acetaldehyde and acetic acid and gas phase products are carbon monoxide, carbon dioxide, methane and ethane. A parallel reaction network of first order model well described the characteristics of the ethanol decomposition to acetaldehyde and acetic acid. Utilisation of the high-pressure steam oxidation process can overcome the problem of pressure tightness of the reactor in supercritical water oxidation, and the process can be employed in practical facilities.

List of contents

Abstract ····· iv

List of contents ····· vi

List of figures ····· ix

List of tables ····· xii

Nomenclature ····· xiii

Chapter 1: Introduction

1.1 Background ····· 1

1.2 Properties of near- and supercritical water ····· 2

1.2.1 Dielectric constant

1.2.3 Ion product

1.3 Hydrothermal oxidation ····· 10

1.3.1 Supercritical water oxidation

1.3.2 Subcritical wet oxidation

1.3.3 High-pressure steam oxidation

1.4 Difference between hydrothermal oxidation and gas-phase combustion ····· 12

1.4.1 Reaction condition

1.4.2 Condensed vapour

1.5 Summary ····· 13

Chapter 2: Review of kinetics in hydrothermal oxidation

2.1 Kinetic studies on hydrothermal oxidation ····· 16

2.1.1 Model compounds
2.2 Chemical reactions for hydrothermal oxidation ····· 19
2.2.1 Supercritical water oxidation
2.2.2 Subcritical wet oxidation
2.3 Hydrothermal oxidation of ethanol ····· 23
2.4 Numerical experiment and simulation of hydrothermal flow for reactor design ····· 23
2.5 Summary ····· 24

Chapter 3: Objectives

3.1 Objectives ····· 25
3.2 Structure of the thesis ····· 26

Chapter 4: Numerical experiments of ethanol oxidation in hot-compressed water

4.1 Introduction ····· 29
4.2 Governing equations ····· 30
4.3 Equation of state for sub/super critical water ····· 31
4.4 Physical properties and mixing lows ····· 35
4.4.1 Thermal properties
4.4.2 Transport properties
4.4.3 Mixing lows
4.5 Reaction rate ····· 38
4.6 Numerical method ····· 39
4.7 Results and discussions ····· 40
3.7.1 Effect of preheat temperature
3.7.2 Effect of flow velocity
3.7.3 Effect of heat loss
4.8 Conclusions ····· 57

Chapter 5: Kinetics of ethanol oxidation in subcritical water

5.1 Introduction ····· 59

5.2 Experimental apparatus and procedures ····· 59

5.3 Analytical techniques ····· 60

5.4 Results and discussion ····· 62

5.4.1 Global kinetics of ethanol oxidation

5.4.2 Oxidation products and reaction pathway

5.4.3 Consecutive four-step reaction

5.5 Conclusions ····· 75

Chapter 6: Kinetics of ethanol oxidation in high-pressure steam

6.1 Introduction ····· 76

6.2 Experimental apparatus and procedures ····· 76

6.3 Analytical techniques ····· 79

6.4 Results and discussion ····· 79

6.4.1 First-order oxidation rate of ethanol

6.4.2 Reaction products

6.5 Conclusions ····· 89

Chapter 7: Conclusions ····· 90

Chapter 8: Suggestions for further research ····· 93

References ····· 94

Appendix - A: Lee-Kesler equation and methodology for estimating properties around the critical point

A.1 Lee-Kesler equation of state ····· 103

A.2 Thermochemical properties ····· 104

A.3 Transport properties ·····106

A.3.1 Viscosity

A.3.2 Thermal conductivity

A.4 Mixing rule ·····109

A.4.1 Mixing rule for Lee-Kesler EOS

A.4.2 Mixing rule for transport properties

List of Figures

1.1 Typical phase diagram of water, whose data points are calculated via REFPROP ver. 8.0 (Lemmon et al., 2007). ····· 6

1.2 Relation among p, ρ and T of water, whose data points are calculated via REFPROP ver. 8.0 (Lemmon et al., 2007), referring to the report by Shaw et al. (1991). ····· 7

1.3 Dielectric constant of water versus temperature at each pressure ranging from 0.1 to 1600 MPa, calculated via equation (1.1) released by IAPWS (1997), (or Fernández et al., 1997). ····· 8

1.4 Ion product of water versus temperature at each pressure ranging from 5 to 100 MPa, calculated via equation (1.2) released by IAPWS (1997), (or Fernández et al., 1997). ····· 9

1.5 Basic supercritical water oxidation process (Marrone et al., 2004). ····· 14

1.6 Basic wet oxidation plant flow sheet (Mishra et al., 1995). ····· 15

2.1 Pseudo first-order Arrhenius plot for oxidation of model compounds in sub- and supercritical water. ····· 18

3.1 Structure of the thesis. ····· 28

4.1 One-dimensional reactor model. ····· 32

4.2 Comparison of state equations of water at 25 MPa. ····· 33

4.3 Comparison of specific enthalpy of water at 25 MPa. ····· 34

4.4 Changes of conversion along the reactor for different preheat temperatures at u_{in} = 1.0 m·s^{-1} under adiabatic condition. ····· 42

4.5 (a) Changes of ΔT and (b) changes of temperature, along the reactor for different preheat temperatures at u_{in} = 1.0 m·s^{-1} under adiabatic condition. ····· 43

4.6 Changes of specific heat: (a) along the reactor for different preheat temperatures, and (b) against temperature for different preheat

temperatures, at u_{in} = 1.0 m·s^{-1} under adiabatic condition. ····· 44

4.7 Changes of reaction rate along the reactor for different preheat temperatures at u_{in} = 1.0 m·s^{-1} under adiabatic condition. ····· 45

4.8 Changes of conversion along the reactor for different flow velocities at $T_{preheat}$ = 350 °C under adiabatic condition. ····· 48

4.9 (a) Changes of ΔT and (b) changes of temperature, along the reactor for different flow velocities at $T_{preheat}$ = 350 °C under adiabatic condition. ····· 49

4.10 Changes of reaction rate along the reactor for different flow velocities at $T_{preheat}$ = 350 °C under adiabatic condition. ····· 50

4.11 Comparison of logarithmic components in the reaction rate equation along the reactor at $T_{preheat}$ = 350 °C under adiabatic condition. ····· 51

4.12 (a) Changes of ΔT and (b) changes of temperature, along the reactor for different heat transfer coefficients at $T_{preheat}$ = 350 °C, u_{in} = 1.0 m·s^{-1} with heat loss. ····· 53

4.13 Changes of isobaric specific heat along the reactor for different heat transfer coefficients at $T_{preheat}$ = 350 °C, u_{in} = 1.0 m·s^{-1} with heat loss. ····· 54

4.14 Changes of conversion along the reactor for different heat transfer coefficients at $T_{preheat}$ = 350 °C, u_{in} = 1.0 m·s^{-1} with heat loss. ····· 55

4.15 Changes of reaction rate along the reactor for different heat transfer coefficients at $T_{preheat}$ = 350 °C, u_{in} = 1.0 m·s^{-1} with heat loss. ····· 56

5.1 Schematic diagram of experimental apparatus for the measurement of reaction rate on subcritical wet oxidation. ····· 61

5.2 First-order reaction rate for ethanol conversion. ····· 63

5.3 Arrhenius plot for the overall conversion rate of ethanol assuming first-order reaction. ····· 64

5.4 Parity plot for the subcritical wet oxidation kinetics of ethanol conversion. ····· 65

5.5 Arrhenius plots of conversion rates of ethanol assuming first-order reaction obtained by different experiments: this work, Hirosaka et al. (2008), Hirosaka et al. (2007), and Schanzenbächer et al. (2002). ····· 66

5.6 Temporal variation of the carbon fraction of ethanol, acetaldehyde, acetic acid, carbon monoxide and carbon dioxide for ethanol

subcritical wet oxidation at 260 °C. ····· 71

5.7 Temporal variation of the carbon fraction of ethanol, acetaldehyde, acetic acid, carbon monoxide and carbon dioxide for ethanol subcritical wet oxidation at 320 °C. ····· 72

5.8 Variation of the carbon fractions of acetaldehyde, acetic acid, carbon monoxide, and carbon dioxide with the ethanol conversion. ····· 73

6.1 Experimental apparatus: (a) whole reactor setup, (b) detail of the mixing cross. ····· 77

6.2 Variation of $\ln(C/C_0)$ versus residence time, for the temperature of 430 °C, 450 °C, 470 °C and 490 °C at p = 10 MPa. ····· 80

6.3 Arrhenius plot for the overall conversion rate of ethanol assuming first-order reaction. ····· 81

6.4 Arrhenius plots of conversion rates of ethanol assuming first-order reaction obtained by different experiments: this work at 10 MPa, Schanzenbächer et al. (2002) at 24.6 MPa, and Koido et al. (2010) at 23.5–25.0 MPa around the critical temperature. ····· 82

6.5 Concentration of unreacted ethanol and liquid phase products i: acetaldehyde and acetic acid, for the experiments at p = 10 MPa, T = 470 °C and C_0 = 40. ····· 85

6.6 Concentration of gas phase products i: carbon monoxide, carbon dioxide, methane and ethane, for the experiments at p = 10 MPa, T = 470 °C and C_0 = 40. ····· 86

List of Tables

1.1 Processes for removing pollutants from wastewaters (Bhargava et al., 2006). ····· 4

1.2 Comparison of properties for water in the three phases: gas, supercritical water and liquid. ····· 5

2.1 Global kinetic parameters for oxidation of model compounds and hazardous biowastes in sub- and supercritical water through continuous plug-flow reactor.. ····· 17

2.2 Summary of detailed chemical kinetics models for SCWO of hydrogen, carbon monoxide, methane, methanol, ethanol, phenol and benzene. ····· 22

4.1 Calculation conditions. Three comparisons (Case 1, 2 and 3) are made for different parameters: temperature, inflow velocity and heat transfer coefficient. ····· 41

5.1 Values of k_1–k_6 kinetic parameters. ····· 67

5.2 Reaction rate equations and their analytical solutions for the reaction network: EtOH → AAL → AAC → CO → CO_2, where AAL and AAC are acetaldehyde and acetic acid, respectively. ····· 70

6.1 Reaction rate equations and their analytical solutions for the reaction network (6.4). ····· 87

Nomenclature

Roman symbols

A	Frequency factor
[AAL]	Concentration of acetaldehyde
[AAC]	Concentration of acetic acid
[CO]	Concentration of carbon monoxide
[CO_2]	Concentration of carbon dioxide
C_p	Isobaric specific heat
C_v	Isochoric specific heat
D_i	Diffusion coefficient
d_0	Cross-sectional diameter
[EtOH]	Concentration of ethanol
E_a	Activation energy
h_i	Specific enthalpy
k	Reaction rate constant
k_B	Boltzmann's constant
M_i	Molar weight
N_A	Avogadro's number
[O_2]	Concentration of oxygen
p	pressure
p_c	Critical pressure
p_r	Reduced pressure
Q	Heat source
q	Heat flux
R	Universal gas constant

r_i	Reaction rate of species *i* on mole basis
T	Temperature
T_c	Critical temperature
T_r	Reduced temperature
V_c	Molar critical volume
$\dot{v}_p$	Total of flow rates at the pump
V_r	Reduced volume
V_R	Volume of the reactor
X_i	Mole fraction of species *i*
Y_i	Mass fraction of species *i*
Z	Compressibility factor
u	Velocity
v_c	Specific volume at critical point
w_i	Reaction rate on mass basis

Greek symbols

α	Heat transfer coefficient
ε	Dielectric constant
ε_0	Permittivity of free space
ϕ	Fuel equivalence ratio
η	Viscosity
λ	Thermal conductivity
μ	Dipole moment
ρ	Density
$\tilde{\rho}$	Molar density
ρ_P	Density of water at feeding conditions
ρ_R	Density of water at reaction conditions
τ_{ind}	Induction period
ω	Acentric factor

Chapter 1: Introduction

1.1 Background

Wet biowastes, e.g. food leftover, animal manure, sewage sludge, etc., are difficult to be incinerated as a fuel due to their high moisture content. Requirements for constructing energy conversion processes with utilisable wet wastes lead to review many technologies treating wet wastes. Processes for removing sewage sludge and reducing total organic carbon (TOC) from wastewater and recovering heat energies and/or biogases from biowastes for suitable conditions are listed in Table 1.1. Biowastes treatments include two different processes, i.e. biological treatment and hydrothermal process. Biological treatment (e.g. methane fermentation) is well-established technology to produce methane as biogas and utilised for various opportunities (Okuno et al., 2003), while hydrothermal process (e.g. subcritical wet oxidation) is viable treatment process. In this thesis, hydrothermal treatments are featured.

The hydrothermal processes are useful energy conversion technologies for the wet biowaste containing a lot of moisture, such as domestic animal excrement, sludge, and organic feedstock (Xu and Matsumura, 1996). The oxidation processes also have been widely studied and applied to an extensive variety of waste materials. The reaction is accomplished in hot-compressed water near or above the critical point (p = 22.1 MPa and T = 374 °C). In addition, comparison of the process with the other energy conversion technologies enlightens several advantages:

- High reactivity and high solubility for organic matters such as wet biowaste, low

quality oils, industrial process water and wastewater.

- Availability of released heat during the oxidation for preheating section
- Recovery of carbon dioxide, NO_x and minerals in exhausted water

1.2 Properties of near- and supercritical water

Typical properties for supercritical water are compared with for gas and liquid water in Table 1.2. Each property for supercritical water has the value intermediate between the values for gas and liquid, except for kinetic viscosity.

1.2.1 Dielectric constant

Close to the critical point, the density ρ can drop sharply with a slight increase in temperature T at a constant pressure p. The dependence of density on temperature at each pressure is shown in Figure 1.2, which is calculated via REFPROP (Lemmon et al., 2007). According to the release by international association for the properties of water and steam, IAPWS (1997), dielectric constant ε is expressed as the functional form of density and temperature,

$$\varepsilon = \frac{1 + A + 5B + \sqrt{9 + 2A + 18B + A^2 + 10AB + 9B^2}}{4 - 4B} \tag{1.1}$$

with

$$A = \frac{N_A \mu^2}{\varepsilon_0 k_B} \cdot g(\tilde{\rho}, T) \cdot \frac{\tilde{\rho}}{T},$$

$$B = \frac{N_A \beta}{\varepsilon_0 k_B} \cdot \tilde{\rho},$$

$$g(\tilde{\rho}, T) = 1 + \sum_{h=1}^{11} N_h \left(\frac{\tilde{\rho}}{\tilde{\rho}_c}\right)^{i_h} \left(\frac{T_c}{T}\right)^{j_h} + N_{12} \left(\frac{\tilde{\rho}}{\tilde{\rho}_c}\right) \left(\frac{T}{228\ \mathrm{K}} - 1\right)^{-1.2}$$

where T is absolute temperature and ρ is molar density, and i_h and j_h are fitting parameters (Fernández et al., 1997). With increasing temperature and density, dielectric constant decrease, shown in Figure 1.3. Above the critical pressure or temperature, it is

possible to control reactions continuously. The decrease in dielectric constant involves the change in solvent polarity. Compared to 80 for ambient temperature, the dielectric constant is 5–6 for water at the critical point, which is the same for a nonpolar organic solvent at ambient condition. Consequently, small organic compounds are highly soluble in high-temperature water.

1.2.2 Ion product

Change in solvent polarity significantly influences on equilibrium in reactions associated with ion. Dependence of ion product on temperature and pressure is displayed in Figure 1.4. The ion product is the measure of how water dissociate to be hydrogen ion (H^+) and hydroxide ion (OH^-) with the reversible reaction, $H_2O \rightleftharpoons H^+ + OH^-$. The ion product is defined as products of hydrogen and hydroxide ion concentration,

$$K_W = [H^+][OH^-]$$

where K_W = 10^{-14} [mol^2 kg^{-2}] at atmospheric pressure and normal temperature. The expression for estimation of $pK_W \equiv -\log_{10} K_W$ is proposed by Bandura et al. (2006) as follows:

$$\begin{aligned} pK_W = &-2n\left[\log_{10}(1+Q) - \frac{Q}{Q+1}\rho(\beta_0 + \beta_1 T^{-1} + \beta_2 \rho)\right] \\ &+ pK_W^G + 2\log_{10}\frac{m^0 M_W}{G} \end{aligned} \tag{1.2}$$

where

$$Q = \left(\frac{\rho}{\rho_0}\right)\exp(\alpha_0 + \alpha_1 T^{-1} + \alpha_2 T^{-2}\rho^{\frac{2}{3}}).$$

With increasing temperature at a constant pressure of 22.1 MPa, K_W reaches around 10^{-11} at 250 °C and then decreases to around 10^{-18} at 400 °C. The high pressure and temperature water is an effective medium for acid and base catalysed reactions of 1- and 2-propannol (Antal et al., 1998; Akiya and Savage, 2002).

Table 1.1 Processes for removing sewage sludge and reducing total organic carbon (TOC) from wastewater and recovering heat energies and/or biogases from biowastes for suitable conditions, referring to Bhargava et al. (2006).

process/process type	comment
adsorption (activated carbon, zeolitic materials, clays)	suitable for removing high-molecular-weight organics
incineration	suitable for high-concentration wastewaters
wet oxidation/catalytic wet oxidation	suitable for medium – high-concentration wastewaters and biowastes
supercritical water oxidation	suitable for persistent substances and wastes
wet peroxide oxidation	suitable for low-concentration wastewaters
coagulation/flocculation	mostly suitable for insoluble pollutants
biological treatment	suitable for nontoxic wastewaters and biowastes
potassium permanganate	suitable for low-concentration wastewaters
photocatalytic processes	suitable for low-concentration wastewaters

Table 1.2 Comparison of properties for water in the three phases: gas, supercritical water and liquid.

Properties	Gas	Supercritical Water	Liquid
Density, ρ [kg m^{-3}]	0.6–2	300–900	700–1600
Diffusion coefficient [10^{-9} m^2 s^{-1}]	1000–4000	20–700	0.2–2
Viscosity [10^{-5} Pa s]	1–3	1–9	200–300
Thermal conductivity [10^{-3} W m^{-1} K^{-1}]	1	1–100	100
Kinetic viscosity [10^{-7} m^2 s^{-1}]	100	1–10	10

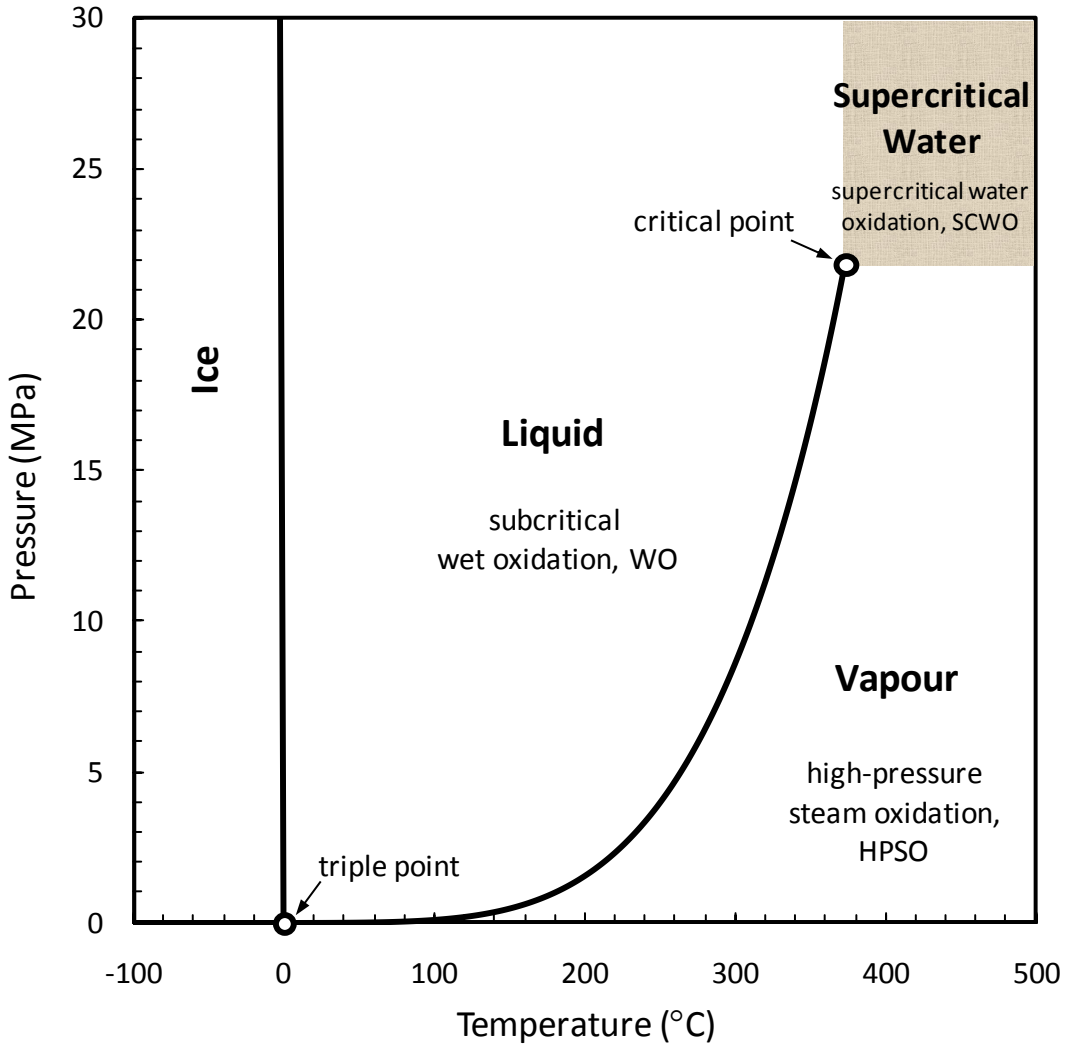

Figure 1.1 Typical phase diagram of water, whose data points are calculated via REFPROP ver. 8.0 (Lemmon et al., 2007).

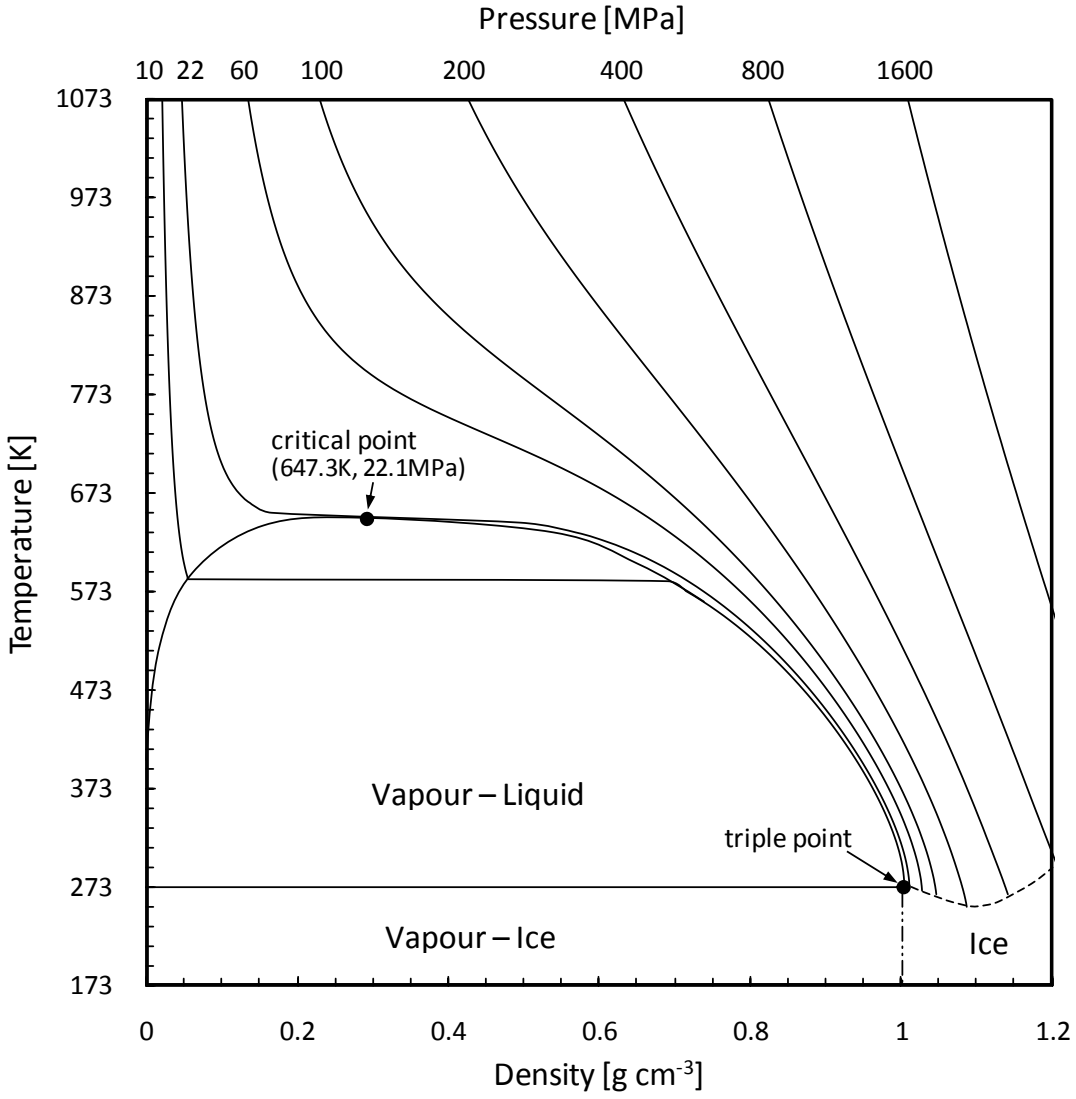

Figure 1.2 Relation among p, ϱ and T of water, whose data points are calculated via REFPROP ver. 8.0 (Lemmon et al., 2007), referring to the report by Shaw et al. (1991).

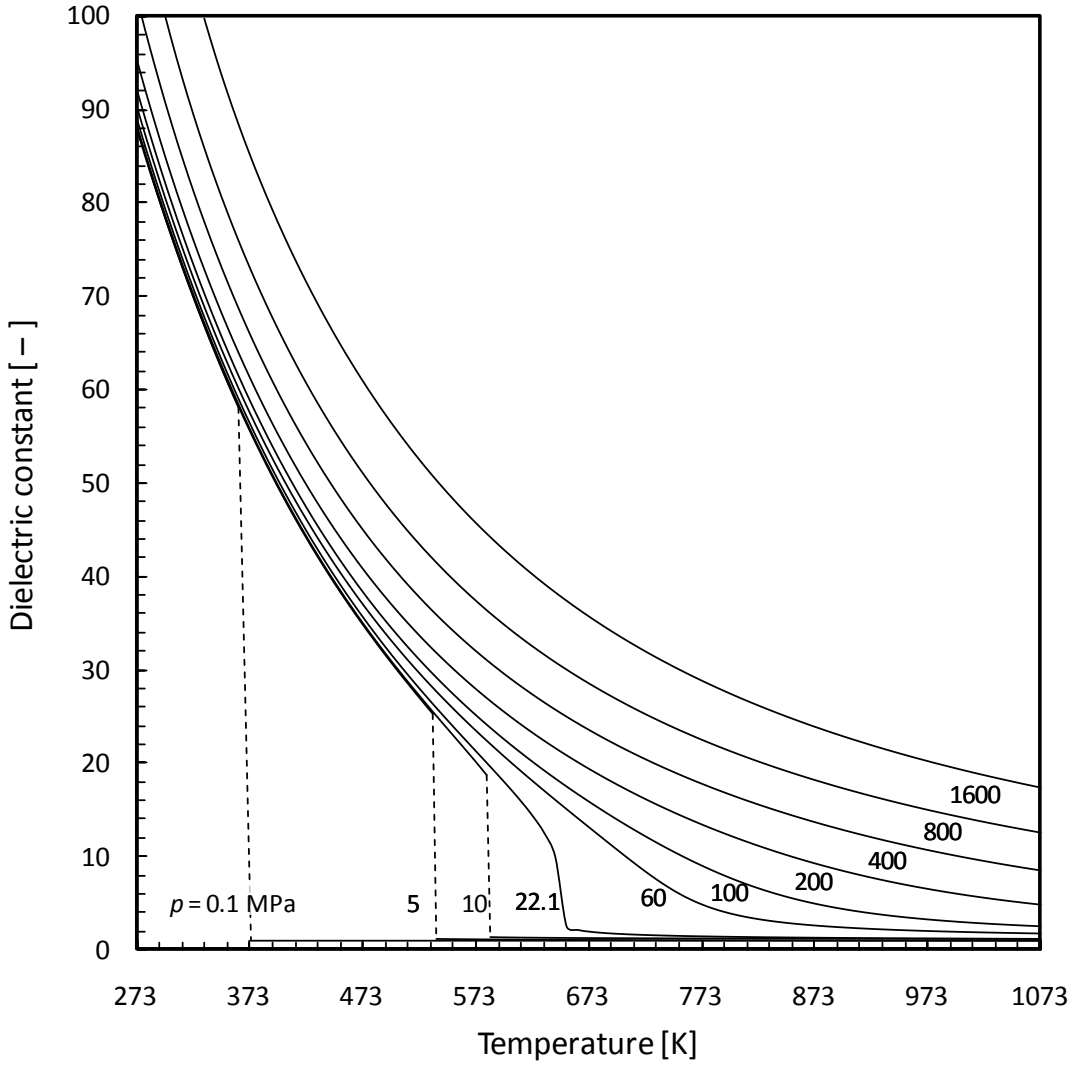

Figure 1.3 Dielectric constant of water versus temperature at each pressure ranging from 0.1 to 1600 MPa, calculated via equation (1.1) released by IAPWS (1997), (or Fernández et al., 1997).

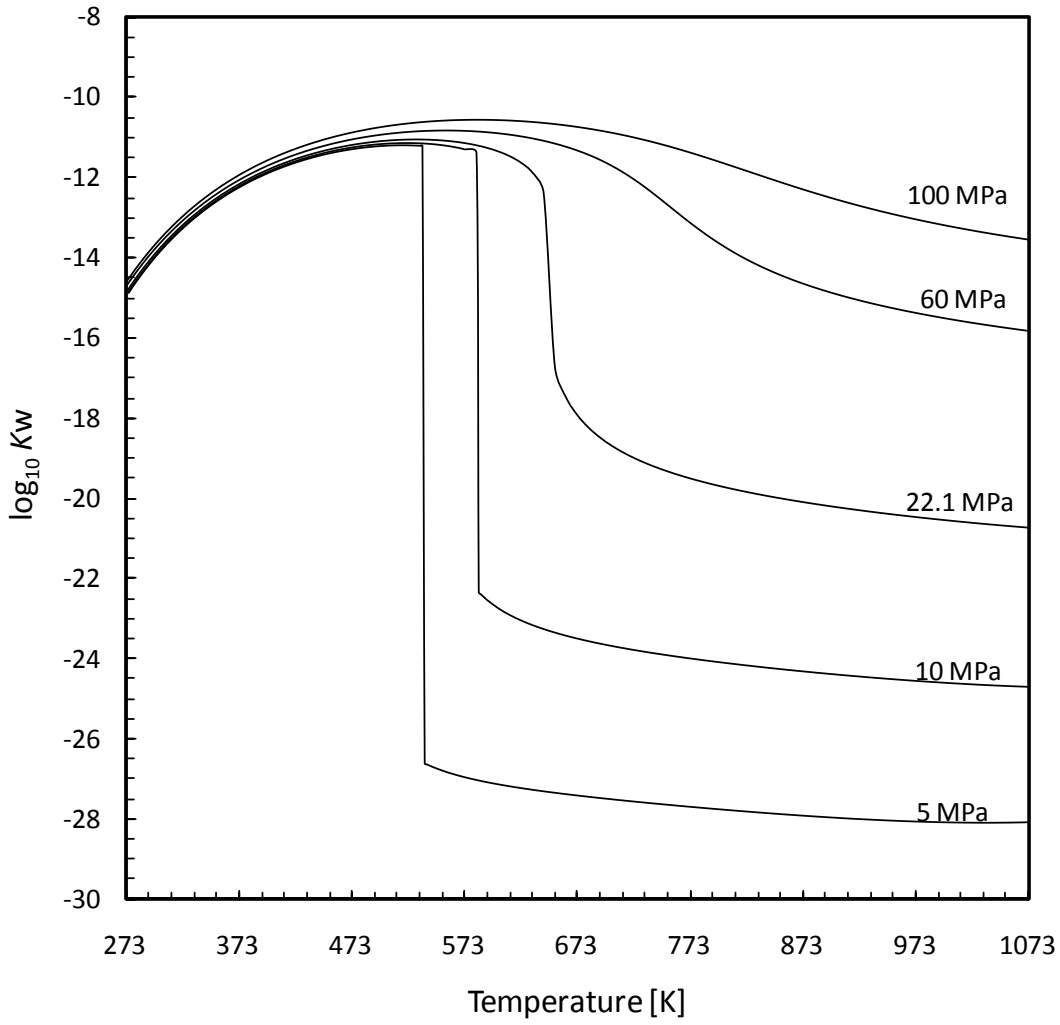

Figure 1.4 Ion product of water versus temperature at constant pressure ranging from 5 to 100 MPa, calculated via equation (1.2) released by IAPWS (1997), (or Fernández et al., 1997).

1.3 Hydrothermal oxidation

Oxidation reaction in water at a condition above the critical point (p = 22.1 MPa and T = 374 °C) is known as supercritical water oxidation (SCWO) (Gloyna and Li, 1995). On the other hand, the oxidation in water at a condition below the critical point using oxygen as the oxidiser is referred to as subcritical wet oxidation (WO), and it is also referred to as wet air oxidation (WAO) when air is used (Mishra et al., 1995). Especially, subcritical WO in the vapour phase is known as high-pressure steam oxidation (HPSO).

1.3.1 Supercritical water oxidation

Supercritical water oxidation (SCWO) is a promising technology, useful to eliminate a wide range of problematic wastes from a broad variety of chemical industries. Although each company has its own specific designs, all SCWO processes consist of the general steps shown in the block flow diagram of Figure 1.5 by Marrone et al. (2004). The waste feed mixture is first prepared, pressurised, and preheated before entering the reactor. The oxidation reaction occurs under supercritical conditions in the reactor. The effluent leaving the reactor is then usually cooled and depressurised prior to separation of gaseous, liquid, and solid products.

SCWO was first patented by Modell (1982) (or Thomason and Modell, 1984) in 1982. Since the inception of the SCWO process, many researchers have proved its effectiveness and have studied the reaction kinetics involved. The process has been preferably used for the treatment of organics with oxygen as the oxidant, because SCWO has strong ability to oxidise reactants to carbon dioxide in a short residence time. Flow diagram for the SCWO process (Marrone et al., 2004) is shown in Figure 1.5. As a result, a significant amount of information describing reactions in this environment has been accumulated. However, its commercial development has been hindered by the problems of corrosion and salt precipitation/solids buildup. Corrosion problems have not been satisfactorily solved (DeSimone, 2002).

1.3.2 Subcritical wet oxidation

Subcritical wet oxidation (WO) was first developed and applied as a commercial process by Zimmerman (1950, 1958), which is often referred to as the Zimpro process. Nowadays, subcritical WO is a well-established technique for waste material treatment, especially when organic wastes are too diluted by water to be incinerated (Baillod et al., 1985). Since 1960, numerous researchers have studied the kinetics involved in the subcritical WO environment.

Commercial systems typically employ a bubble column reactor. Oxidant, i.e. oxygen or air, is bubbled through a vertical column full of the hot and pressurised wastewater. Fresh wastewater enters the bottom of the column and oxidised wastewater goes out the top. The heat released during the oxidation is used to maintain the operating temperature at preheating section. Figure 1.6 shows a basic flow diagram of a WAO plant described by Luck (1996, 1999), which consists mainly of a high-pressure pump, an air or oxygen compressor, a heat-exchanger, and a reactor with a relief valve and a downstream separator (Mishra et al., 1995).

The works on WO process were reviewed in detail by Bhargava et al. (2006) for the research from 1995 to 2006, and by Mishra et al. (1995) for the works before 1995. The WO processes was first issued as a patent by Zimmerman in 1950. The complete oxidation of organics in liquid water with oxygen or air as an oxidant eliminates sludge and COD from wastewater to obtain carbon dioxide. Basic wet oxidation plant flow sheet (Mishra et al., 1995) is shown in Figure 1.6. This process is clean because it involves no chemical reagent, and the end products through the process are carbon dioxide and water when they are completely oxidised.

The WO process, however, has significant disadvantages, or requirements for reaction conditions. To oxidise many organics to a high conversion in appropriate residence times, it is usually necessary to prepare high pressure and temperature. Partial oxidation occurs when the conditions of temperature and residence time are inadequate. In most cases, low-molecular alcohols and organic acids are formed from the oxidation of high-molecular organics, which is difficult to be oxidised. Therefore, many researches performed the WO of many low-molecular alcohols (e.g. Ito et al., 1989 for methanol, ethanol, propanol, butanol and pentanol; Imamura et al., 1982 for methanol; Levec, 1990 for butyl alcohol) and organic acids (e.g. Imamura et al., 1982, 1999; Dietrich et al., 1985; Shende and Levec, 1999; Shende and Mahajani, 1997; Bjerre and Sorensen, 1992 for formic

acid; Shende and Levec, 1999; de Leitenburg et al., 1996; Barbier et al., 1998; Wakabayashi and Okuwaki, 1988; Foussard et al., 1989 for acetic acid; Day et al., 1973; Imamura et al., 1982; Furuya et al., 1985; Imamura et al., 1999 for propionic aicd).

1.3.3 High-pressure steam oxidation

High-pressure and temperature water vapour is described as superheated steam. The oxidation technology using superheated steam is defined as high-pressure steam oxidation (HPSO). This oxidation technology has not already explored as hydrothermal oxidation. The HPSO generates heat via exothermic reactions, whereas steam gasification produces gas through water-gas shift reaction. In the HPSO process, complete oxidation occurs and released heat can be recovered when adequate residence time, temperature and pressure are retained for an operation. On the other hand, partial oxidation occurs when these conditions are insufficient or when the reactants are liquid and/or solid in operation, from which generated heat and substances can be recovered.

1.4 Difference between hydrothermal oxidation and gas-phase combustion

1.4.1 Reaction condition

Whereas gas phase combustion occurs at around 600–800 °C, hydrothermal oxidation usually arises at around 300–500 °C and high pressure. Heat loss through the oxidation process in water is extremely lower than for the gas phase combustion process, because the reaction occurs in water where released heat can be recovered. Such heat generation can be utilised for hot-water boiler.

1.4.2 Condensed vapour

For hydrothermal oxidation, an excessive amount of water exists in the oxidation system,

while ambient air exists in the system for gas phase combustion. Therefore hot-compressed water participate the reaction, playing some roles as reactant/product and collision partner, acid/base catalyst, and medium of mass, heat and inter-molecular energy transfer, as well as solvent (Akiya and Savage, 2002).

1.5 Summary

Hydrothermal oxidation of wet biowastes is promising approach to recover heat energy. This process uses water whose properties at near- and supercritical conditions are presented in this section. Dielectric constant and ion product decrease dramatically at around the critical point. Hydrothermal oxidation consists of supercritical water oxidation, subcritical wet oxidation and high-pressure steam oxidation. The differences between these oxidation processes and gas-phase are elucidated for reaction condition and roles of media.

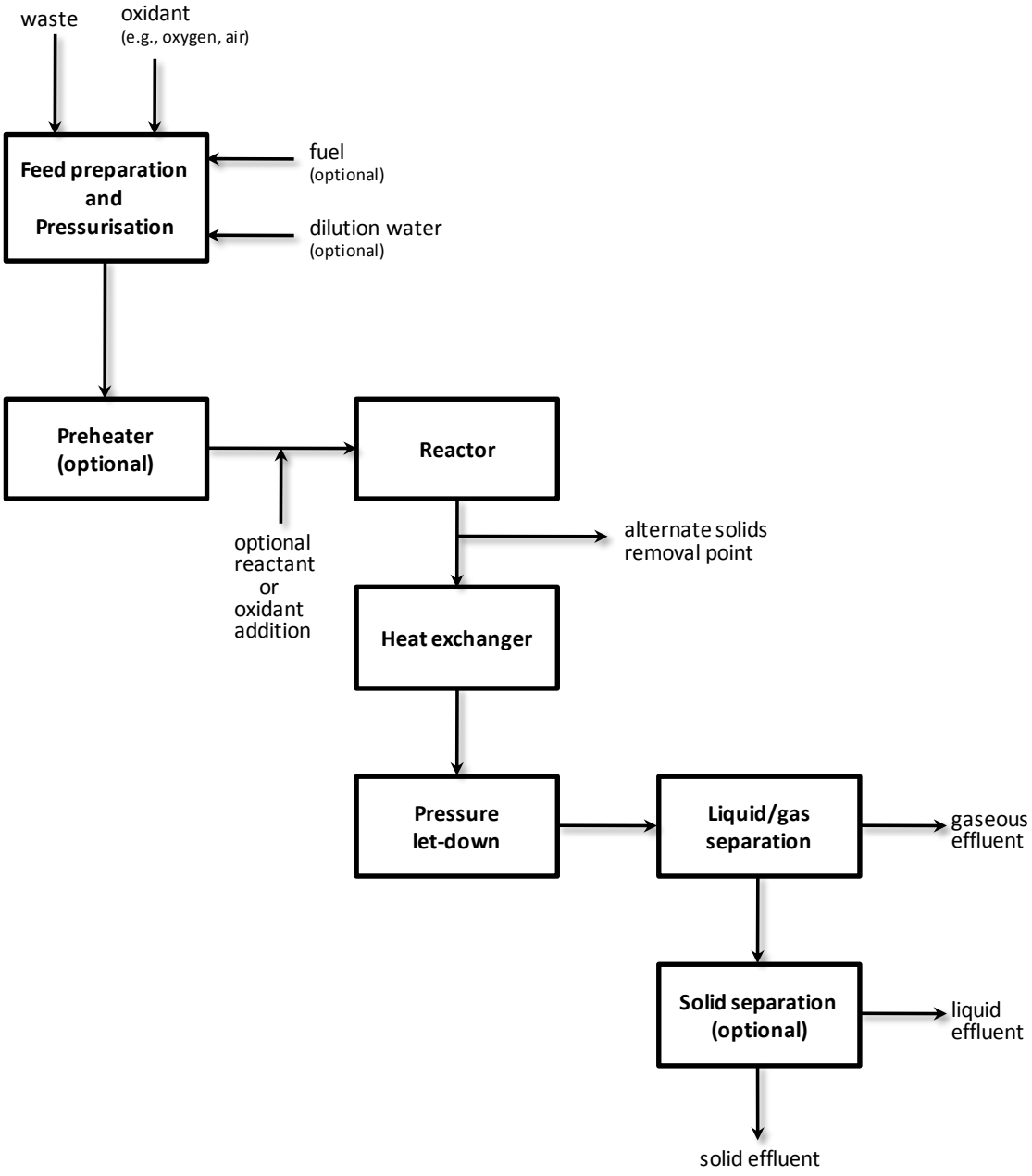

Figure 1.5 Basic supercritical water oxidation process (Marrone et al., 2004).

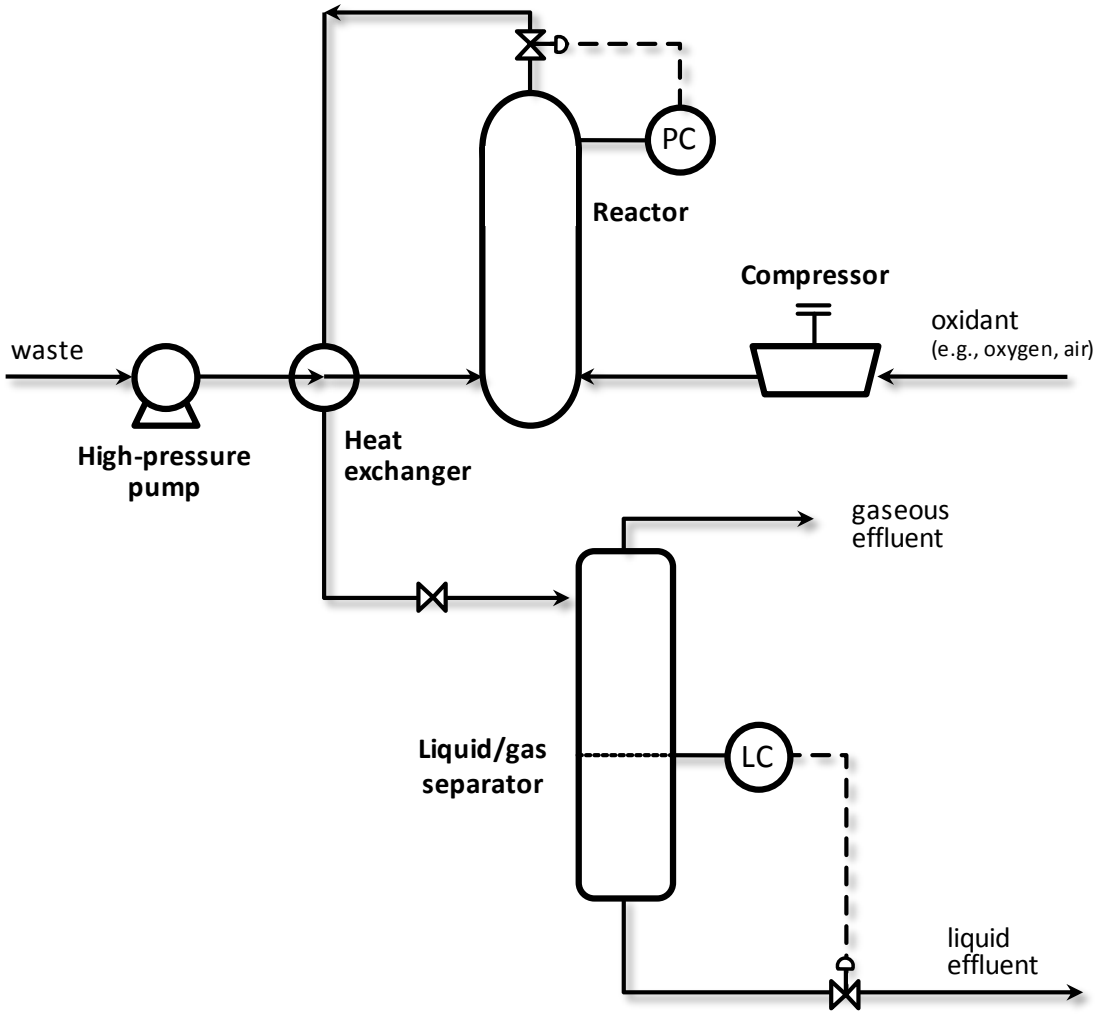

Figure 1.6 Basic wet oxidation plant flow sheet (Mishra et al., 1995).

Chapter 2: Review of kinetics in hydrothermal oxidation

2.1 Kinetic studies of hydrothermal oxidation

2.1.1 Model compounds

Model compounds for hydrothermal oxidation include acetic acid, phenol, ammonia, methanol and ethanol. The relevant preceding researches are summarised in Table 2.1. It tabulates global kinetic parameters for oxidation of model compounds, hazardous wastes and biowastes in sub- and supercritical water through continuous flow type reactor.

Kinetics data are available from the literatures for several compounds, e.g. acetic acid (Meyer et al., 1995); phenol (Gopalan and Savage, 1995); ammonia (Helling and Tester, 1988); methanol (Anitescu et al., 1996; Brock et al., 1996); and ethanol (Schanzenbächer et al., 2002; Helling and Tester, 1988; Hirosaka et al., 2007, 2008). Figure 2.1 shows pseudo first-order Arrhenius plot for oxidation of model compounds in sub- and supercritical water.

Several experimental studies related to hydrothermal oxidation under supercritical conditions have been reported (Rice et al., 1996; Brock et al, 1996; Hirosaka et al., 2007; Helling and Tester, 1988; Schanzenbächer et al., 2002; Rice and Croiset, 2001). In some studies (Rice et al., 1996; Brock et al, 1996), methanol (CH_3OH) was selected as a reactant. Its oxidation kinetics was measured experimentally and also calculated numerically using elemental chemical reactions. On the other hand, Rice, et al. (Rice and Croiset, 2001) studied ethanol (C_2H_5OH) oxidation in supercritical water. They showed an elementary

Table 2.1. Global kinetic parameters for oxidation of model compounds and hazardous biowastes in sub- and supercritical water through continuous plug-flow reactor.

$$d[C]/dt = -A \exp(-E_a/RT)[C]^a[O_2]^b[H_2O]^c$$

compound	$\log_{10}A$	E_a	a	b	c	conditions	source
carbon monoxide	6.52	112	1	0	0	24.6 MPa, 400–540 °C	Helling and Tester (1988)
methane	11.4	179	0.99	0.66	0	24.6 MPa, 560–650 °C	Webley and Tester (1991)
methanol	26.2	409	1	0	0	24.6 MPa, 450–550 °C	Webley (1989); Tester et al. (1993)
	21.3	78	1	0	0	24.9 MPa, 500–589 °C	Brock et al. (1996)
	5.33	85.9	1	0	0	27.6 MPa, 442–574 °C	Rice and Steeper (1998)
	11.8	178	1	0	0	25.3 MPa, 400–500 °C	Anitescu et al. (1999)
ammonia	6.5	157	1	0	0	24.6 MPa, 650–700 °C	Webley et al. (1990, 1991)
ethanol	21.8	340	1	0	0	24.6 MPa, 484–541 °C	Helling and Tester (1988)
	17.23	213.9	1.34	0.55	0	24.6 MPa, 433–494 °C	Schanzenbächer et al. (2002)
	2.46	41.1	1	0	0	26–28 MPa, 200–320 °C	Hirosaka et al. (2007)
	2.05	61.1	0.86	1.15	0	23.5 MPa, 170–230 °C	Hirosaka et al. (2008)
acetic acid	18.0	231	1	1	0	40.0–44.5 MPa, 338–445 °C	Wightman (1981)
	9.9	168	0.72	0.15	0	24.6 MPa, 425–600 °C	Meyer et al. (1995)
	13.6	208	1	0	0	27.6 MPa, 441–533 °C	Rice and Steeper (1998)
phenol	5.4	64	1	1	0	29.6–40.3 MPa, 284–429 °C	Wightman (1981)
	2.5	52	1	0.5	0.7	19.0–28.2 MPa, 300–420 °C	Thornton and Savage (1992)
	2.34	12.4	0.85	0.50	0.42	25.0 MPa, 380–480 °C	Gopalan and Savage (1995)
	6.42	108	1	0	0	27.6 MPa, 504–585 °C	Rice and Steeper (1998)
acetamide	3.6	69	1	0	0	23.3–33.9 MPa, 400–525 °C	Lee and Gloyna (1992)

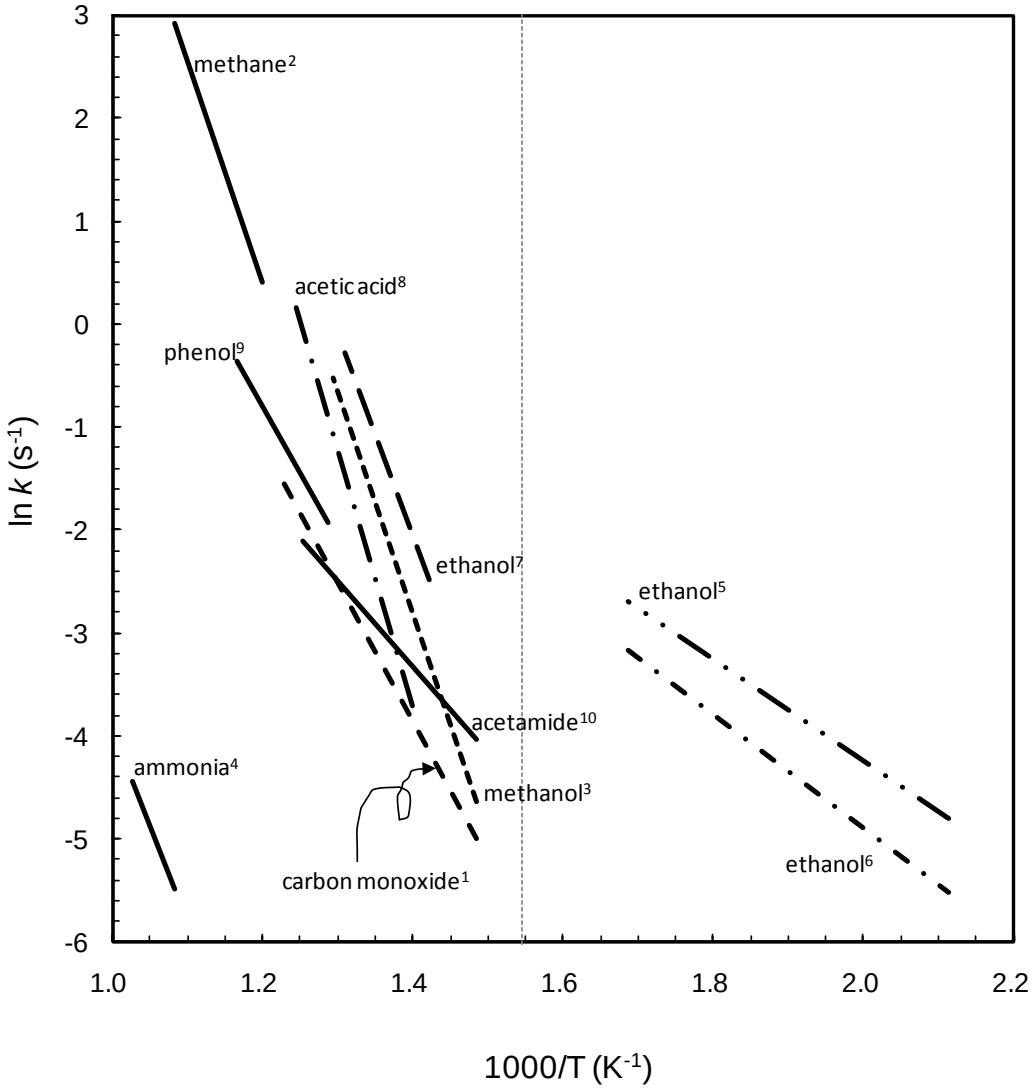

Literature cited:

1. Helling and Tester (1988)
2. Webley and Tester (1991)
3. Anitescu et al. (1999)
4. Webley et al. (1990, 1991)
5. Hirosaka et al. (2007)
6. Hirosaka et al. (2008)
7. Schanzenbächer et al. (2002)
8. Rice and Steeper (1998)
9. Rice and Steeper (1998)
10. Lee and Gloyna (1992)

Figure 2.1 Pseudo first-order Arrhenius plot for oxidation of model compounds in sub- and supercritical water.

reaction mechanism based on the work of Marinov (1999) and proved that the formaldehyde was the primary stable organic intermediate. Hirosaka et al. (Hirosaka et al., 2007, 2008) have experimentally studied hydrothermal oxidation of ethanol under subcritical conditions. They confirmed that the temperature increased up to 120 °C owing to exothermic reaction and obtained the first-order reaction rate for ethanol oxidation. Similarly, Helling and Tester (1988) and Schanzenbächer et al. (2002) reported hydrothermal oxidation rates of ethanol under supercritical conditions. Helling and Tester (1988) assumed the first-order reaction of ethanol with ignoring oxygen concentration and determined the oxidation rate of ethanol by measuring the conversion at one residence time for each temperature. However, they provided only preliminary data on oxidation kinetics. Schanzenbächer et al. made several improvements to their reactor system and provided detailed kinetic data for the oxidation of ethanol in supercritical water (SCW) under well-defined conditions. They investigated the dependency of the reaction rate on oxygen concentration and determined the rate expression.

2.2 Chemical reactions for hydrothermal oxidation

2.2.1 Supercritical water oxidation

In high-pressure and hot conditions of water, e.g. SCW, water itself plays several roles. During hydrothermal oxidation, water behaves as the reactants and products participating in some reactions. The elementary reactions that water takes part in are as follows:

$$H_2O + M \rightleftharpoons OH + H + M \tag{2.1}$$
$$H_2O + H \rightleftharpoons OH + H_2 \tag{2.2}$$
$$H_2O + O \rightleftharpoons OH + OH \tag{2.3}$$
$$OH + HO_2 \rightleftharpoons H_2O + O_2 \tag{2.4}$$
$$OH + HR \rightleftharpoons H_2O + R \tag{2.5}$$
$$H_2O + HO_2 \rightleftharpoons OH + H_2O_2 \tag{2.6}$$

Examples of such reactions appear in detailed chemical kinetics model for SCWO of hydrogen, carbon monoxide, methane, methanol, ethanol and benzene summarised in

Table 2.2. These reactions can play an important role of the overall kinetics. M is a collision partner in this reaction.

The works of detailed ethanol oxidation chemistry is proposed by Marinov (1999) for gas phase combustion at ambient pressure and Rice and Croiset (2001) for supercritical water oxidation, which involve many radical reactions. On the other hand, there are several researches for kinetics of phenol oxidation in supercritical water (i.e. Hayashi et al., 2005, 2007), which suggest that the oxidation occur radical and via ion elementary reactions.

2.2.2 Subcritical wet oxidation

Free radical reactions

Among the researchers in this field, it is general consensus that wet oxidation occurs by means of a combination of elementary radical reactions. The radical reactions are mainly divided into three types, i.e. initiation, propagation and termination. Examples of the different types of free-radical reactions, which can occur through WO, are shown in Equations 2.7–2.32.

Although many researchers suggest that WO occur through radical reactions (Bhargava et al., 2006), there is just one report that supports the radical reaction from experiments, i.e. Robert et al. (2002).

- Initiation

Bimolecular reactions:

$$RH + O_2 \rightarrow R^{\bullet} + HO_2^{\bullet}$$ (Mantzavinos et al., 1997) (2.7)

$$H_2O + O_2 \rightarrow H_2O_2 + O^{\bullet}$$ (Ingale et al., 1996) (2.8)

$$H_2O + O_2 \rightarrow HO_2^{\bullet} + OH^{\bullet}$$ (Ingale et al., 1996) (2.9)

Unimolecular reactions:

$$RH \rightarrow R^{\bullet} + H^{\bullet}$$ (Robert et al., 2002) (2.10)

$$O_2 \rightarrow O^{\bullet} + O^{\bullet}$$ (Ingale et al., 1996) (2.11)

$$H_2O \rightarrow OH^{\bullet} + H^{\bullet}$$ (Rivas et al., 1998) (2.12)

Trimolecular reactions:

$$RH + O_2 + RH \rightarrow 2R^{\bullet} + H_2O_2$$ (Emanuel et al., 1980) (2.13)

Alkaline solution only:

$$XCH_2^{-} + O_2 \rightarrow XCH_2^{\bullet} + O_2^{\bullet -}$$ (Wakabayashi & Okuwaki, 1988) (2.14)

$$C_6H_5O^{-} + O_2 \rightarrow C_6H_5O^{\bullet} + O_2^{\bullet -}$$ (Rivas et al., 1998) (2.15)

$$O_2 + e^- \rightarrow R^\bullet + {}^\bullet O_2^-$$ (Eyer, 2001) (2.16)

(X = carboxylate group)

- Propagation

$$R^\bullet + O_2 \rightarrow ROO^\bullet$$ (Mantzavinos et al., 1997) (2.17a)

$$ROO^\bullet + RH \rightarrow RCOOH + R^\bullet$$ (Mantzavinos et al., 1997) (2.17b)

$$O^\bullet + H_2O \rightarrow HO^\bullet + HO^\bullet$$ (Ingale et al., 1996) (2.18)

$$RH + HO_2^\bullet \rightarrow R^\bullet + H_2O_2$$ (Li et al., 1991) (2.19)

$$H^\bullet + H_2O \rightarrow HO^\bullet + H_2$$ (Robert et al., 2002) (2.20)

$$ROOH \rightarrow RO^\bullet + HO^\bullet$$ (Robert et al., 2002) (2.21)

$$RH + HO^\bullet \rightarrow R^\bullet + H_2O$$ (Robert et al., 2002) (2.22)

Alkaline solution only:

$$XCH_2OO^\bullet + XCH_2^- \rightarrow XCH_2OO^- + XCH_2^\bullet$$

(Wakabayashi & Okuwaki, 1988) (2.23)

(X = carboxylate group)

- Termination

$$2ROO^\bullet \rightarrow ROOR + O_2$$ (Mantzavinos et al., 1997) (2.24)

$$2HO_2^\bullet \rightarrow H_2O_2 + O_2$$ (Farhataziz & Ross, 1977) (2.25)

$$HO_2^\bullet + OH^\bullet \rightarrow H_2O + O_2$$ (Farhataziz & Ross, 1977) (2.26)

Alkaline solution only:

$$XCH_2OO^\bullet + O_2^{\bullet-} \rightarrow XCH_2^- + 2O_2$$ (Wakabayashi & Okuwaki, 1988) (2.27)

$$2O_2^{\bullet-} + H_2O \rightarrow HOO^- + HO^- + O_2$$ (Patterson et al., 2001) (2.28)

$$HO^\bullet + CO_3^{2-} \rightarrow {}^-OH + {}^\bullet CO_3^-$$ (Patterson et al., 2001) (2.29)

$$O_2^{\bullet-} + {}^\bullet CO_3^{2-} \rightarrow O_2 + CO_3^{2-}$$ (Glaze et al., 1995) (2.30)

$$HO^\bullet + HCO_3^- \rightarrow H_2O + {}^\bullet CO_3^-$$ (Robert et al., 2002) (2.31)

$$ROO^\bullet + O_2^{\bullet-} \rightarrow ROO^- + O_2$$ (Ichinose & Okuwaki, 1990) (2.32)

(X = carboxylate group)

Non free radical (ionic) reactions

Ion reactions also participate in the oxidation of organics (Bhargava et al., 2006), whereas few ion reactions are known today, e.g. the ionic reactions involving

Carbanion formation:

$$XCH_3 + {}^-OH \rightarrow XCH_2^- + H_2O$$ (Wakabayashi & Okuwaki, 1988) (2.33)

(X = carboxylate group)

Alkoxide formation:

$$C_6H_5OH + {}^-OH \rightarrow C_6H_5O^- + H_2O$$ (Rivas et al., 1998) (2.34)

Retro aldol reaction:

$$C_6H_8O_7 + {}^-OH \rightarrow CH_3CO_2H + HO_2CCOCH_2CO_2H + {}^-OH$$

(Roberts, 1979) (2.35)

Table 2.2 Summary of detailed chemical kinetics models for SCWO of hydrogen, carbon monoxide, methane, methanol, ethanol, phenol and benzene.

substance	source
hydrogen	Holgate and Tester (1993,1994); Brock and Savage (1995)
carbon monoxide	Helling and Tester (1987); Holgate et al. (1992); Holgate and Tester (1994)
methane	Webley and Tester (1991); Brock and Savage (1995)
methanol	Wbley and Tester (1989); Brock and Savage (1995); Brock et al. (1996)
ethanol	Rice and Croiset (2001)
phenol	Gopalan and Savage (1995)
benzene	DiNaro et al. (2000)

2.3 Hydrothermal oxidation of ethanol

Some works for reaction rates of ethanol hydrothermal oxidation are reported. For SCWO of ethanol, the oxidation rates were measured by Schanzenbächer et al. (2002) and Helling and Tester (1988). In the work by Schanzenbächer et al. (2002), ethanol oxidation rates were investigated in supercritical water using a lab-scale plug-flow reactor system at temperatures from 433 to 494 °C and a fixed pressure of 24.6 MPa. The oxidation rate obtained is

$$-\frac{\mathrm{d[EtOH]}}{\mathrm{d}t} = 10^{17.23\pm1.65}\exp(-213.9\pm18.3/RT)[\mathrm{EtOH}]^{1.34\pm0.11}[\mathrm{O_2}]^{0.55\pm0.19}. \quad (2.36)$$

The pioneer works by Helling and Tester (1988) are also famous in this field.

On the other hand, the reactions rate for subcritical WO of ethanol were obtained by Hirosaka et al. (2007, 2008) for T = 170–230 °C and p = 23.5 MPa,

$$-\frac{\mathrm{d[EtOH]}}{\mathrm{d}t} = 10^{2.05\pm0.24}\exp(-61\pm3/RT)[\mathrm{EtOH}]^{0.86\pm0.03}[\mathrm{O_2}]^{1.15\pm0.05}, \quad (2.37)$$

and for T = 200–320 °C and p = 26–28 MPa,

$$-\frac{\mathrm{d[EtOH]}}{\mathrm{d}t} = 10^{2.46\pm0.06}\exp(-41.1\pm1.0/RT)[\mathrm{EtOH}]. \quad (2.38)$$

For high-pressure steam oxidation, there is no report on reaction rate.

2.4 Numerical experiment and simulation of hydrothermal flow for the reactor design

A number of numerical approaches have been reported to assist the experimental study. Oka et al. (2000) developed a programme for fluid and reaction analysis of supercritical fluid (SCF). They calculated the hydrothermal decomposition and oxidation of coffee residue in a SCF reactor as an example of waste material. Distributions of thermody-

namic quantities in the cylindrical reactor vessel were investigated in their study.

Works that Dutournié et al. (2003, 2004, 2005) conducted consist of numerical model to simulate the critical behaviour of the fluid in a tubular oxidation reactor during stationary and non-stationary operation. Their model was validated from experimental temperature profiles with a quasi-adiabatic hydrothermal oxidation tubular reactor. The simulation results showed that thermal operation of the hydrothermal oxidation reactor could be considered to be stable.

An investigation developed by Vielcazals et al. (2006) shows a mathematical model of a reactor for hydrothermal oxidation, which is based on the plug flow assumption. This reactor is horizontal and tubular and is designed with multi-injection points of oxidant. The comparison of computed profiles of temperature and concentration of chemical species with experimental profiles obtained in the case of supercritical oxidation of methanol showed good agreement.

2.5 Summary

This chapter reviewed literature for kinetic studies on hydrothermal oxidation of model compounds, e.g. acetic acid, phenol, ammonia, methanol, ethanol, etc. Detailed chemical reactions are also reviewed for supercritical water oxidation and subcritical wet oxidation. The literatures for several studies on numerical simulation are presented in this chapter.

Chapter 3: Objectives

3.1 Objectives

The primary objectives of this research were to develop the code of numerical simulation of hydrothermal flow and to obtain kinetic data for oxidation of ethanol as the basis for development of accurate models of numerical experiments as a reactor design tool for boiler system via hydrothermal oxidation of wet biowaste.

Ethanol as a reactant

Some waste substances are hydrolysed in subcritical water to produce miscible substances such as alcohols and fatty acids (Hashaikeh, 2005; Holliday, 1997). Moreover, the literature (Li, 1991), including specific description of subcritical WO reaction mechanisms, states that stable intermediates in WO of waste materials are mainly methanol, ethanol and acetic acid. Particularly, ethanol (C_2H_5OH or EtOH) is among the simplest compounds that contain C, H and O atoms, all of which are prevalent in waste materials, and also easy to handle in experiment for its non-toxicity. Therefore, in this study, ethanol was selected as a model reactant for wet oxidation at subcritical conditions.

For design of hot-water boiler

As viewed from the perspective of practical applications, this research will be used for design of hot-water boiler processes, which is available for food processors as a heat conversion system. The study that involves heat release and reaction kinetics in the

reactor is necessary to develop hot-water boiler system via hydrothermal oxidation. Validity and consistency of the results obtained from the numerical experiments for hydrothermal flow in this research can be examined in further research.

For improvement of the reliability of numerical experiments as a design tool

The products and reaction paths are identified, and the overall reaction rates are obtained for the hydrothermal oxidation. This research is carried out to collect information which provide criterion to decide a better phase condition for hot-water boiler via subcritical water.

3.2 Structure of the thesis

The structure of this thesis is illustrated in Figure 3.1 and summarised below:

- Chapter 1 explains background and outlines fundamental properties of near- and supercritical water. The difference between hydrothermal oxidation and gas-phase combustion are also described.

- Chapter 2 presents a brief literature review relating to kinetics of hydrothermal oxidation, detailed chemical reaction for hydrothermal oxidation and numerical experiments of hydrothermal flow for reactor design.

- Chapter 4 explains a parametric study to develop a design method for hot-water boiler via numerical experiments. The reaction conditions are at preheating temperature of 350 (below the critical temperature in liquid phase) or 400 (above the critical temperature in supercritical water). The exothermic reaction occurred continuously through subcritical to supercritical temperature.

- The reaction rates, products and oxidation reaction pathways are clarified for

hot-compressed water in Chapter 5 and for high-pressure steam in Chapter 6. This information provide criterion to decide which phase is the better condition for hot-water boiler by means of subcritical water. In addition, the knowledge of products and pathways can help to calculate more precise results.

- Chapter 7 summarises the key conclusions from this work. The implications of this research work are also highlighted.

- Chapter 8 provides several suggestions for further work.

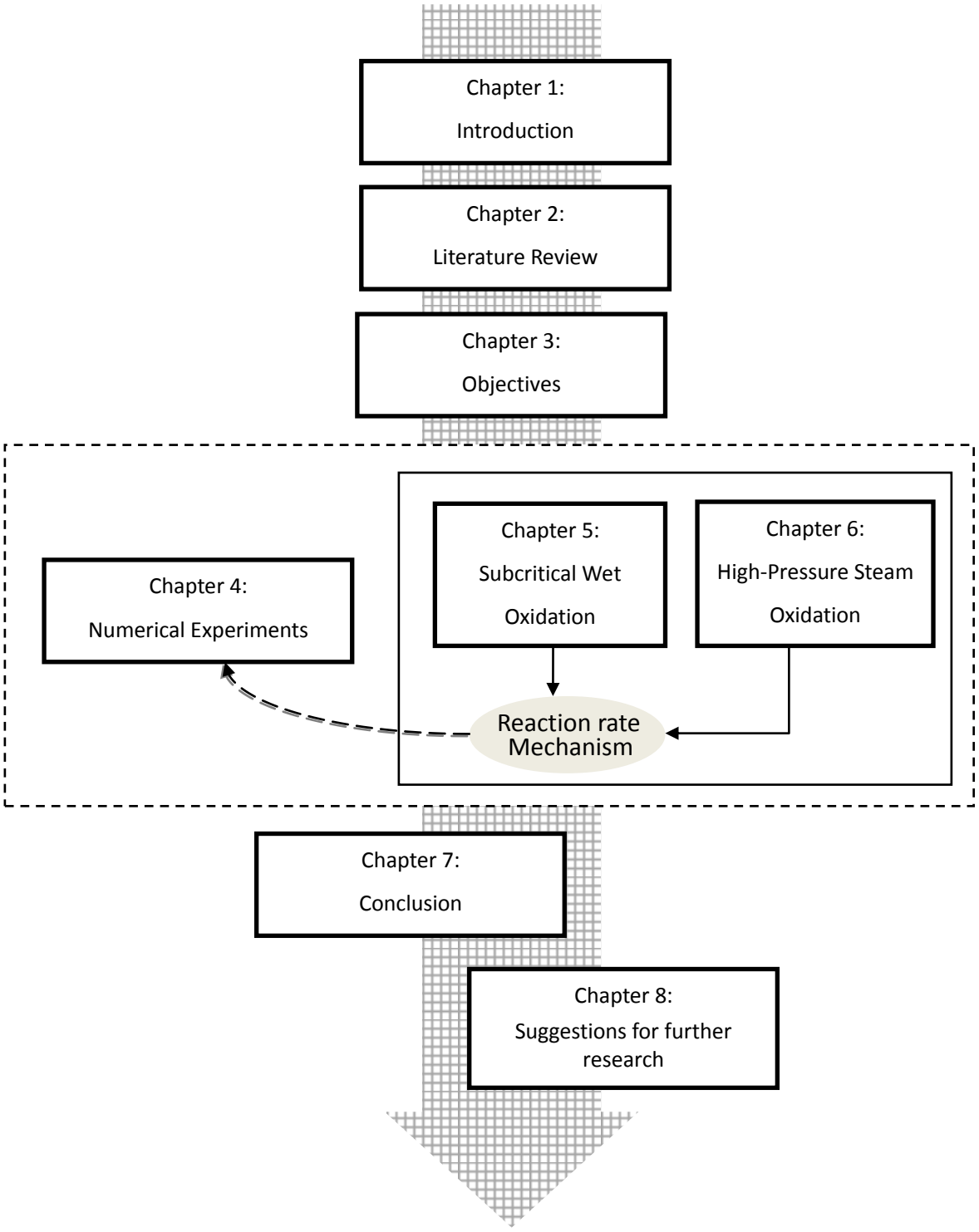

Figure 3.1 Structure of the thesis.

Chapter 4: Numerical experiments of ethanol oxidation in hot-compressed water

4.1 Introduction

In the preceding researches described above, several efforts were made to predict thermal behaviours of the fluids through the reactors via numerical simulation of hydrothermal oxidation flow. Most of these papers assumed that the chemical reaction rate was first order in fuel (waste substances) and independent on oxidant, because the concentration of oxidant was enough to completely oxidise the fuel. Furthermore, the concentration of reactants (fuel and oxidant) was relatively smaller and thus thermal and transport properties of fluids were evaluated as those of pure water. Oka et al. used the equation of state (EOS), which can deal with mixture properties. They simulated the mixture reactive flow with a Peng-Robinson EOS, because the Peng-Robinson equation is generally used for supercritical state. On the other hand, some papers e.g. Yamamoto et al. (2005) adopted an appropriate EOS for their own objective. They analysed thermal flow field in near-critical carbon dioxide by using the Peng-Robinson EOS. In this way, it is important to discuss what EOS to employ. Especially, dealing with the near-critical media where physical properties vary remarkably is of considerable significance.

Macroscopic properties are important qualities for utilisation of sub- and supercritical water. Many operation conditions for pressure and temperature involve the change in water phase from supercritical to subcritical water and vice versa. When the

different phase compounds coexist, e.g. liquid and solid, it is also important that estimate the equilibrium properties for each phase compound. The macroscopic transport and thermo chemical properties for each component are necessary for calculating heat and mass transfer in sub- and supercritical water.

In the current study, the macroscopic properties of water in sub- and supercritical water are used for the simulation by assuming a global one-step reaction including fuel and oxidiser concentrations and use experimental data for reaction order of reactants from a literature. We also discuss what EOS is suitable for simulating hydrothermal flow around the critical point and for using mixing rules of thermal and transport properties. The flow field is one dimensional, i.e. plug flow, which is often used in preceding literatures (Dutournié et al., 2003, 2004, 2005, 2007). Ethanol is adopted as the fuel of hydrothermal oxidation reactants, while Oka et al. (2000) used coffee residue, Dutournié et al. (2004, 2005, 2007) used phenol and methanol, and Vielcazals et al. (2006) used methanol. Ethanol is considered to be one of the stable intermediate products of biomass. Behaviours of ethanol oxidation under sub/super critical conditions are numerically simulated and effects of preheat temperature, heat loss and flow velocity are addressed.

4.2 Governing equations

Oxidation of ethanol was assumed to be one-step irreversible reaction:

$$C_2H_5OH + 3O_2 \rightarrow 3H_2O + 2CO_2, \tag{4.1}$$

which is a complete oxidation formula of ethanol to water and carbon dioxide. The calculation geometry is a plug flow tubular reactor with length 1 m and heater of 0.1 m as shown in Figure 4.1. The wall surface is heated at inlet side of the reactor and the mixture of water and reactants flows into the reactor at far left. Governing equations for the one-dimensional hydrothermal flow shown in Figure 4.1 are written below:

Mass conservation:

$$\frac{\partial \rho}{\partial t} + \frac{\partial \rho u}{\partial x} = 0 \tag{4.2}$$

Momentum conservation:

$$\rho\frac{\partial u}{\partial t}+\rho u\frac{\partial u}{\partial x}=-\frac{\partial p}{\partial x}+\frac{\partial}{\partial x}\left(\frac{4}{3}\overline{\eta}\frac{\partial u}{\partial x}\right) \tag{4.3}$$

Energy conservation:

$$\rho\overline{c}_p\frac{\partial T}{\partial t}+\rho\overline{c}_p u\frac{\partial T}{\partial x}=\frac{\partial}{\partial x}\left(\overline{\lambda}\frac{\partial T}{\partial x}\right)-\sum_i h_i w_i+Q(x) \tag{4.4}$$

Species conservation:

$$\rho\frac{\partial Y_i}{\partial t}+\rho u\frac{\partial Y_i}{\partial x}=\frac{\partial}{\partial x}\left(\rho D_i\frac{\partial Y_i}{\partial x}\right)+w_i \tag{4.5}$$

where $\overline{\eta}$, $\overline{\lambda}$, and $\overline{c}_p$ denote viscosity, thermal conductivity and isobaric specific heats for the mixture, respectively. D_i denotes diffusion coefficient of *i*-th species in water and $Q(x)$ denotes heat source or heat loss.

4.3 Equation of state for sub-/super critical water

There are several types of equation of state proposed for sub-/super critical fluids: 1) Helmholtz type equation in which Helmholtz free energy is first estimated at a certain density and temperature then pressure is obtained by the derivative of Helmholtz free energy with respect to volume (Span and Wagner (1996), etc.); 2) van der Waals type equation (Peng-Robinson equation (Peng and Robinson, 1976), Soave-Redlich-Kwong equation (Soave, 1972), etc.), which is a modified equation of state of ideal gas considering real gas effect such as attractive and repulsive forces of molecules; 3) BWR type equation (BWRS equation (Benedict et al., 1940), Nishiumi-Saito equation (Nishiumi and Saito, 1975), etc.), which uses an empirical Birial expansion of pressure by density; and 4) Lee-Kesler equation (Lee and Kelser, 1975) that estimates compression coefficient: $Z = pV/RT$.

Several types of equations of state for water are compared with steam data from the IAPWS formation (Wagner and Kruse, 1998) as shown in Figures 4.2 and 4.3. Figure 4.2 shows density change against temperature under constant pressure of 25 MPa. The

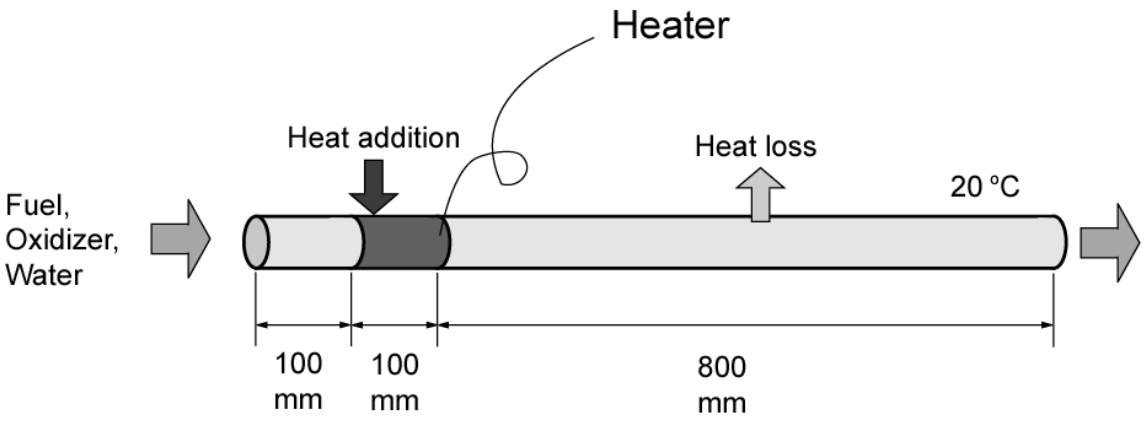

Figure 4.1 One-dimensional reactor model.

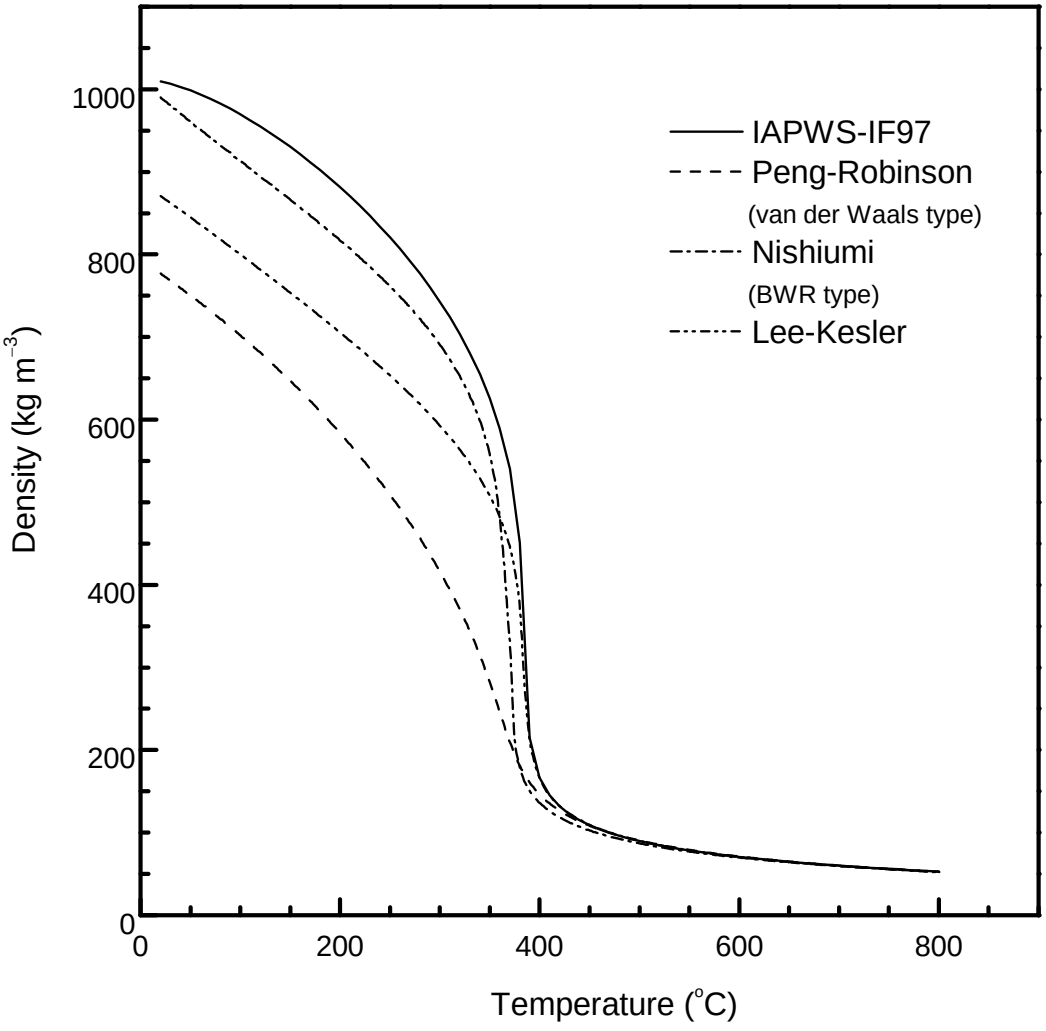

Figure 4.2 Comparison of state equations of water at 25 MPa.

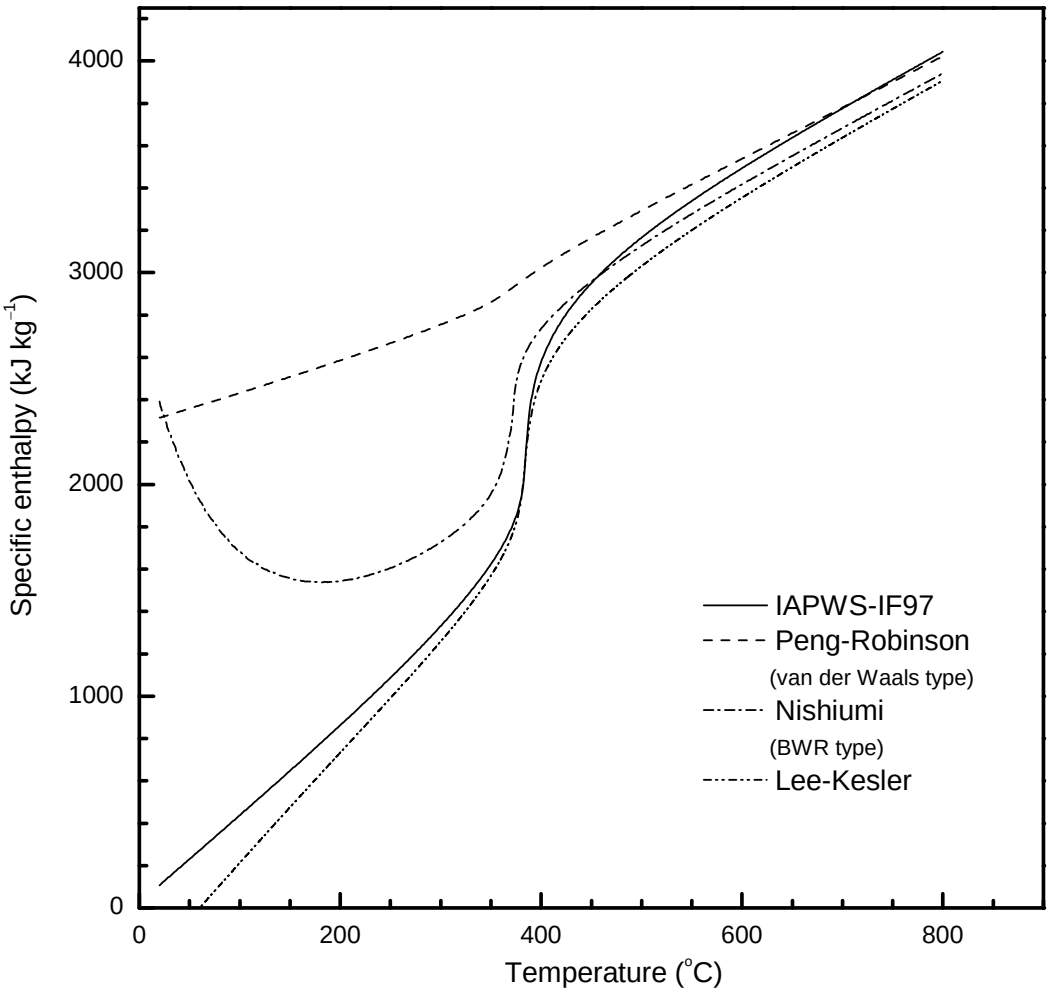

Figure 4.3 Comparison of specific enthalpy of water at 25 MPa.

Peng-Robinson equation (Peng and Robinson, 1976) agrees well with the steam data above the critical point, i.e. 374 °C, but estimates much lower density under the critical point. The Nishiumi-Saito equation (Nishiumi and Saito, 1975) predicts almost similar change as the steam data for all temperature range, but it estimates much different density from the steam data near the critical point, where the density changes dramatically by the temperature. The Lee-Kesler equation of state (Lee and Kesler, 1975) predicts the density change quite well above and just below the critical point, though it estimates lower density far below the critical point.

Figure 4.3 shows enthalpy change against temperature under the constant pressure of 25 MPa. The Peng-Robinson equation (Peng and Robinson, 1976) agrees well with the steam data above the critical temperature, but estimates higher enthalpy around and below the critical temperature. The Nishiumi-Saito equation (Nishiumi and Saito, 1975) predicts well the change of enthalpy above the critical temperature, but it estimates higher enthalpy than the steam data below the critical temperature. The Lee-Kesler equation of state (Lee and Kesler, 1975) predicts the enthalpy change quite well just around the critical point, though it estimates a little lower enthalpy than the steam data above and below the critical point. As the Lee-Kesler equation of state has a discrepancy for ethanol due to its large acentric factor, but the concentration of ethanol is 1.81 mol% (4.31 wt%) in this study and it has a small influence on the evaluation of the state of the mixture.

These comparisons made us decide to adopt Lee-Kesler equation for simulation, because it could represent correctly the drastic change of physical properties across the critical point. The Lee-Kesler equation of state is written as

$$Z = Z^{(0)} + \frac{\omega}{\omega^{(r)}} \left(Z^{(r)} - Z^{(0)} \right) \tag{4.6}$$

where Z is the compression coefficient. Detail derivation of the compression coefficient is described in at A.1 in Appendix A.

4.4 Physical properties and mixing lows

4.4.2 Thermal properties

For the estimation of thermal properties such as isobaric specific heat and specific enthalpy, we used the method by Lee-Kesler. First, specific heat of ideal gas is estimated using following equation (Moore, 1972):

$$C_p^{id} = a + bT + cT^2 + dT^3 \tag{4.7}$$

By the isobaric specific heat departure from ideal gas (or liquid), equation (4.6) may be transformed to be following equation:

$$\frac{C_p - C_p^{id}}{R} = \left(\frac{C_p - C_p^{id}}{R}\right)^{(0)} + \frac{\omega}{\omega^{(r)}}\left[\left(\frac{C_p - C_p^{id}}{R}\right)^{(r)} - \left(\frac{C_p - C_p^{id}}{R}\right)^{(0)}\right]. \tag{4.8}$$

In equation (8), the right-hand side is calculated by

$$\left(\frac{C_p - C_p^{id}}{R}\right)^{(i)} = \left[\frac{C_v - C_v^{id}}{R} - 1 - T_r\left(\frac{\partial p_r}{\partial T_r}\right)_{V_r}^2 \Big/ \left(\frac{\partial p_r}{\partial V_r}\right)_{T_r}\right]^{(i)} \tag{4.8a}$$

where $i = 0$ for simple fluids and $i = r$ for reference fluids.

Specific enthalpy for ideal gas is expressed as

$$h^{id} = h_0 + \int_{T_0}^{T} C_p^{id} dT \tag{4.9}$$

where the superscript *id* denotes ideal gas (or liquid). The isothermal enthalpy departure from ideal gas (or liquid) is also estimated by

$$\frac{h - h^{id}}{RT_c} = \left(\frac{h - h^{id}}{RT_c}\right)^{(0)} + \frac{\omega}{\omega^{(r)}}\left[\left(\frac{h - h^{id}}{RT_c}\right)^{(r)} - \left(\frac{h - h^{id}}{RT_c}\right)^{(0)}\right] \tag{4.10}$$

In an analogous way to calculate specific heat, the right-hand side of equation (4.10) is calculated by

$$\left(\frac{h - h^{id}}{RT_c}\right)^{(i)} = \left\{T_r\left(Z - 1 - \frac{b_2 + 2b_3/T_r + 3b_4/T_r^2}{T_r V_r} - \frac{c_2 + 3c_3/T_r^2}{2T_r V_r^2} + \frac{d_2}{5T_r V_r^5} + 3E\right)\right\}^{(i)} \tag{4.10a}$$

where $i = 0$ for simple fluids and $i = r$ for reference fluids (See details at A.2 in Appendix A).

4.4.3 Transport properties

Equations obtained by Chung et al. (1988) and Wilke and Chung (1955) are used for estimation of transport properties such as viscosity, thermal conductivity, and diffusion coefficient. Details are described at A.3 in Appendix A.

For viscosity,

$$\eta = \eta_k + \eta_p \tag{4.11}$$

with $\eta_k = \eta_0(1/G_2 + A_6 Y)$, $\eta_p = \{36.344\times10^{-6}(M_r T_c)^{1/2}/V_c^{2/3}\}A_7 Y^2 G_2 \exp(A_8 + A_9/T^* + A_{10}/T^{*2})$. For thermal conductivity,

$$\lambda = \lambda_k + \lambda_p \tag{4.12}$$

with $\lambda_k = \lambda_0(1/H_2 + B_6 Y)$, $\lambda_p = \{3.039\times10^{-4}(T_c/M_r)^{1/2}/V_c^{2/3}\}B_7 Y^2 H_2 T_r^2$. For diffusion coefficient,

$$D_i = \frac{7.4\times10^{-8}(\beta M_2)^{1/2}T}{\eta_2 V_{b,i}^{0.6}} \tag{4.13}$$

where subscript 2 denotes water as diffuse solvent, β is associated factor which has the value of 2.6 for water solution. $V_{b,i}$ is molar volume at the boiling point for molecule *i*, and related to that at critical point:

$$V_{b,i} = 0.285 V_{c,i}^{1.048} \tag{4.14}$$

which is estimated by Tyn et al. (1975).

4.4.4 Mixing lows

In this simulation, four different chemical species, C_2H_5OH, O_2, CO_2, and H_2O, are considered as reactants and products of the reaction (4.1). Hence, mixing laws should be applied to equation of state and transport properties, e.g. viscosity and thermal conductivity. Mixing laws for equation of state and thermal properties are obtained by Plöcker et al. (1978) and those for transport properties are obtained by Chung et al. (1988). Details are described at A.4 in Appendix A.

4.5 Reaction rate

There are some expressions for oxidation reaction rate of ethanol under various conditions and various reaction orders in literatures. When the concentration of ethanol is much smaller than the oxidiser, first-order oxidation of ethanol could be assumed. Hirosaka et al. (2007) obtained the oxidation rate of ethanol under sub-critical conditions around 26–28 MPa and 200–320 °C.

$$-r_{\mathrm{EtOH}} = 10^{2.46\pm0.06} \times \exp\left(\frac{-41.1 \pm 1.0\,(\mathrm{kJ\cdot mol^{-1}})}{RT}\right)[\mathrm{EtOH}] \tag{4.15}$$

Under supercritical conditions of 25.6 MPa and 433 to 494 °C, Schanzenbächer et al. (2002) determined the oxidation rate of ethanol, which was assumed to be first-order in ethanol and zero-order in oxygen:

$$-r_{\mathrm{EtOH}} = 10^{11.1\pm4.5} \times \exp\left(\frac{-163.9 \pm 3.3\,(\mathrm{kJ\cdot mol^{-1}})}{RT}\right)[\mathrm{EtOH}]\cdot \tag{4.16}$$

The activation energy for supercritical condition is approximately four times larger and the order of the frequency factor is about 10^{10} times greater than those under sub-critical conditions. One reason of this discrepancy is attributed to the dramatic increase of oxidation rate and change in reaction mechanism when the reaction field changes from sub-critical condition to supercritical condition.

When considering effect of oxygen concentration, oxidation rate should depend on the equivalence ratio, which ranges from $\phi \leq 1$ to $\phi \geq 1$. Under supercritical condition, Schanzenbächer et al. (2002) obtained the expression:

$$-r_{\mathrm{EtOH}} = 10^{17.23\pm1.65} \exp\left(-\frac{214 \pm 18\ (\mathrm{kJ\cdot mol^{-1}})}{RT}\right)[\mathrm{EtOH}]^{1.34\pm0.11}[\mathrm{O_2}]^{0.55\pm0.19} \tag{4.17}$$

which could express the dependence on the oxygen concentration. For the examination of the oxygen dependence, they varied the fuel equivalence ratio ϕ between 0.5 and 1.9 at a temperature of 433 to 494 °C and a pressure of 24.6 MPa. The resulting pre-exponential factor was 17.23 ± 1.65, the activation energy was 213.9 ± 18.3 kJ·mol^{-1} and the reaction orders for ethanol and oxygen were 1.34 ± 0.11 and 0.55 ± 0.19.

On the other hand, Hirosaka et al. (2008) obtained the expression for subcritical conditions:

$$-r_{\mathrm{EtOH}} = 10^{2.05\pm0.24} \exp\left(-\frac{61.1 \pm 3.1\ (\mathrm{kJ\cdot mol^{-1}})}{RT}\right) [\mathrm{EtOH}]^{0.86\pm0.03}[\mathrm{O_2}]^{1.15\pm0.05} \tag{4.18}$$

using a plug-flow reactor system at temperatures between 170 °C and 230 °C and a fixed pressure 23.5MPa. The fuel equivalence ratio ranges from 0.5 to 1.5 with the initial concentration of ethanol 0.131 mol%. The reaction orders for ethanol and oxygen are 0.86 ± 0.03 and 1.15 ± 0.05, respectively. The resulting activation energy and the pre-exponential factor are 61.1 ± 3.12 kJ·mol^{-1} and $10^{2.05 \pm 0.24}$, respectively. To confirm whether this obtained oxidation rate is applicable at the condition of higher ethanol concentration, they conducted numerical simulation of hydrothermal oxidation of ethanol in sub-critical water with the initial concentration of ethanol 10.9 mol%. The simulation results agree with the experimental results qualitatively.

In the present study, the expression (4.17) by Schanzenbächer et al. (2002) is used as the reaction rate, because the reaction temperature in our study (above 350 °C) is closer to the temperature range used by Schanzenbächer et al. (2002) than that of Hirosaka et al (2008). Though the concentration of ethanol in the experiment of Schanzenbächer et al. (2002) is 0.0472 mol%, which is much lower than that used for our calculation, i.e. 1.82 mol%, Hirosaka et al. (2008) demonstrated that a numerical simulation using the reaction rate obtained by the experiment with lower concentration of ethanol (0.131 mol%) well agreed with the experimental results obtained with higher concentration of ethanol (10.9 mol%).

4.6 Numerical methods

The second-order central finite volume method was used for space, Euler's implicit method was used for time integration and the fractional step method was used for solving pressure field. The initial pressure was 25 MPa and boundary conditions were

$$u, T \text{ and } Y_i = \text{const.} \qquad \text{at inlet boundary,} \tag{4.19}$$

$$\frac{\partial u}{\partial x} = \frac{\partial T}{\partial x} = \frac{\partial Y_i}{\partial x} = 0 \qquad \text{at outlet boundary.} \tag{4.20}$$

Concentrations of ethanol and oxygen were 1.8 mol% (4.3 wt%) and 5.4 mol% (9 wt%), respectively ($\phi = 1.0$). Conditions of simulation are listed in Table 4.1. Case 1: Preheat temperature of the reactants was 350 °C (sub-critical condition) and 400 °C (supercritical condition), initial flow velocity was 1.0 $m \cdot s^{-1}$ and without heat loss. Case 2: The initial flow velocity was 1.0 $m \cdot s^{-1}$, 2.0 $m \cdot s^{-1}$ and 3.0 $m \cdot s^{-1}$, while the preheat temperature was 350 °C and without hear loss. Case 3: The heat transfer coefficient varies as 0.0 $W \cdot m^{-2} \cdot K^{-1}$, 10^6 $W \cdot m^{-2} \cdot K^{-1}$ and 10^7 $W \cdot m^{-2} \cdot K^{-1}$, while the preheat temperature was 350 °C and initial flow velocity was 1.0 $m \cdot s^{-1}$.

4.7 Results and discussions

4.7.1 Effect of preheat temperature

Figure 4.4 shows the conversion along the reactor for preheat temperature of 350 °C and 400 °C. Conversion is defined by

$$\frac{Y_{\text{ethanol}}(0) - Y_{\text{ethanol}}(x)}{Y_{\text{ethanol}}(0)} \times 100 \quad [\%] \tag{4.21}$$

where $Y_{\text{ethanol}}(x)$ means the ethanol mass fraction at the distance from inlet, x. In Figure 4.4, ethanol is converted almost completely at preheated temperatures of 350 °C and 400 °C. Figure 4.5a shows changes of ΔT, which is the difference between temperatures with and without chemical reaction, along the reactor for different preheat temperatures at $u_{\text{in}} = 1.0$ $m \cdot s^{-1}$, while Figure 4.5b shows changes of temperature along the reactor for different preheat temperatures.

The value of ΔT for 400 °C becomes up to 280 °C in the preheated region in Figure 4.5a, while the increase of temperature for 350 °C becomes only 80 °C. This is caused by the behaviour of the specific heat, which has a peak at the critical point, i.e. 374 °C, 25 MPa. In the case of 350 °C, most of the heating value is absorbed by the increasing specific heat because exothermic reaction occurs around the critical point. But for 400 °C, where the condition is supercritical, heating value is mostly used to increase temperature because after passing through the critical point exothermic reaction occurs.

Table 4.1: Calculation conditions. Three comparisons (Case 1, 2 and 3) are made for different parameters: temperature, inflow velocity and heat transfer coefficient.

Case	Temperature [°C]	Inflow velocity [$m \cdot s^{-1}$]	Heat transfer coefficient [$W \cdot m^{-2} \cdot K^{-1}$]
1	350, 400	1	0 (adiabatic)
2	350	1, 2, 3	0 (adiabatic)
3	350	1	0, 2500, 25000

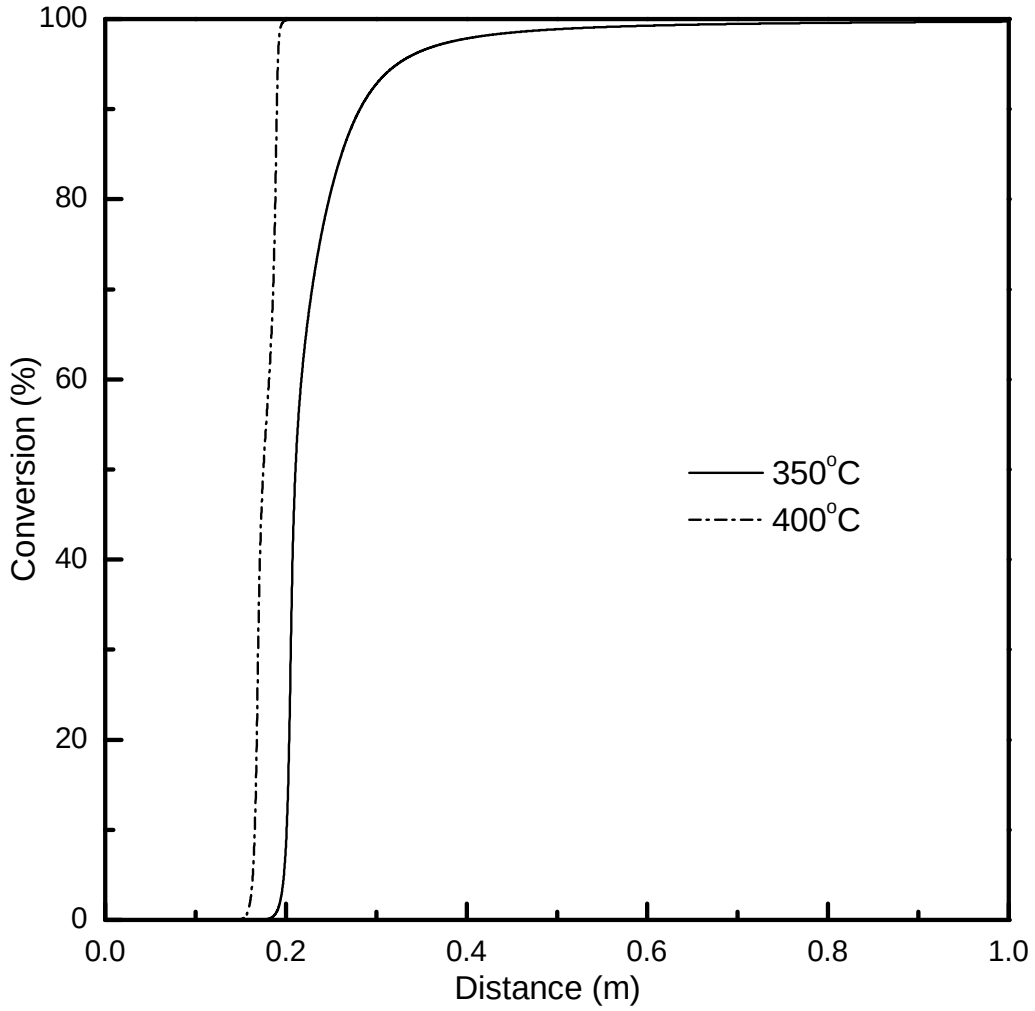

Figure 4.4 Changes of conversion along the reactor for different preheat temperatures at u_{in} = 1.0 m·s^{-1} under adiabatic condition.

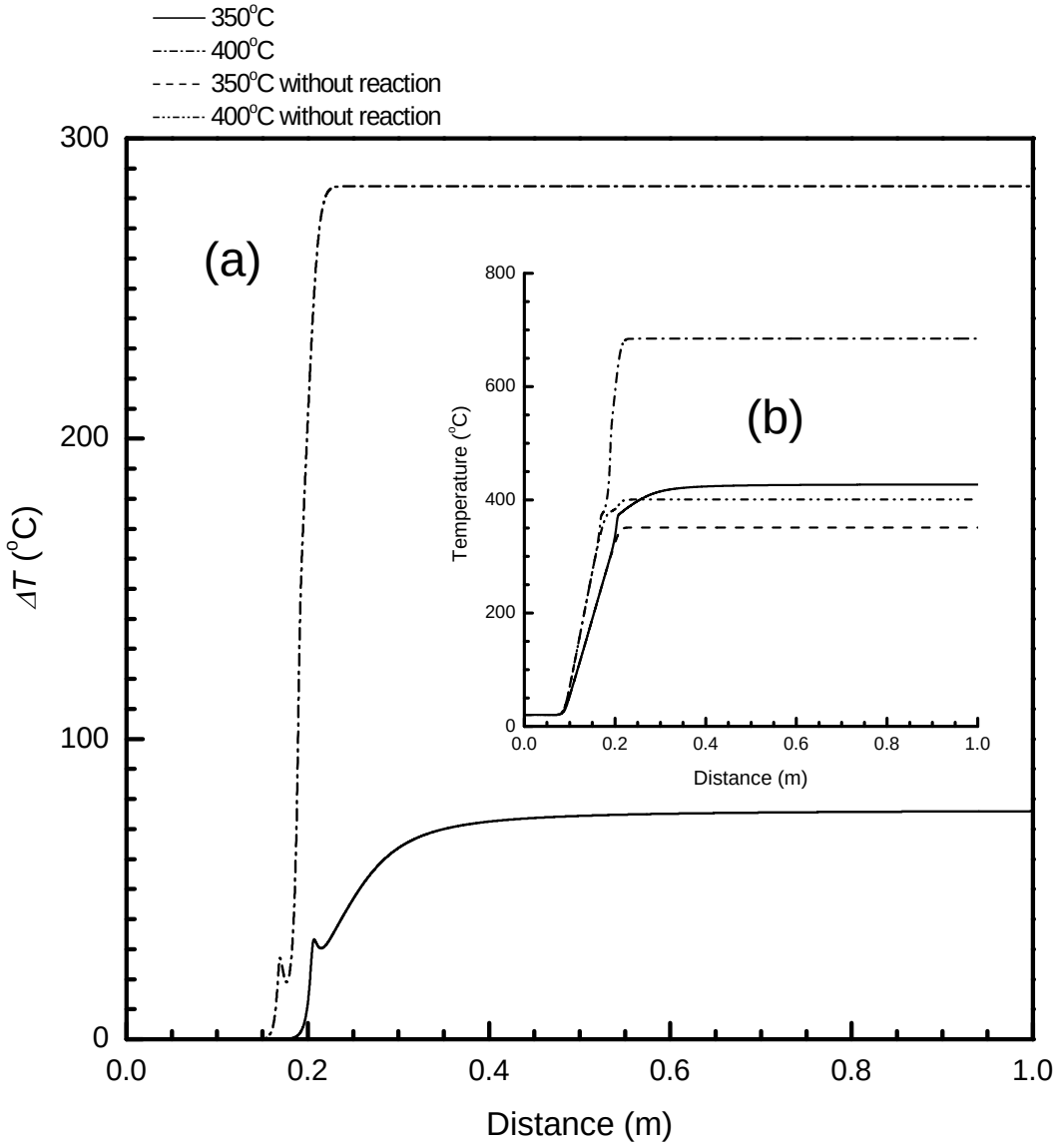

Figure 4.5 (a) Changes of ΔT and (b) changes of temperature, along the reactor for different preheat temperatures at u_{in} = 1.0 m·s^{-1} under adiabatic condition.

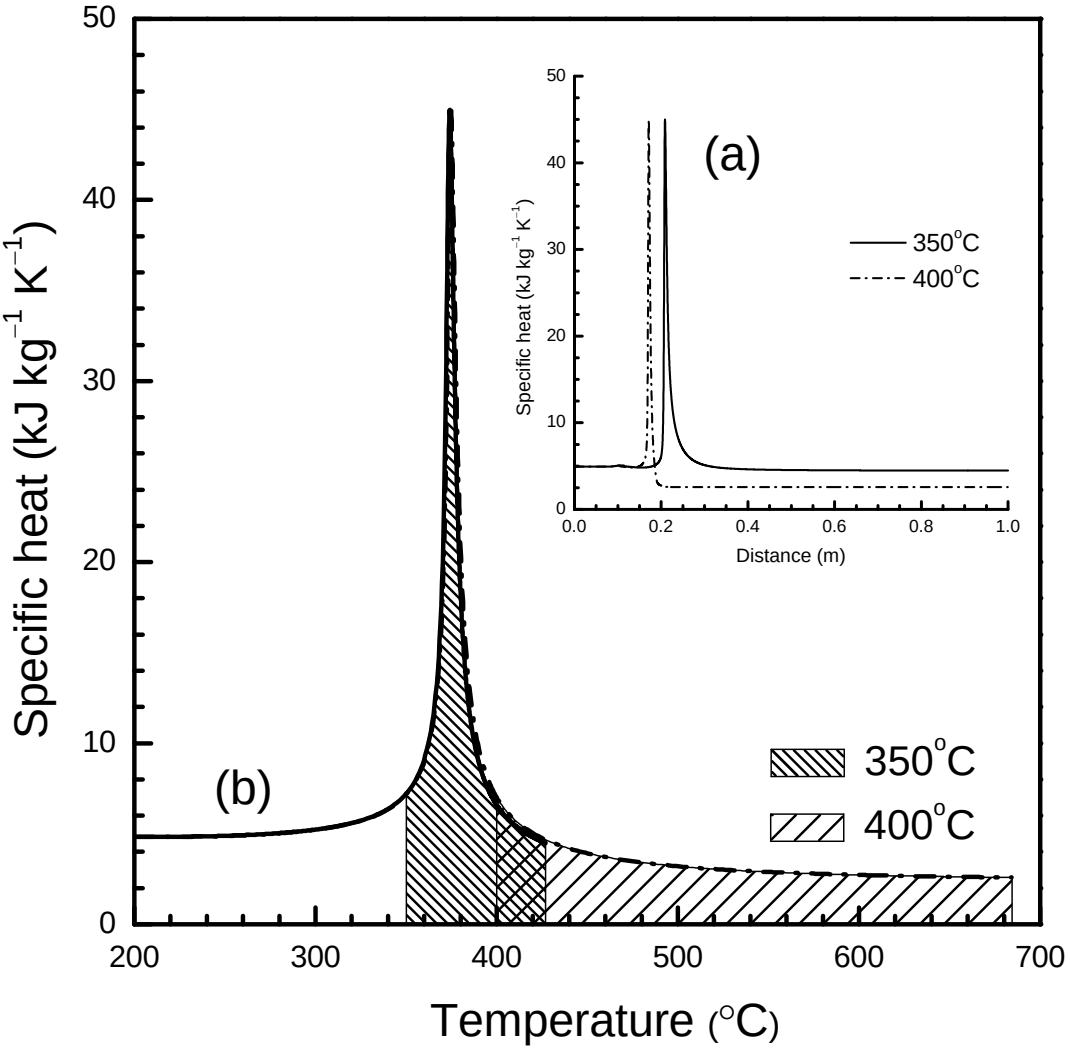

Figure 4.6 Changes of specific heat: (a) along the reactor for different preheat temperatures, and (b) against temperature for different preheat temperatures, at u_{in} = 1.0 m·s^{-1} under adiabatic condition.

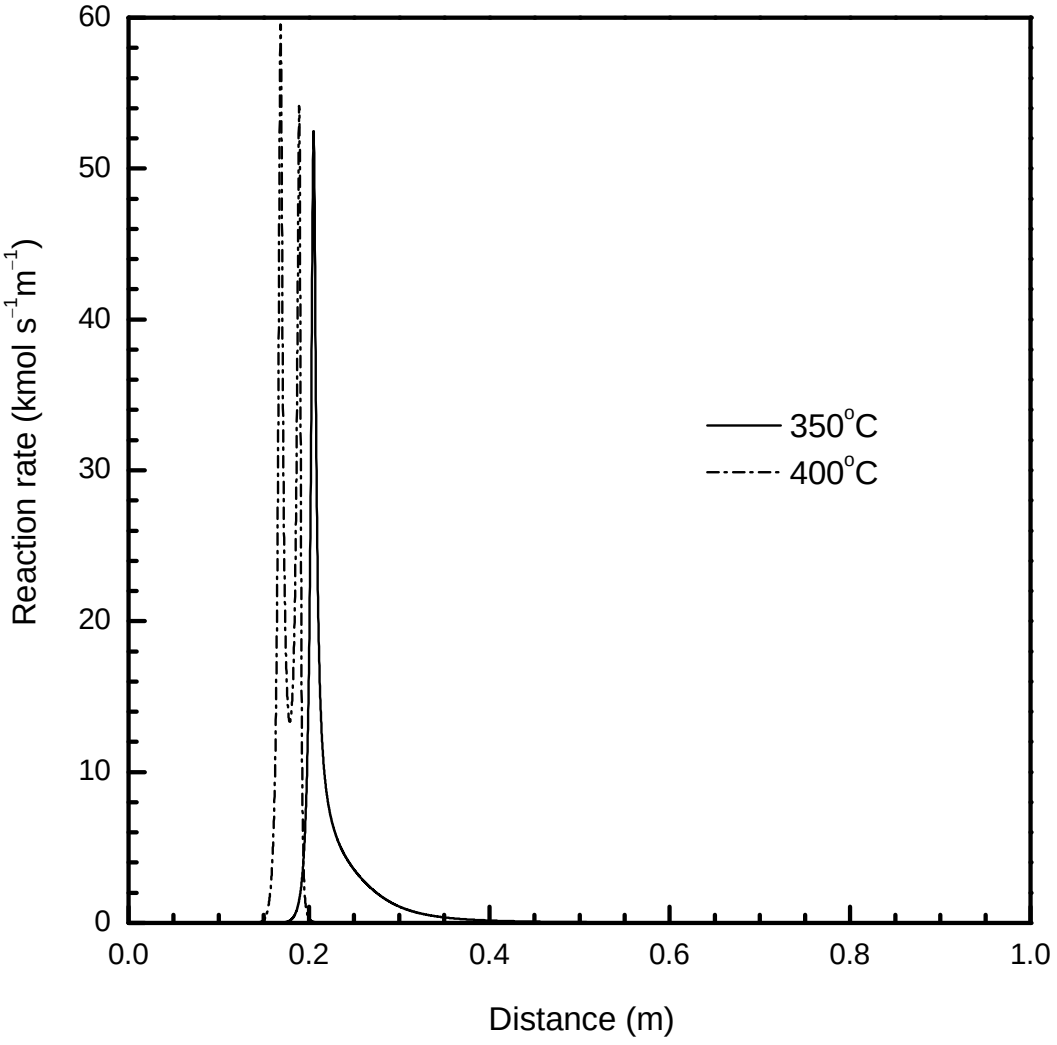

Figure 4.7 Changes of reaction rate along the reactor for different preheat temperatures at u_{in} = 1.0 m·s^{-1} under adiabatic condition.

The relation between the specific heat and temperature increase ΔT is explained in Figure 4.6. An abrupt increase of the isobaric specific heat appears for both preheat temperature of 350 °C and 400 °C, because the isobaric specific heat becomes large across the critical temperature of the reactant. Each of heating values is calculated by integration of specific heat as a function of temperature:

$$h = h_0 + \int_{T_0}^{T} C_p dT \,. \tag{4.9a}$$

Hence, the heating value corresponds to the area of hatching in Figure 4.6b which is changes of specific heat against temperature for different preheat temperatures.

On the other hand, Figure 4.6a shows changes of specific vs. distance for different preheat temperatures. The heating values for the both cases have almost same value because ethanol is, in fact, almost completely converted in each case as mentioned above in Figure 4.4, and the corresponding areas of hatching are approximately the same. Here, one of the reasons why ΔT differs from each other is that ΔT is affected by specific heat peak as shown in Figure 4.6b. Namely, for the case of 350 °C, most of the heating value is absorbed by the increasing specific heat because exothermic reaction occurs around the critical point. But for 400 °C, where the condition is supercritical, heating value is mostly used to increase temperature because exothermic reaction occurs after passing through the critical point. Increase of temperature ΔT is the difference of maximum and minimum coordinate value of abscissa axis corresponding to hatching area. Thus the temperature increase ΔT differs from each other.

Figure 4.7 shows reaction rate change for both preheat temperature of 350 °C and 400 °C. In the case of 400 °C, slope of the ΔT curve in Figure 4.5 fall into negative around x = 0.18 m where specific heat has a peak in Figure 4.6a. Thus the reaction rate rises rapidly and then decreases suddenly as shown in Figure 4.7. Because the reaction zone is located in the heated region, the calorie of the heater makes ethanol oxidation to be reactivated. Thus the reaction rate has the second peak, and consequently reaction rate has double peaks in the case of 400 °C.

4.7.2 Effect of flow velocity

Figure 4.8 shows changes of conversion for different flow velocities of 1 $m \cdot s^{-1}$, 2 $m \cdot s^{-1}$

and 3 $m \cdot s^{-1}$ when the preheat temperature is fixed at 350 °C. Change of velocities corresponds to change of flow rates. It is obvious that larger flow velocity causes slower increase of conversion. Figure 4.9a shows changes of ΔT with different flow velocities and Figure 4.9b is the changes of temperature along the reactor for different flow velocities. It is indicated that ΔT increases slower for larger flow velocity and that ΔT for all the cases are the same around the outlet of the reactor. Changes of reaction rate for different flow velocities in Figure 4.10 shows that larger flow velocity causes thicker reaction zone than that for smaller one. The possible reason why reaction zone becomes thicker for larger flow velocity is the fluid advection. In particular, ratio of distance between $x = 0.2$ m (point a in Figure 4.8) where ethanol oxidation begins and points at conversion of 80 % (b, c and d in Figure 4.8) is approximately 1:2:3, which is proportional to the ratio of inlet flow velocity. This agreement quite simply represents that flow advection have a great influence on the thickness of reaction zone.

Analysis of the reaction rate equation is conducted to clarify why the magnitude of reaction rate depends on the flow velocity as shown in Figure 4.10. For the reaction rate equation:

$$-r_{\mathrm{EtOH}} = 10^{17.23} \times \exp\left(\frac{-214\ (\mathrm{kJ\ mol^{-1}})}{RT}\right)[\mathrm{EtOH}]^{1.34}[\mathrm{O_2}]^{0.55}, \tag{4.17a}$$

the natural logarithm of positive both sides gives

$$\ln\ -r_{\mathrm{EtOH}} = \ln(10^{17.23}) + \frac{-214\ (\mathrm{kJ\ mol^{-1}})}{RT} + \ln([\mathrm{EtOH}]^{1.34}[\mathrm{O_2}]^{0.55}). \tag{4.22}$$

In this equation, the left-hand side is predominantly determined by a function of the second and third terms of the right-hand side, since the first term in the right-hand side is constant. The second term is an inverse function of temperature and the third term is a function of concentration of ethanol and oxygen. Figure 4.11 shows that distribution of $214\ (\mathrm{kJ \cdot mol^{-1}})/RT$ has almost no difference behind the preheated region. On the other hand, $\ln([\mathrm{EtOH}]^{1.34}[\mathrm{O_2}]^{0.55})$ for larger flow velocity becomes larger behind the heater, because the increased flow velocity transports more reactants downstream without oxidation. Therefore the difference of $\ln([\mathrm{EtOH}]^{1.34}[\mathrm{O_2}]^{0.55})$ affects absolute value of the reaction rate. In other words, different concentration profiles of ethanol and oxygen, which are caused by the difference of inlet flow velocities, result in difference of reaction rates.

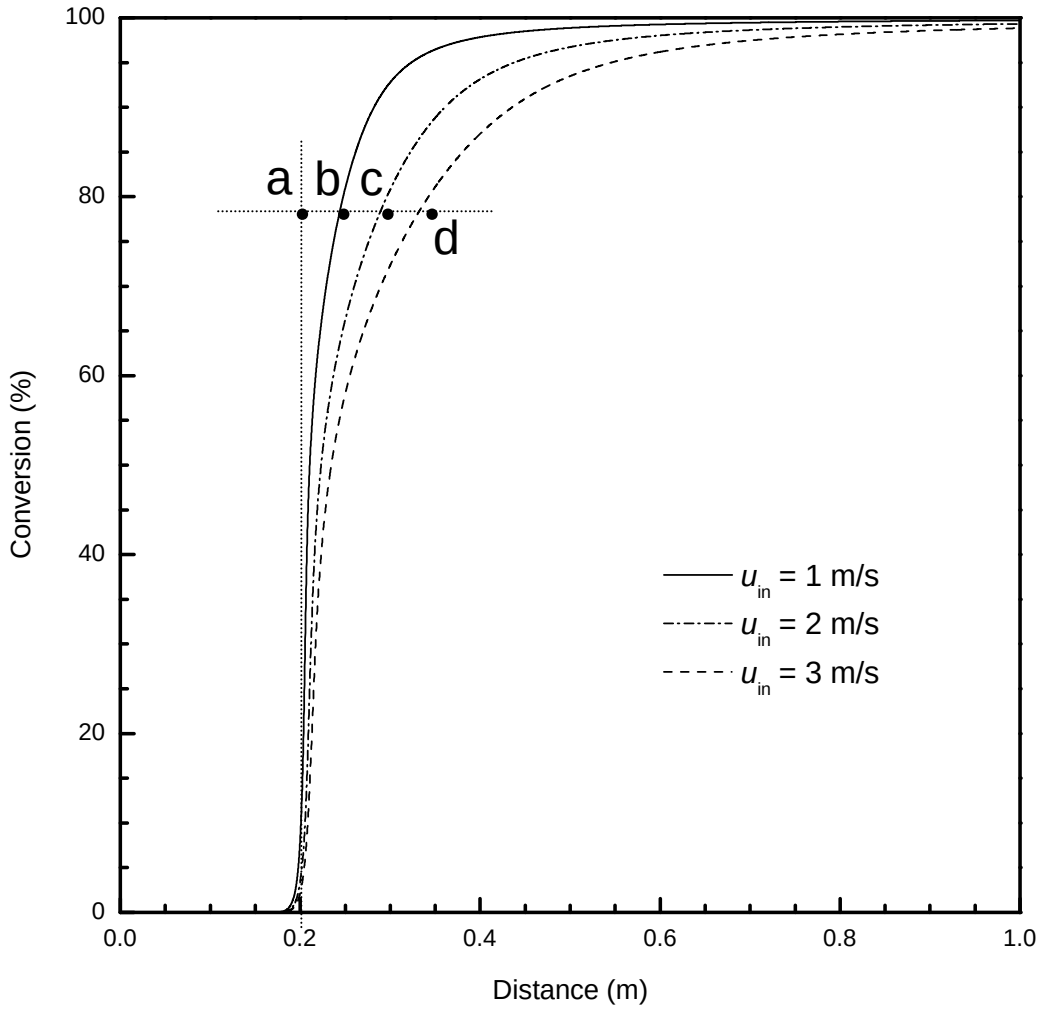

Figure 4.8 Changes of conversion along the reactor for different flow velocities at $T_{preheat}$ = 350 °C under adiabatic condition.

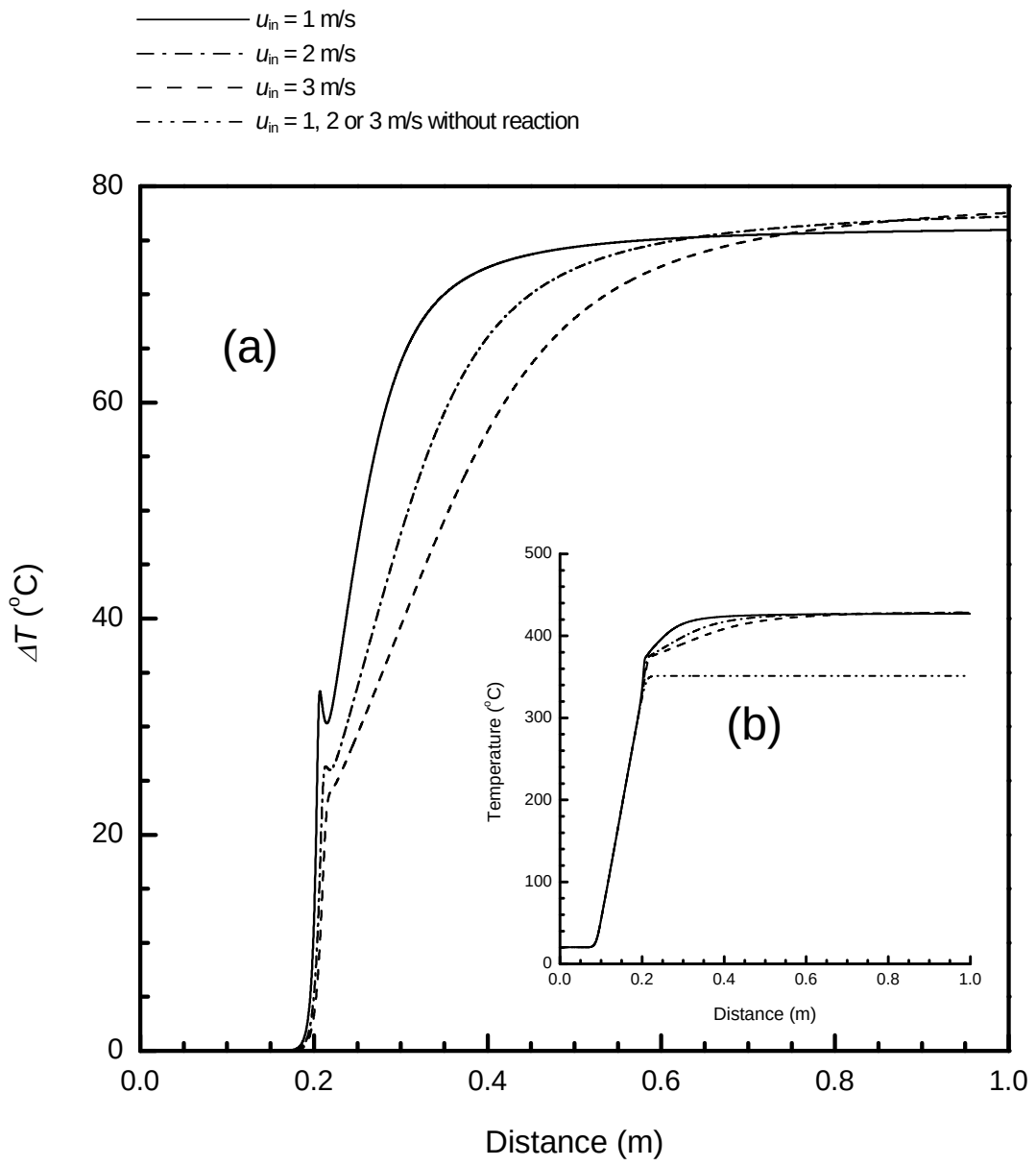

Figure 4.9 (a) Changes of ΔT and (b) changes of temperature, along the reactor for different flow velocities at $T_{preheat}$ = 350 °C under adiabatic condition.

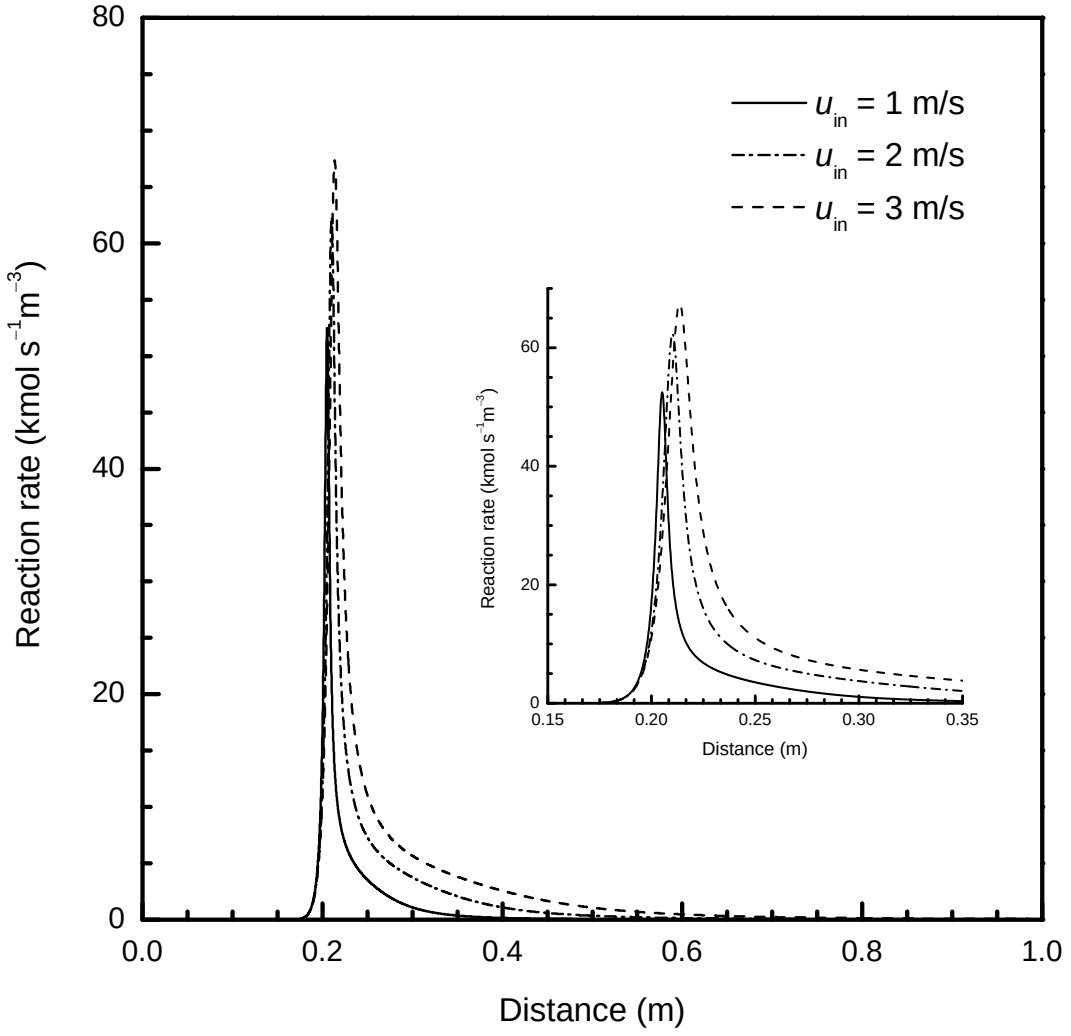

Figure 4.10 Changes of reaction rate along the reactor for different flow velocities at $T_{preheat}$ = 350 °C under adiabatic condition.

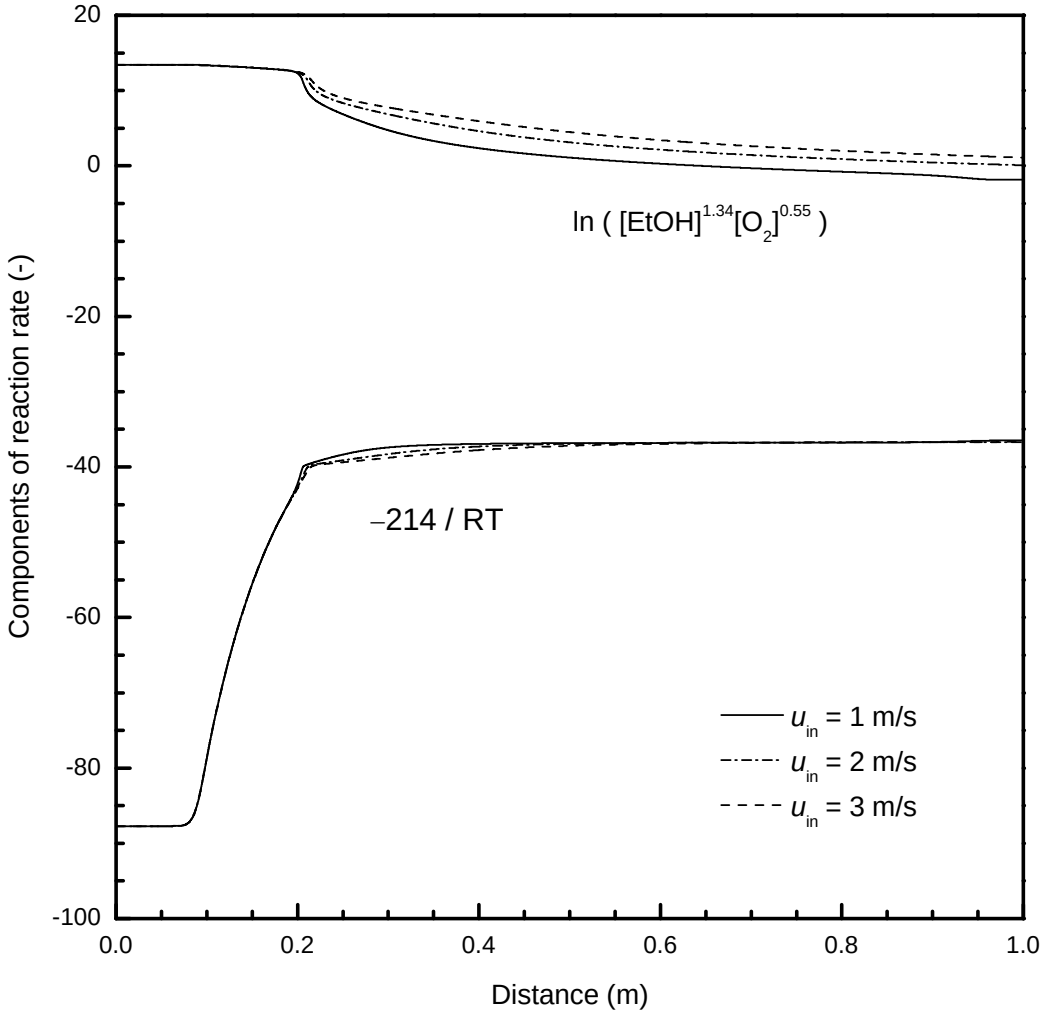

Figure 4.11 Comparison of logarithmic components in the reaction rate equation along the reactor at T_{preheat} = 350 °C under adiabatic condition.

4.7.3 Effect of heat loss

Heat loss effect is considered here by giving a heat flux $q = \alpha\,(T - T_w)$ (Newton's low) as an energy source term. The symbols α, T and T_w indicate the heat transfer coefficient, the temperature of fluid and the wall temperature, respectively. The term $Q(x)$ in equation (4.2), which is the heat source or heat loss, is rewritten as

$$Q(x) = \frac{q \cdot (\pi d_0) \cdot \mathrm{d}x}{\left(\frac{\pi d_0^2}{4}\right) \cdot \mathrm{d}x} = \frac{q}{d_0 / 4} = \frac{\alpha}{d_0 / 4}(T - T_w) \tag{4.23}$$

where the cross-sectional diameter d_0 is set to be 1 cm.

Changes of ΔT for different heat transfer coefficients are shown in Figure 4.12a when the preheat temperature and inlet flow velocity are respectively fixed at 350 °C and 1 $m \cdot s^{-1}$. Figure 4.12b shows changes of temperature for different heat transfer coefficients. The T_w is set to be 20 °C. It is proved that ΔT once decreases down to about 20 °C and then drops down again to –175 °C from the preheat temperature at the outlet of reactor for $\alpha = 2.5 \times 10^4$ $m^{-2} \cdot K^{-1}$. This large value of alpha is used to see the behaviour of fluids cooling down to the sub-critical condition. On the other hand, ΔT gradually falls down to 40 °C at the outlet of reactor for $\alpha = 2.5 \times 10^3$ $W \cdot m^{-2} \cdot K^{-1}$.

The two-step temperature decrease for $\alpha = 2.5 \times 10^4$ $W \cdot m^{-2} \cdot K^{-1}$ may be attributed to the ·behaviour of the isobaric specific heat around the critical point. In Figure 4.13, the isobaric specific heat for all the cases of α have a peak around $x = 0.2$ m, which means the temperature exceeds the critical value. Then, the specific heat for $\alpha = 2.5 \times 10^4$ $W \cdot m^{-2} \cdot K^{-1}$ has a second peak, while that for $\alpha = 2.5 \times 10^3$ $W \cdot m^{-2} \cdot K^{-1}$ shows a small augmentation toward the outlet of the reactor. Thus in the case of $\alpha = 2.5 \times 10^4$ $W \cdot m^{-2} \cdot K^{-1}$, the temperature decreases by heat loss, but when the temperature reaches the critical temperature, the isobaric specific heat increases again and change of ΔT becomes smaller. The increase of temperature ΔT subsequently decreases drastically because the specific heat becomes smaller. On the other hand, in the case of $\alpha = 2.5 \times 10^3$ $W \cdot m^{-2} \cdot K^{-1}$, the temperature does not reaches down the critical temperature, and thus the temperature decreases gradually by the heat loss.

Figure 4.14 shows the change of conversion for different heat transfer coefficients. It is proved that heat loss inhibits complete conversion of ethanol, because the temperature is

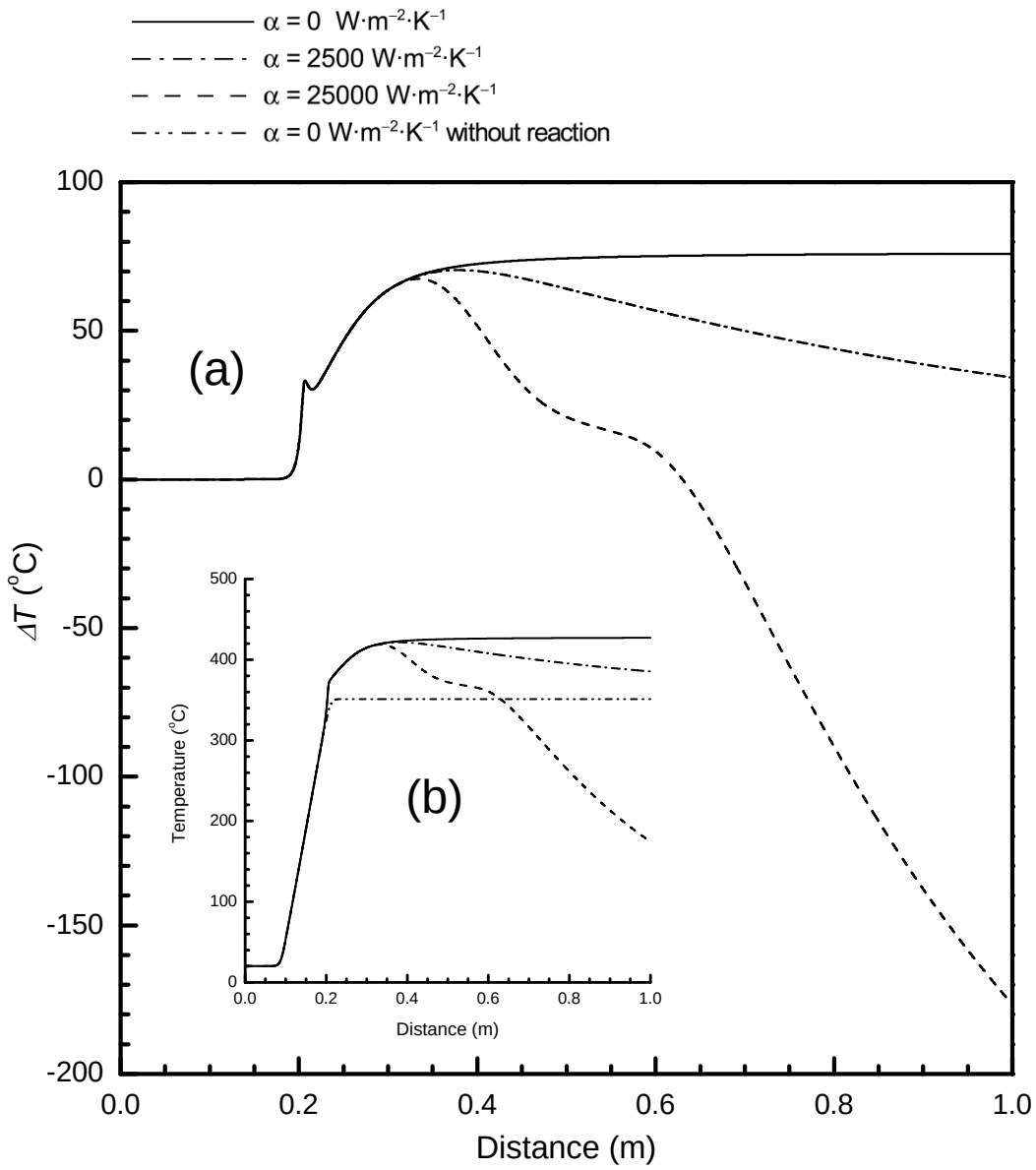

Figure 4.12 (a) Changes of ΔT and (b) changes of temperature, along the reactor for different heat transfer coefficients at T_{preheat} = 350 °C and u_{in} = 1.0 m·s^{-1} with heat loss.

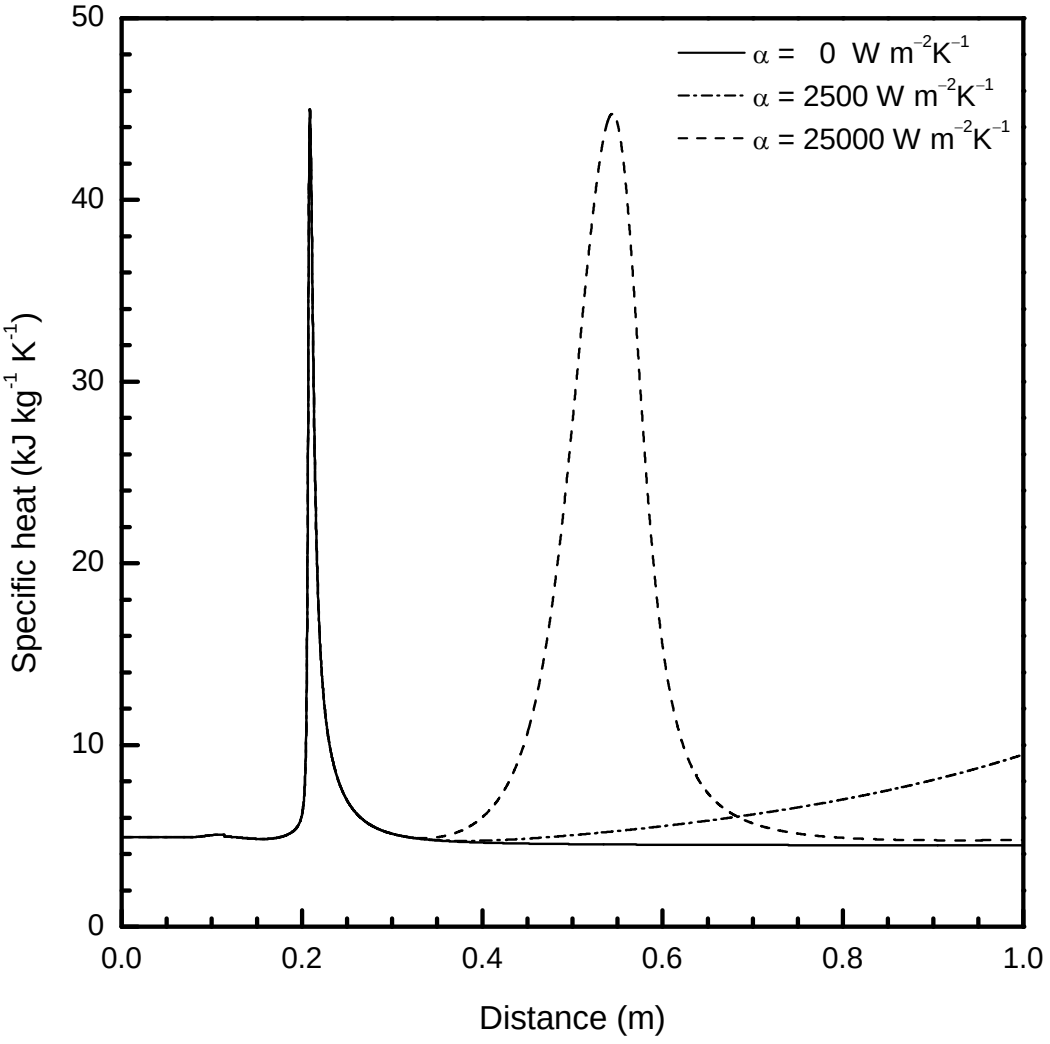

Figure 4.13 Changes of isobaric specific heat along the reactor for different heat transfer coefficients at T_{preheat} = 350 °C and u_{in} = 1.0 m·s^{-1} with heat loss. Lines are overlapped between x = 0 and 0.3 m.

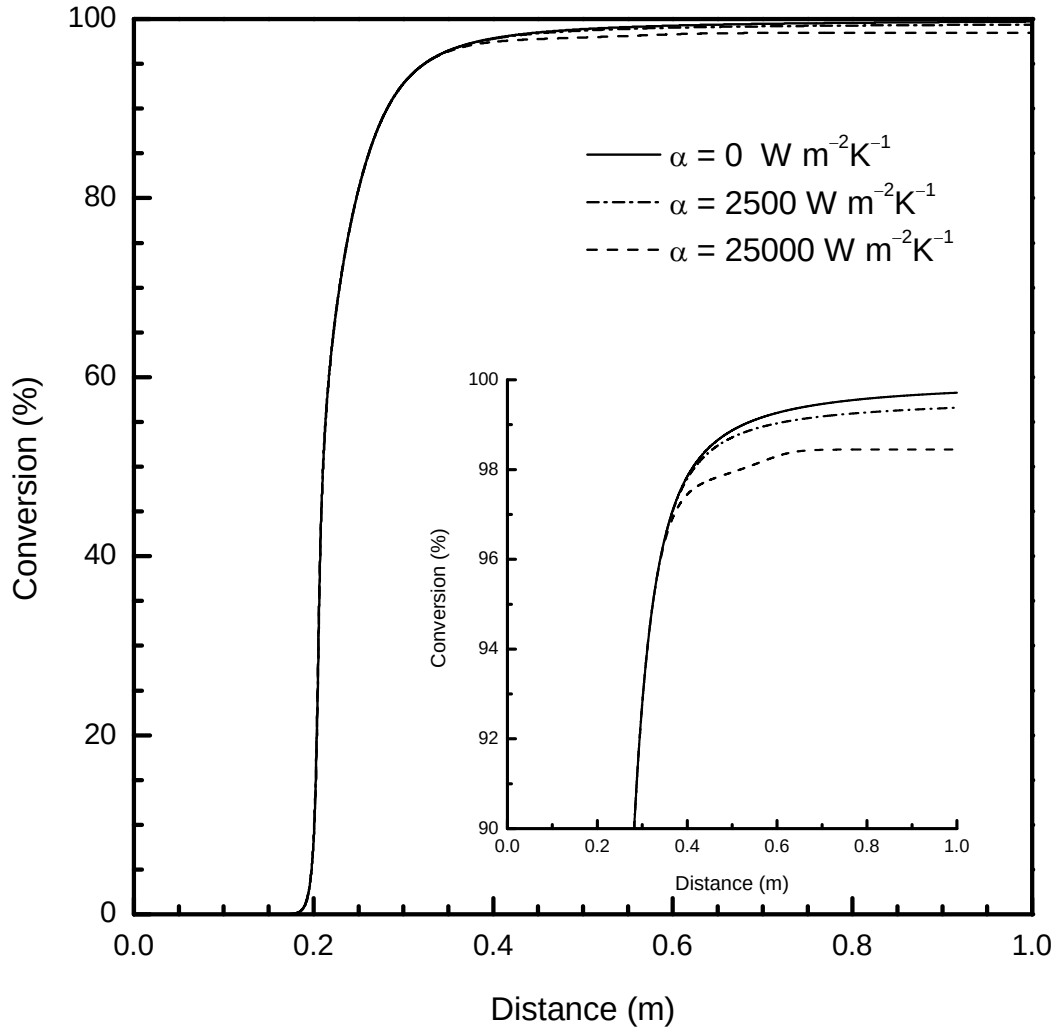

Figure 4.14 Changes of conversion along the reactor for different heat transfer coefficients at $T_{preheat}$ = 350 °C and u_{in} = 1.0 m·s^{-1} with heat loss.

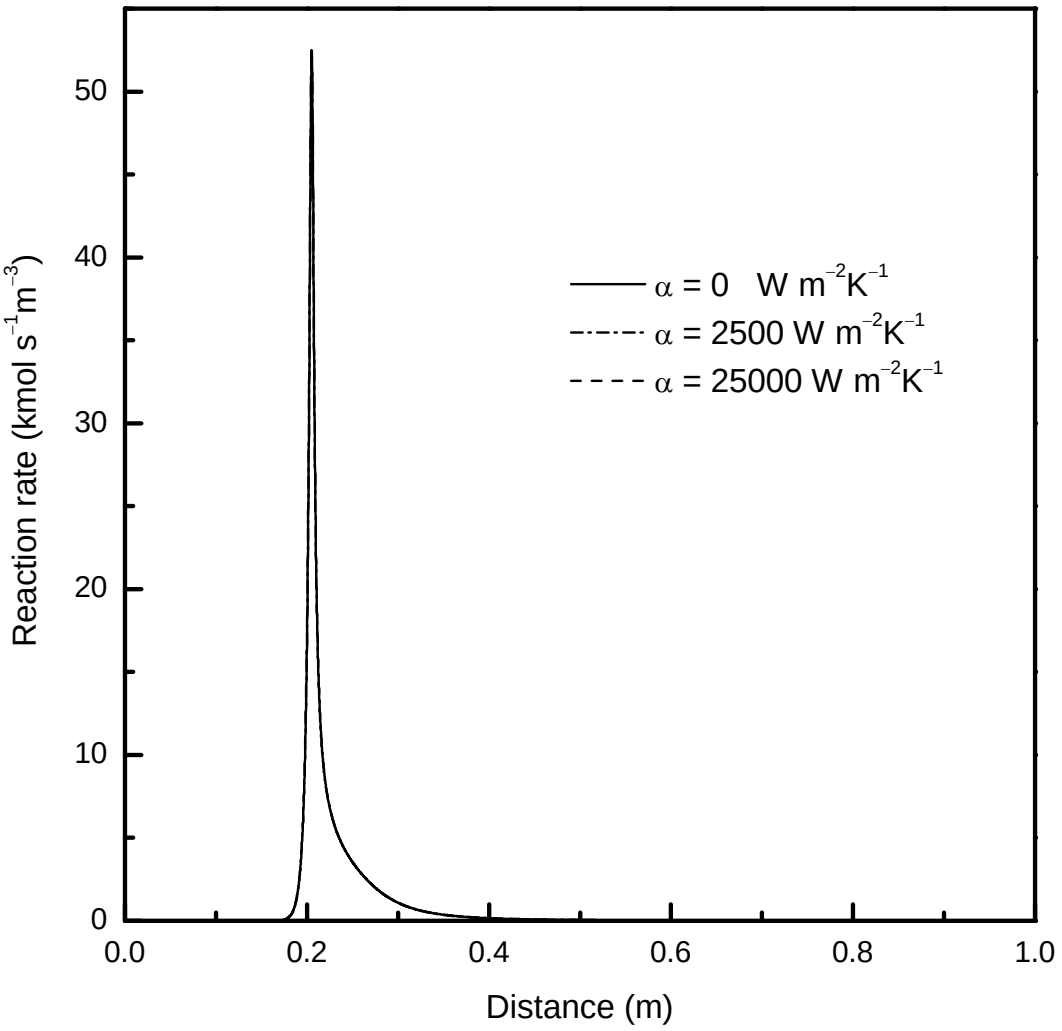

Figure 4.15 Changes of reaction rate along the reactor for different heat transfer coefficients at $T_{preheat}$ = 350 °C and u_{in} = 1.0 m·s^{-1} with heat loss. Lines are overlapped.

decreased by the increase of specific heat. The changes of ΔT and conversion for different heat transfer coefficients differ from one another from x = 0.3 m to 1.0 m in Figures 4.12a and 14. This region is after the reaction zone where the reactants are almost completely converted. The heat loss, however, has almost no effects on the reaction rates in Figure 4.15. This is because the reaction rate on a reaction zone is extremely large in comparison with the reaction rate having the effects of heat loss.

4.8 Conclusions

In this work, premixed combustion of ethanol by hydrothermal oxidation was numerically studied by using the rate expression by Schanzenbächer et al. Behaviours of oxidation reaction and heat release under sub-/super critical conditions of water were studied to elucidate effects of preheat temperature, heat release and reaction kinetics as well as equations of state and oxidation rate equations. Obtained results are as follows.

- Effect of preheat temperature: Ethanol is almost completely converted in both cases of preheat temperature 350 and 400 °C. Increase of temperature, ΔT becomes up to 280 °C in the preheated region for the case of 400 °C, while ΔT for 350 °C becomes only 80 °C behind the preheated region. This means that ΔT for the case of 400 °C is about three times as much as that of 350 °C, whereas heating values are the same. The reason is as follows: for the case of 350 °C, most of the heating value is absorbed by the increasing specific heat because exothermic reaction occurs around the critical point. But for 400 °C, where the condition is supercritical, heating value is mostly used to increase temperature because exothermic reaction occurs after passing through the critical point. Increase of temperature ΔT is the difference of maximum and minimum coordinate value of abscissa axis corresponding to hatching area. Thus the temperature increase ΔT differs from each other.

- Effect of flow velocity: It is easy to understand that the fluid advection limits the reaction phenomenon. The results show that larger flow velocity causes slower

increase of conversion. For larger flow velocity ΔT increases slower but ΔT for all the cases are the same around the outlet of the reactor. Changes of reaction rate for different flow velocities shows that larger flow velocity causes thicker reaction zone and higher reaction peak than that for smaller one. From analysis of the reaction rate equation, the difference of $\ln([EtOH]^{1.34}[O_2]^{0.55})$, which is a function of concentration of ethanol and oxygen, affects absolute value of the reaction rate.

- Effect of heat loss: Heat loss effect is considered by giving a heat flux $q = \alpha\ (T_f - T_\infty)$ as an energy source term. It is proved that ΔT once decreases down to about 20 °C and then drops down again to –175 °C at the outlet of reactor for $\alpha = 10^7$ W·m^{-2}·K^{-1}. On the other hand, ΔT gradually falls down to 40 °C at the outlet of reactor for $\alpha = 10^6$ W·m^{-2}·K^{-1}. The two-step temperature decrease for $\alpha = 10^7$ W·m^{-2}·K^{-1} may be attributed to the behaviour of the isobaric specific heat around the critical point.

Chapter 5: Kinetics of ethanol oxidation in subcritical water

5.1 Introduction

First-order kinetics for subcritical WO of ethanol was measured by Hirosaka et al. (2007). They reported the estimation of capacity for ethanol oxidation in subcritical water as a heat source. At the same time, Hirosaka (2008) and Koido (2009) have worked on the numerical simulation of the behaviour of reactive flow in the reactor. These studies have been implemented with a single step reaction rate of reactants considering decomposition of ethanol into acetic acid. The desire for the more realistic numerical simulation requires a multiple step reaction rate and decomposition of ethanol into carbon dioxide (CO_2) and water. The multiple step reaction pathways are constructed and the oxidation rates are decided.

5.2 Experimental apparatus and procedures

Oxidation reactions were accomplished in a flow reactor, which was operated at subcritical conditions. Figure 5.1 shows a schematic diagram of the continuous flow reactor system. All parts of the reactor, between the pumps and the back pressure regulator, were made of SUS316. The reactor was constructed from several different lengths (80, 130, 200, 270, 450 and 640 mm) of 19.1 mm o.d. (11 mm i.d.) tubes. The oxidant was prepared by dissolving hydrogen peroxide (H_2O_2) into distilled water in one feed tank. Another feed

tank was loaded with an aqueous solution of ethanol. The two feed streams were separately pressurised by two high-pressure metering pumps and then preheated in an electrical muffle furnace. In order to assure that H2O2 is completely decomposed into O2 and H2O, the oxidant was pre-heated through 2.7 m of coiled 1/8 inch o.d. (1.8 mm i.d.) tube fixed in the muffle furnace. According to the study of Croiset et al. (1997), H_2O_2 could be completely decomposed in the pre-heating tube for various experimental conditions of this study. Ethanol feed stream was preheated through 2 m coiled 1/16 inch o.d. (0.59 mm i.d.) tube submerged in the muffle furnace. After preheating, the two lines of oxygen and ethanol were mixed at the reactor en-trance.

In our experimental condition at 25 MPa, solubility of oxygen calculated by the equation of Tromans (1998) was ranging from 520 $mmol \cdot l^{-1}$ at 260 °C to 1180 $mmol \cdot l^{-1}$ at 350 °C, while oxygen concentration at the outlet of preheat section was 125 $mmol \cdot l^{-1}$. Therefore oxygen was completely dissolved in liquid water. On the other hand, oxygen-dissolved water was injected into the main flow of ethanol at a tee union (Figure 5.1) with the Reynolds number of 2471–3641, thus two fluids were mixed rapidly by turbulence. Above facts supported that the flow condition was adequate for plug flow reactor analysis.

The temperature in the furnace was supposed to be uniform, because the furnace had a stir-ring fan, and was referred to be the reaction temperature. After flowing out from the reactor, the effluent was cooled rapidly in a counter-flow heat exchanger and afterwards, the system pressure was reduced by using a backpressure regulator. The product was then separated into liquid and vapour phases. Gas samples were collected in a water pool containing solution of hydrochloric acid 0.1 $mol \cdot l^{-1}$ to prevent CO_2 dissolution, as shown in Figure 5.1. The liquid and gas samples were analysed by gas chromatographs.

5.3 Analytical techniques

Liquid phase products were identified using gas chromatography-mass spectrometer (GC-MS), Shimadzu QP-5050, equipped with Rtx-1701 column (Shimadzu, 60 m × 0.25mm i.d. × 1.0 μm film thickness) with helium as the carrier gas. Subsequently, the

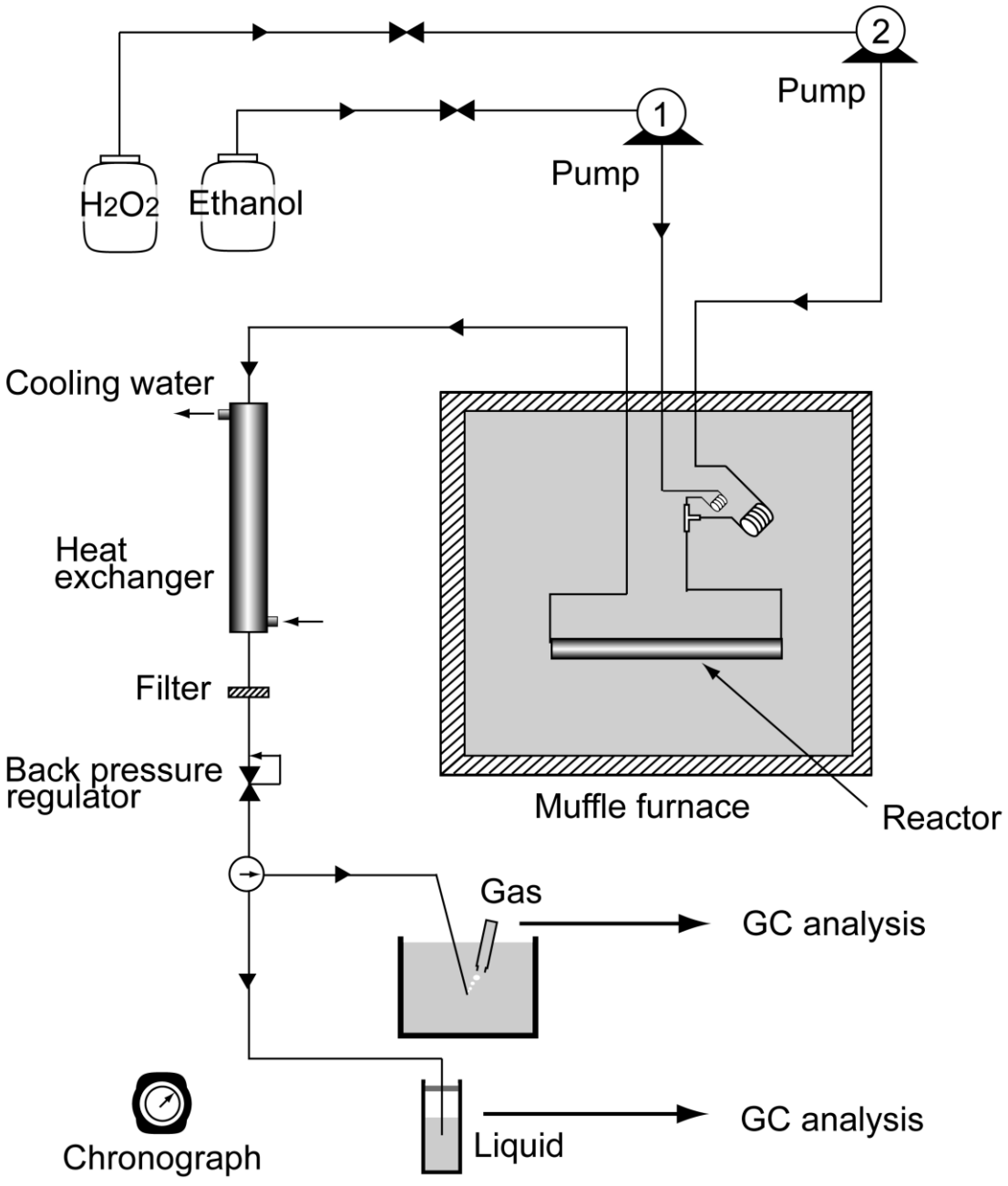

Figure 5.1 Schematic diagram of experimental apparatus for the measurement of reaction rate on subcritical wet oxidation.

samples were quantitatively analysed by a Hewlett-Packard 5890 gas chromatograph (GC), which was equipped with a flame ionisation detector (FID) and supplied nitrogen as a carrier gas. Separation of the compositions was accomplished using a 30 m × 0.25 mm i.d. × 0.25 μm film thickness Pure-WAX column by GL Sciences Inc. The concentrations of unreacted ethanol, acetaldehyde and acetic acid were determined by the GC-FID.

The gas composition was determined by manually injecting three 400 μl vapour sample into GC, Shimadzu GC-14B. The GC was used in a thermal conductivity detector (TCD) mode of operation, and helium was employed as the carrier gas. The gaseous sample was analysed using two columns: the column packed with Porapak Q for detection of carbon dioxide and with MS-5A for carbon monoxide.

Residence times were calculated by considering the flow rates of the ethanol and oxidiser into the system. On the basis of the mass balance of the materials at the input and output of the plug-flow reactor, an equation for the residence time can be obtained in the simple form:

$$\tau = V_{\mathrm{R}}(\rho_{\mathrm{out}} / \rho_{\mathrm{in}}) / \dot{v}_{\mathrm{in}} \tag{5.1}$$

In this equation, the residence time, τ, is calculated from both the volume of the reactor, V_{R}, and the initial flow rate of the liquid reactants at ambient conditions, $\dot{v}_{\mathrm{in}}$, while the density of water at reaction conditions is calculated using the Reference Fluid Thermodynamic and Transport Properties Database (REFPROP ver.8) by National Institute of Standards and Technology (NIST) (Lemmon et al., 2007).

5.4 Results and discussion

Pressure for the experiments was kept at about 25 MPa for all cases, while temperature was varied as 260, 290, 320 and 350 °C. Concentration of ethanol was 25 mmol·l^{-1} and that of O_2 was 125 mmol·l^{-1}, i.e., equivalence ratio was $\phi = 0.6$. Residence time was controlled by changing the length of reactor. Carbon fraction in Figures 5.6–5.8 is defined as:

$$\text{Carbon fraction} = \frac{\text{moles of carbon in product}}{\text{moles of carbon in feed}} \tag{5.2}$$

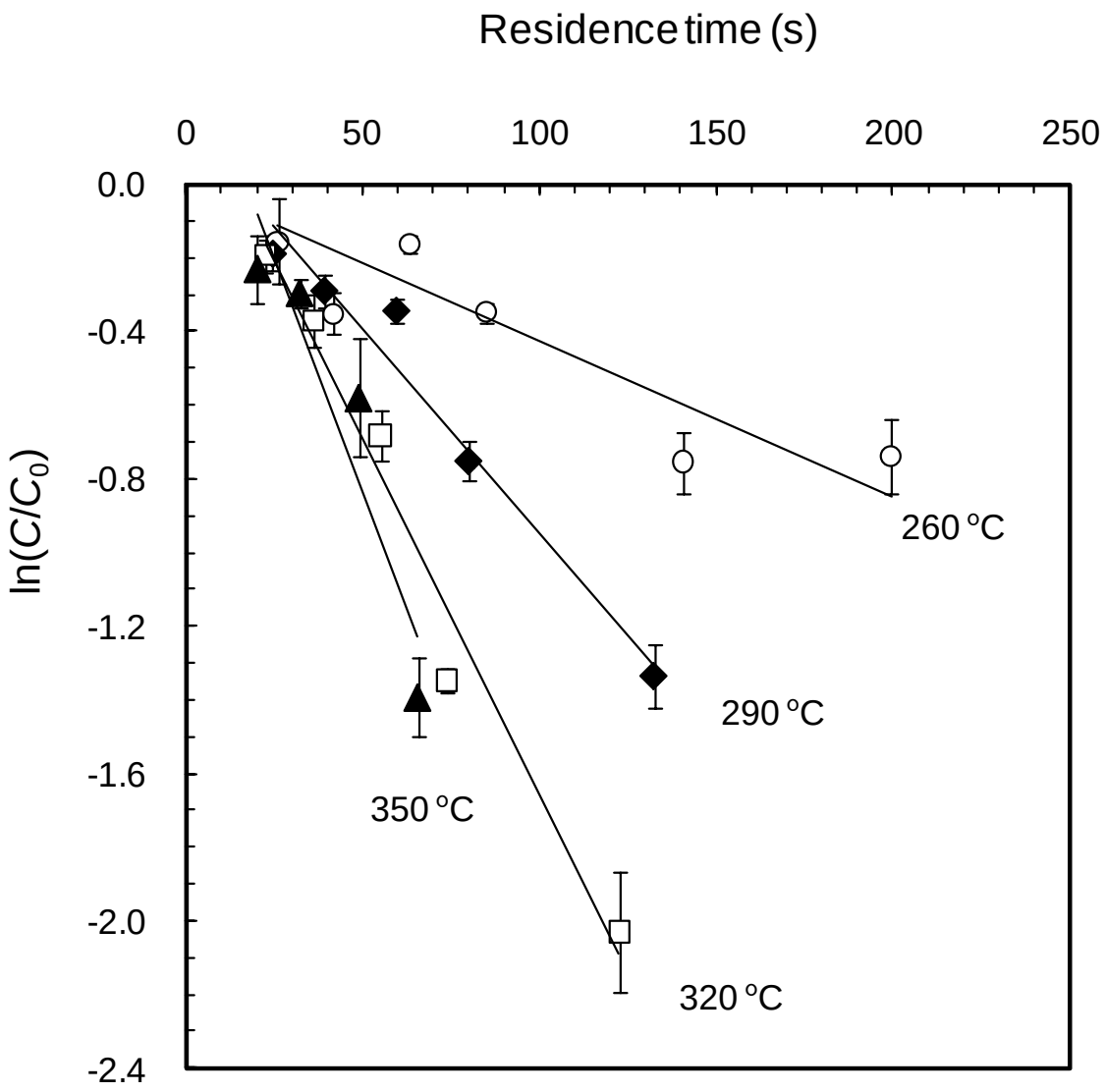

Figure 5.2 First-order reaction rate for ethanol conversion. The lines represent approximation of the experimental data, $\ln(C/C_0) = -k (\tau - \tau_{ind})$ at 260 °C (○), 290 °C (◆), 320 °C (□) and 350 °C (▲).

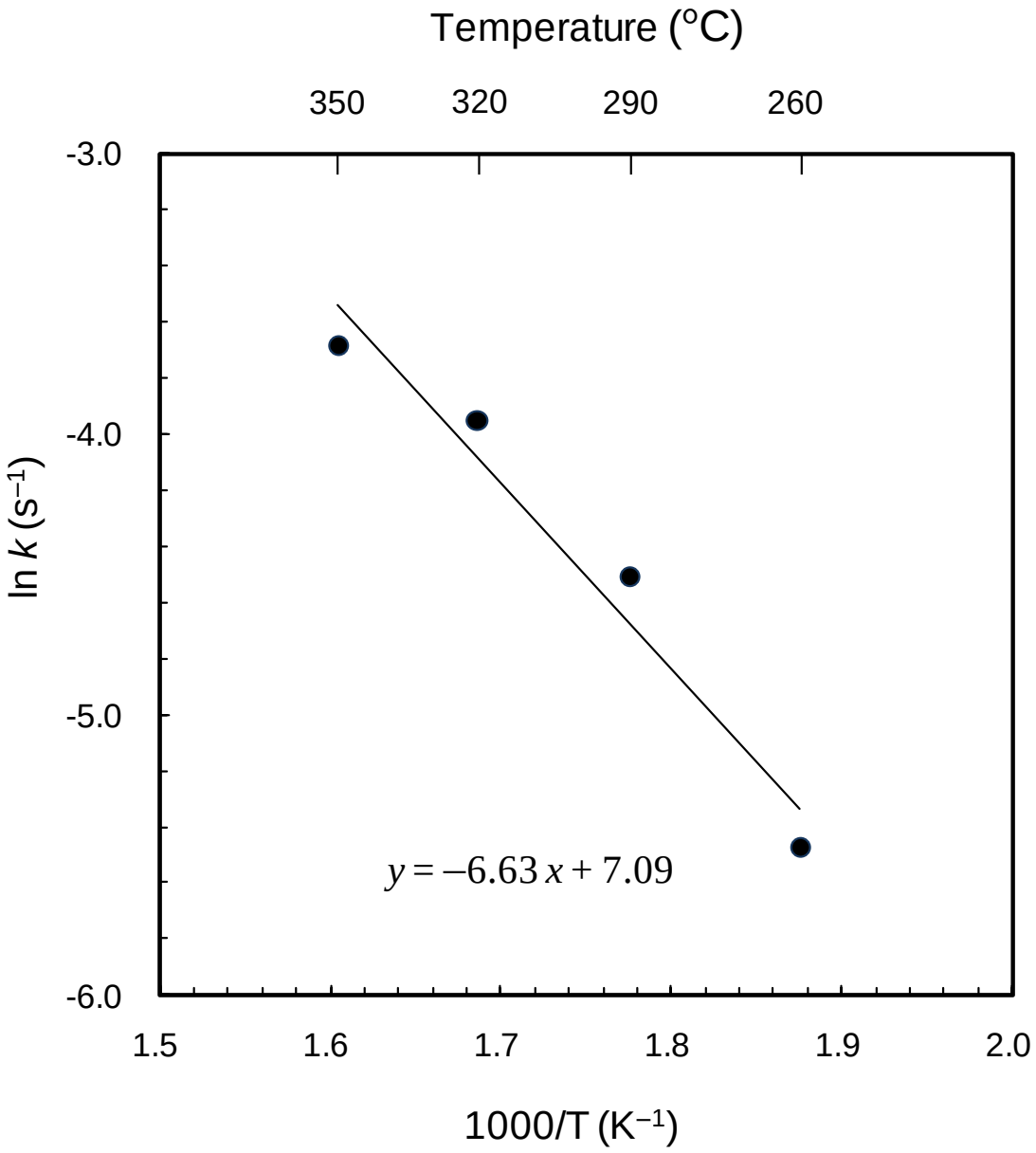

Figure 5.3 Arrhenius plot for the overall conversion rate of ethanol assuming first-order reaction, $dC/dt = -kC$.

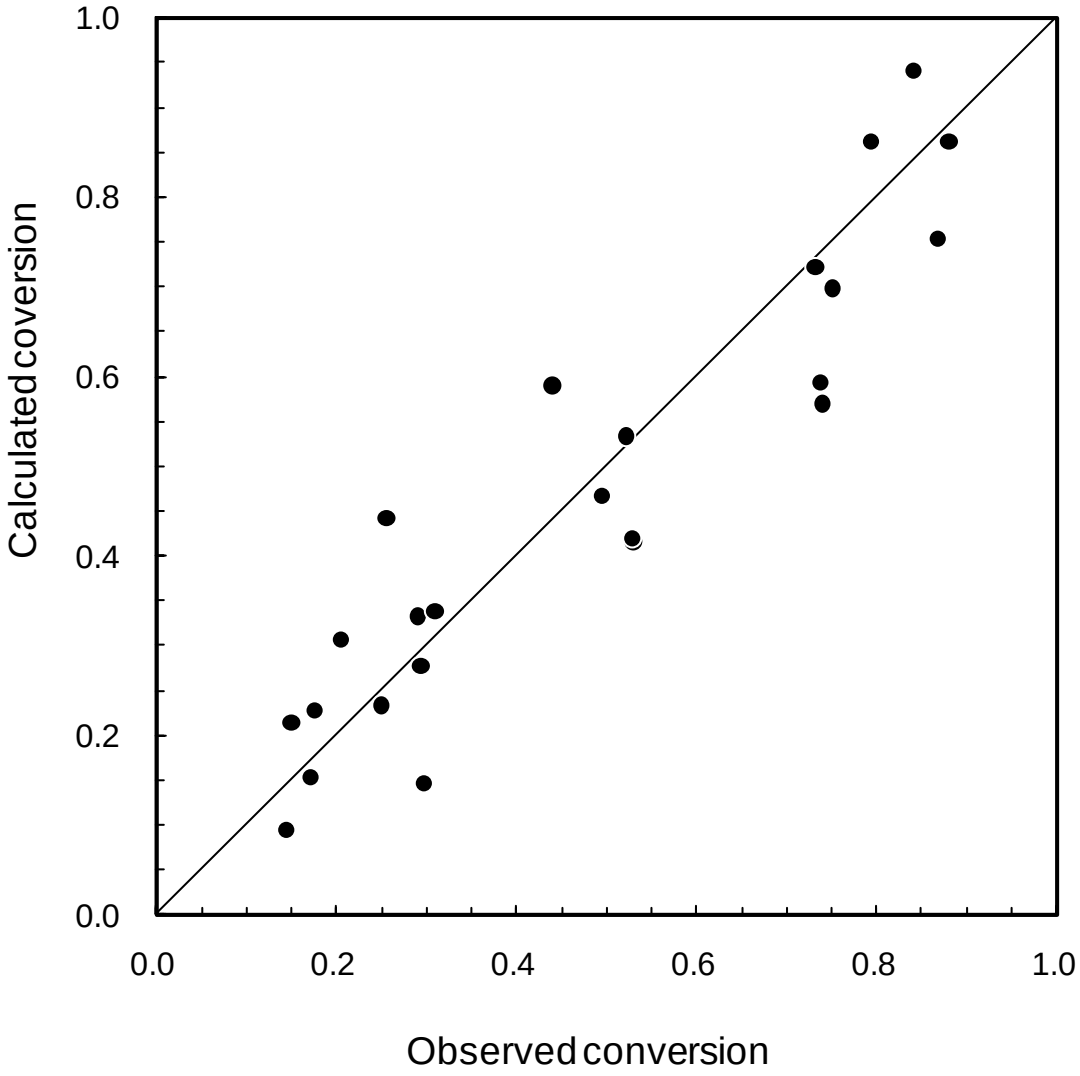

Figure 5.4 Parity plot for the subcritical wet oxidation kinetics of ethanol conversion.

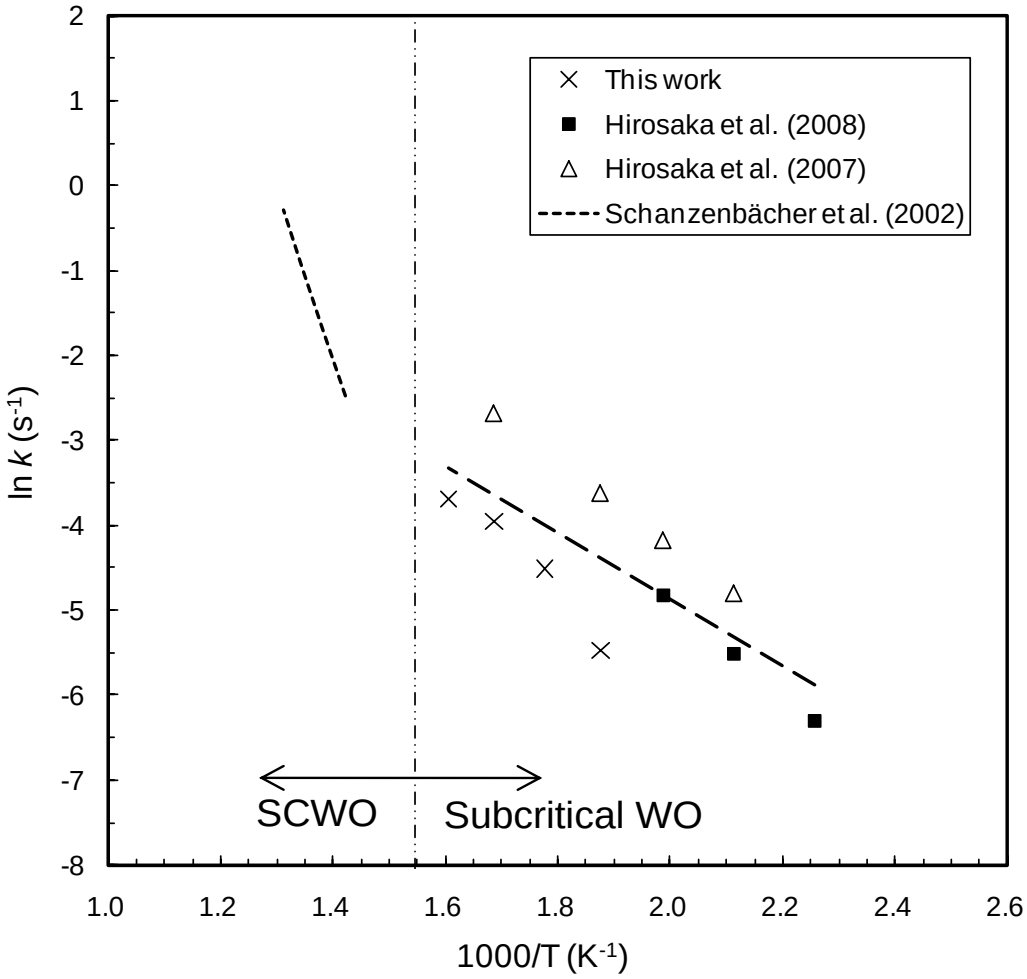

Figure 5.5 Arrhenius plots of conversion rates of ethanol assuming first-order reaction obtained by different experiments: this work (□), Hirosaka et al. (2008) (■), Hirosaka et al. (2007) (△), and Schanzenbächer et al. (2002) (dashed-dotted line). The dashed line is obtained from a combination of the present data with the previous data. The rate constant is $k = 10^{2.7\pm0.3}\times\exp(-47.2\pm5.7 / RT)$.

Table 5.1 Values of k_1–k_6 kinetic parameters.

	temperature (°C)				ln A (s^{-1})	E_a ($kJ \cdot mol^{-1}$)
	260	290	320	350		
k_1 (s^{-1})	0.005	0.011	0.022	0.019	4.97	44.9
k_2 (s^{-1})	0.033	0.068	0.134	0.153	7.78	49.5
k_3 (s^{-1})	0.064	0.045	0.048	0.078	–1.78	5.2
k_4 (s^{-1})	–	2.55	1.32	1.19		
τ_{ind} (s)	0.2	14.9	18.4	10.3		

5.4.1 Global kinetics of ethanol oxidation

The global conversion rate of ethanol by subcritical WO can be evaluated by assuming that the reaction rate is proportional to the ethanol concentration in the reactor at a given time and independent of water and oxygen concentration because of the fuel lean condition (fuel equivalence ratio = 0.6).

For first-order kinetics, a plot of $\ln(C/C_0)$ against the residence time should give a straight line at each temperature. Figure 5.2 shows that the obtained data can be approximated by straight lines. The lines do not pass through the origin, but rather intersect the *x*-axis at positive residence times. The *x*-intercept for each line provides estimation of the induction period, and the slope provides estimation of the rate constant. The kinetics parameters resulting from this analysis appear in Table 5.1. Figure 5.3 shows an Arrhenius plot of the overall first-order rate constant, k_1, for ethanol oxidation. The Arrhenius parameters for k_1 with 95 % confidence level are $A = 10^{2.9 \pm 0.4}$ s^{-1} as a frequency factor and E_a = 53.8 ± 4.6 kJ·mol^{-1} as an activation energy. Thus the oxidation rate for ethanol conversion is expressed by the following equation:

$$-\frac{\mathrm{d[EtOH]}}{\mathrm{d}t} = 10^{2.9\pm0.4}\exp\left(\frac{-53.8 \pm 4.6\ \mathrm{kJ\cdot mol^{-1}}}{RT}\right)[\mathrm{EtOH}] \qquad (5.3)$$

Figure 5.4 compares the conversions calculated from equation (5.3) with those observed in experiment. This parity plot demonstrates the acceptable fit of the data provided by the optimised parameters. The deviation of the model from the experimental data does not exhibit any systematic errors.

The activation energy obtained by our experimental data is relatively close to that reported by Hirosaka et al. (2008) at subcritical conditions: 45.6 ± 0.6 kJ·mol^{-1} (170–230 °C at 23.5 MPa), but much lower than the values reported by Schanzenbächer et al. (2002) at supercritical conditions: 163.9 ± 3.3 kJ·mol^{-1} (433–494 °C at 24.6 MPa). More comprehensive kinetic constants, k_1^*, (T = 170–350 °C, p = 23.5–25.0 MPa) is obtained as

$$k_1^* = 10^{2.7\pm0.3}\exp\left(\frac{-47.2 \pm 5.7\ \mathrm{kJ\cdot mol^{-1}}}{RT}\right) \qquad (5.4)$$

by combining the present data with the reference data (Hirosaka et al., 2007, 2008). The constant, k_1^*, is compared with that for SCWO rate constant by Schanzenbächer (2002) in Figure 5.5. Above the critical temperature T_c, the rate constant increases more sharply

with temperature than below the critical temperature. The reaction mechanism shifts across the critical temperature, that is, ionic reaction dominates in the subcritical region and non-ionic reaction (radical reaction) dominates in the supercritical region (Rice and Croiset, 2001; Taylor et al., 2001).

5.4.2 Oxidation products and reaction pathway

GC-TCD analysis revealed that CO_2 and CO were detected as gaseous products, while CH_4 and C_2H_4 were not detected. Analysis of gas chromatograph-mass spectrometer (GC-MS) also revealed that ethanol, acetaldehyde and acetic acid were detected as liquid products, while methanol (CH_3OH), formaldehyde (HCHO) and formic acid (HCOOH) were not detected. Despite all of these detailed analyses, we had inadequate carbon balance closure, especially for longer residence times. This is probably caused by dissolution of CO_2 in the effluents, in spite of using water substitution with lean hydrochloric acid. Therefore we assumed that a portion of produced CO_2 was dissolved in the effluents.

The global conversion rate of subcritical WO or SCWO depends on the rate of formation of final product as well as those of formation and destruction of stable intermediates. A typical stable intermediate coming from ethanol is acetic acid. Li et al. (1991) showed that acetic acid was rate-limiting intermediate, which had smaller rate constant than for the other alcohols. They proposed a generalised model which consisted of three groups of organic compounds and was compared with the experimental data derived from literature. The comparison showed that the generalised model prediction results agreed with the experimental data for subcritical wet oxidation of activated sludge, black liquor, biological sludge, phenol and 2-chlorophenol, and supercritical water oxidation of industrial activated sludge. Rice et al. (2001) used Raman spectroscopy to detect and measure the formation of acetaldehyde and carbon dioxide from SCWO of ethanol. Their results showed that concentration of formaldehyde initially increased and then decreased with increasing residence time at a given temperature.

5.4.3 Consecutive four-step reaction

Table 5.2 Reaction rate equations and their analytical solutions for the reaction network: EtOH → AAL → AAC → CO → CO_2, where AAL and AAC are acetaldehyde and acetic acid, respectively.

eq.	rate equation	analytical solution
5.6	$r_{\mathrm{EtOH}} = \mathrm{d[EtOH]}/\mathrm{d}t = -k_1[\mathrm{EtOH}]$	$[\mathrm{EtOH}] = [\mathrm{EtOH}]_0 e^{-k_1(t-\tau_{\mathrm{ind}})}$
5.7	$r_{\mathrm{AAL}} = \mathrm{d[AAL]}/\mathrm{d}t = k_1[\mathrm{EtOH}] - k_2[\mathrm{AAL}]$	$[\mathrm{AAL}] = [\mathrm{EtOH}]_0 k_1 \ \ e^{-k_1(t-\tau_{\mathrm{ind}})}/(k_2-k_1) - e^{-k_1(t-\tau_{\mathrm{ind}})}/(k_1-k_2)$
5.8	$r_{\mathrm{AAC}} = \mathrm{d[AAC]}/\mathrm{d}t = k_2[\mathrm{AAL}] - k_3[\mathrm{AAC}]$	$[\mathrm{AAC}] = [\mathrm{EtOH}]_0 k_1 k_2 \ \ (k_2-k_1)^{-1}(k_3-k_1)^{-1}e^{-k_1(t-\tau_{\mathrm{ind}})} + (k_1-k_2)^{-1}$ $(k_3-k_2)^{-1}e^{-k_2(t-\tau_{\mathrm{ind}})} + (k_1-k_3)^{-1}(k_2-k_3)^{-1}e^{-k_3(t-\tau_{\mathrm{ind}})}$
5.9	$r_{\mathrm{CO}} = \mathrm{d[CO]}/\mathrm{d}t = k_3[\mathrm{AAC}] - k_4[\mathrm{CO}]$	$[\mathrm{CO}] = [\mathrm{EtOH}]_0 k_1 k_2 k_3 \ \ (k_2-k_1)^{-1}(k_3-k_1)^{-1}(k_4-k_1)^{-1}e^{-k_1(t-\tau_{\mathrm{ind}})}$ $+ (k_1-k_2)^{-1}(k_3-k_2)^{-1}(k_4-k_2)^{-1}e^{-k_2(t-\tau_{\mathrm{ind}})} + (k_1-k_3)^{-1}$ $(k_2-k_3)^{-1}(k_4-k_3)^{-1}e^{-k_3(t-\tau_{\mathrm{ind}})} + (k_1-k_4)^{-1}(k_2-k_4)^{-1}$ $(k_3-k_4)^{-1}e^{-k_4(t-\tau_{\mathrm{ind}})}$
5.10	$r_{\mathrm{CO_2}} = \mathrm{d[CO_2]}/\mathrm{d}t = k_4[\mathrm{CO}]$	$[\mathrm{CO_2}] = [\mathrm{EtOH}]_0 - [\mathrm{EtOH}] - [\mathrm{AAL}] - [\mathrm{AAC}] - [\mathrm{CO}]$
5.11	at $t = 0$: $[\mathrm{EtOH}] = [\mathrm{EtOH}]_0$ and $[\mathrm{AAL}] = [\mathrm{AAC}] = [\mathrm{CO}] = [\mathrm{CO_2}] = 0$	

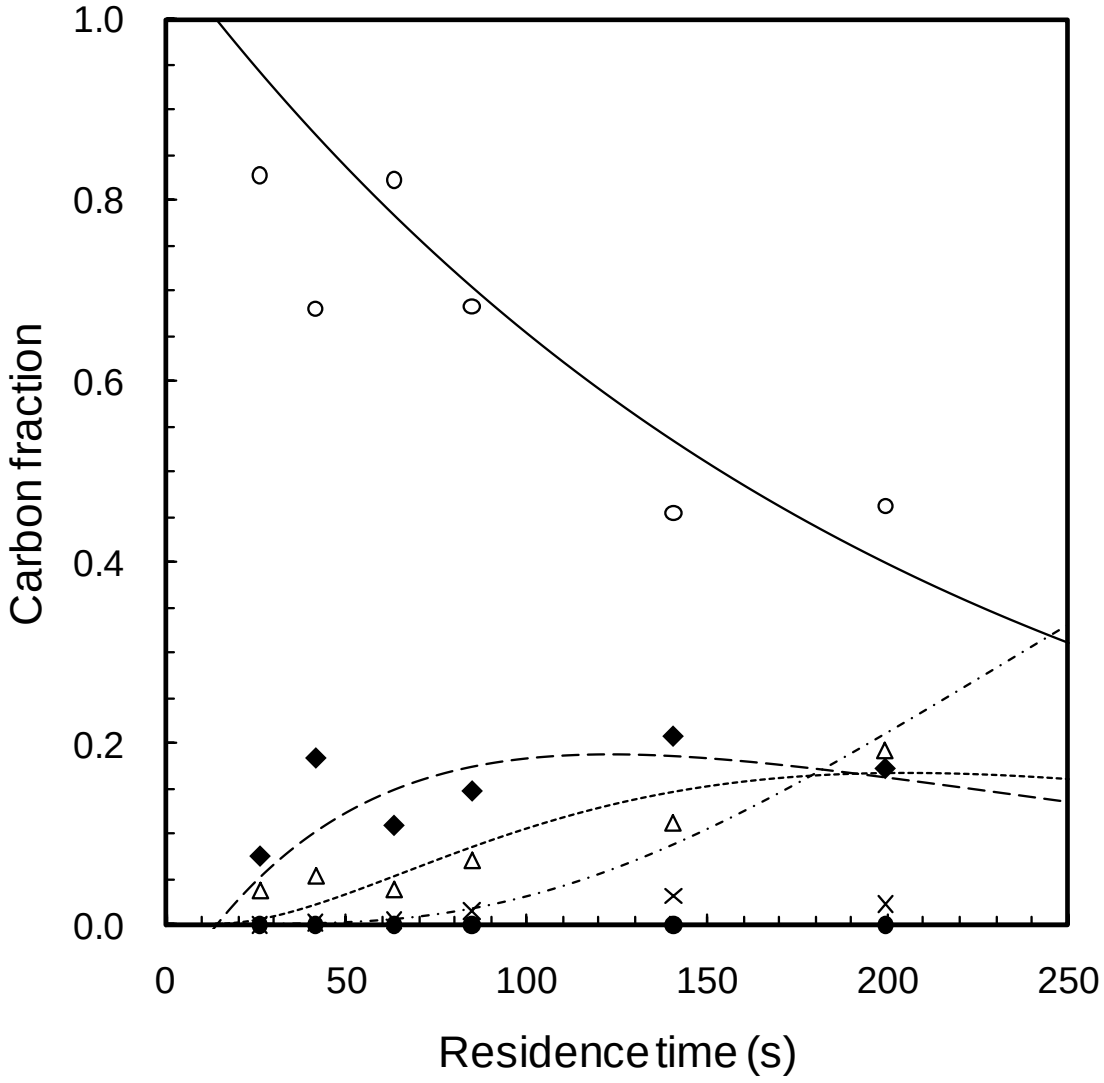

Figure 5.6 Temporal variation of the carbon fraction of ethanol (○), acetaldehyde (◆), acetic acid (△), carbon monoxide (●) and carbon dioxide (×) for ethanol subcritical wet oxidation at 260 °C.

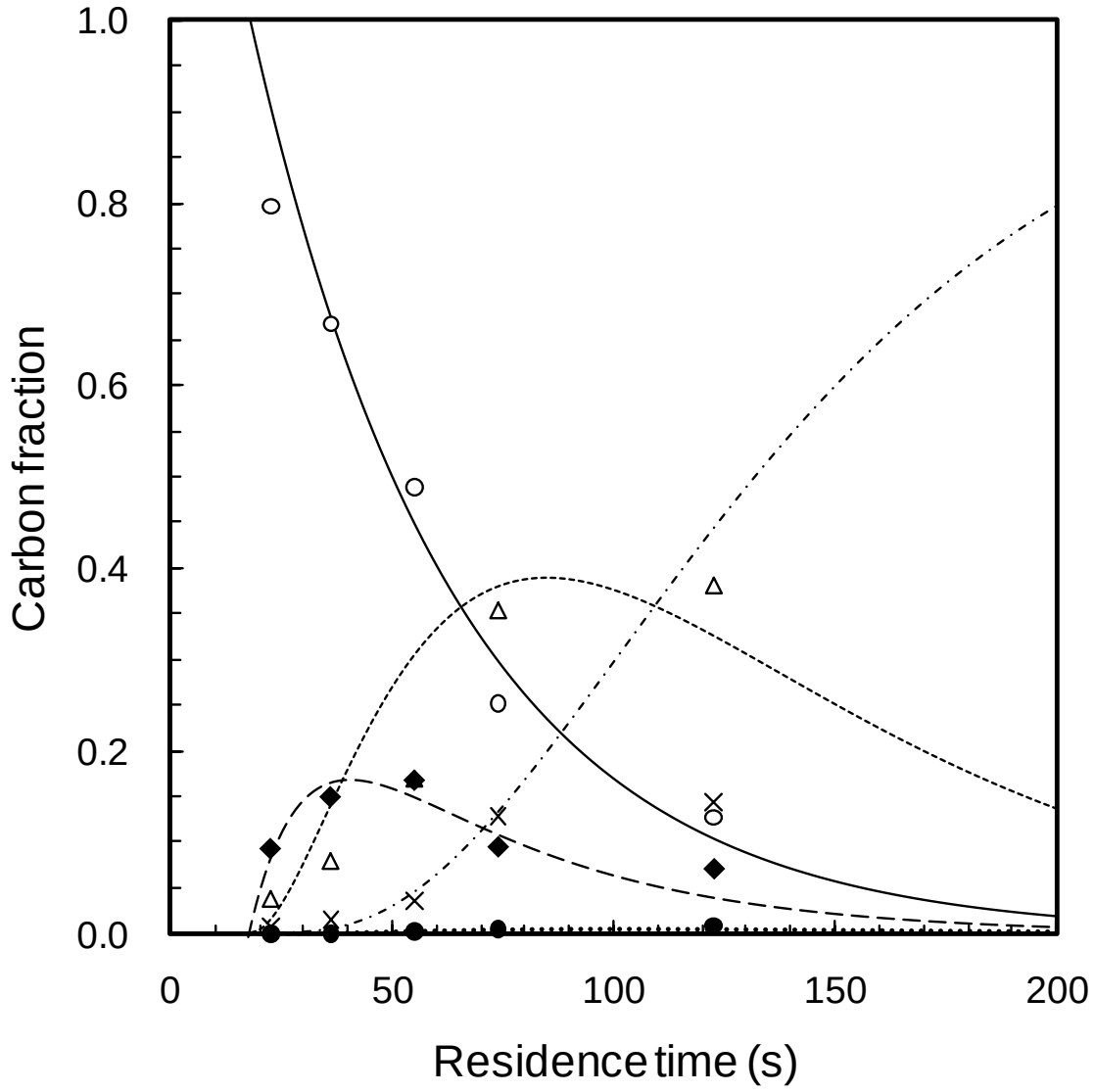

Figure 5.7 Temporal variation of the carbon fraction of ethanol (○), acetaldehyde (◆), acetic acid (△), carbon monoxide (●) and carbon dioxide (×) for ethanol subcritical wet oxidation at 320 °C.

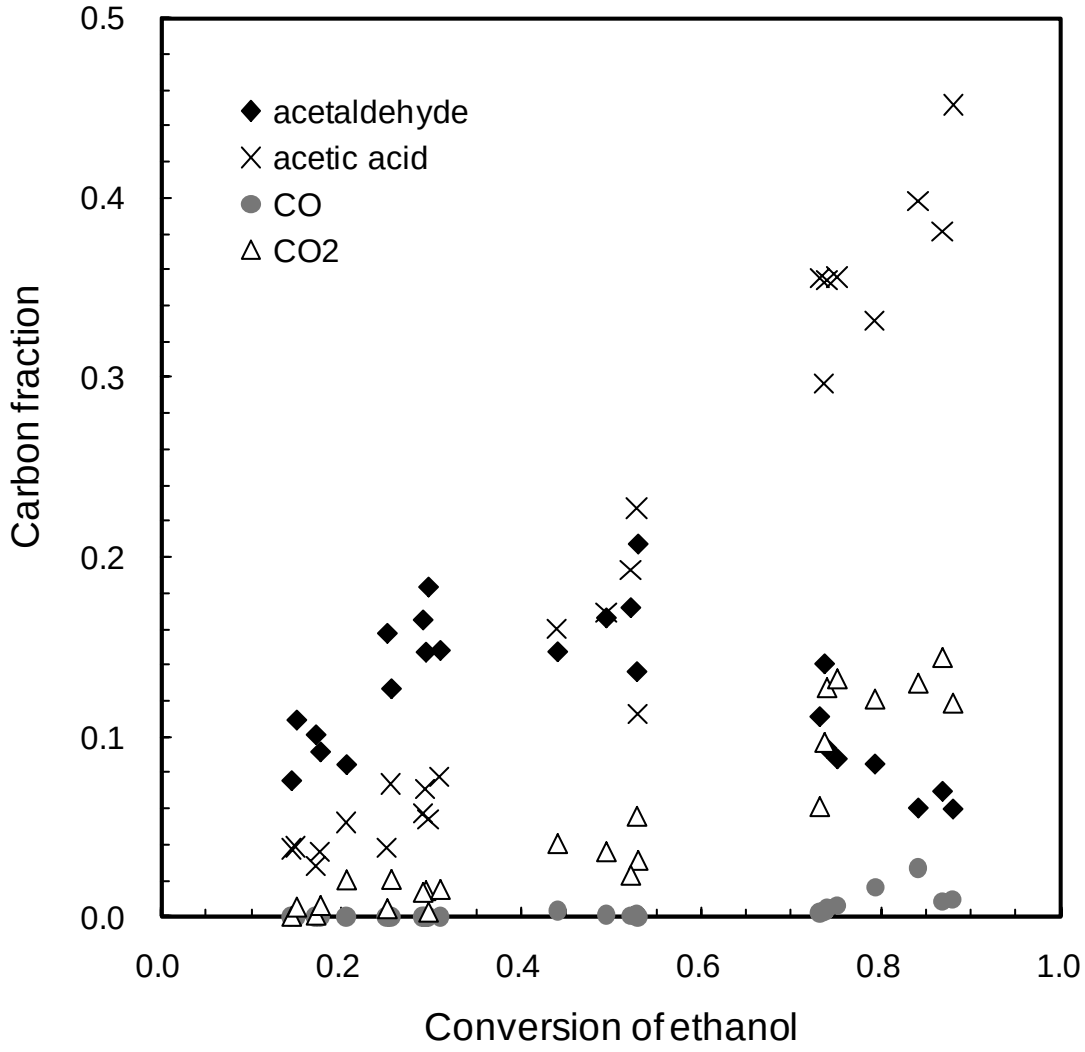

Figure 5.8 Variation of the carbon fractions of acetaldehyde (◆), acetic acid (×), carbon monoxide (●), and carbon dioxide (△) with the ethanol conversion.

Consecutive reaction path is constructed for SCWO by many researchers because of its simplicity, e.g. the research conducted by Anitescu et al. (1999) for SCWO of methanol, whereas the more complex reaction pathways are proposed by Rice et al. (2001) for SCWO of ethanol. However, the mechanisms for WO of ethanol are not addressed, although the intermediate substances are examined by Li et al. (1991).

As described above, analyses of liquid and gas phase effluent in our experiment revealed that ethanol (EtOH), acetaldehyde (AAL), acetic acid (AAC), carbon monoxide (CO) and carbon dioxide (CO_2) were major species appearing in the subcritical water oxidation of ethanol. Accordingly, the global reaction network for subcritical WO of ethanol based on our experimental data is supposed to be a consecutive reaction:

$$\mathrm{EtOH} \xrightarrow{k_1} \mathrm{AAL} \xrightarrow{k_2} \mathrm{AAC} \xrightarrow{k_3} \mathrm{CO} \xrightarrow{k_4} \mathrm{CO_2} \tag{5.5}$$

Assuming that the above oxidation steps depend on first-order reaction kinetics because of the lower concentrations of the reactant and products (i.e. ≤ 25 mmol·l^{-1}) and higher concentration of oxygen (i.e. ~ 125 mmol·l^{-1}), one can write the rate equations as equations (5.6)–(5.10) in Table 5.2, where [EtOH], [AAL], [AAC], [CO] and [CO_2] are concentration of ethanol, acetaldehyde, acetic acid, carbon monoxide, and carbon dioxide, respectively.

These differential equations are integrated with the initial conditions, [EtOH] = [EtOH]$_0$ and [AAL] = [AAC] = [FAC] = [CO] = [CO_2] = 0, giving the analytical solutions of equations (5.6)–(5.10) in Table 5.2, where [EtOH]$_0$ is initial concentration of ethanol and τ_{ind} is induction period. Furthermore, the system of differential equations for *n*-step reaction scheme is solved by Rodiguin and Rodiguina (1964).

Figures 5.6 and 5.7 show composition of the liquid and gas phase effluents as a function of residence time at T = 260 °C and 320 °C, respectively. The global rate constant for ethanol conversion, k_1, and induction period, τ_{ind}, were obtained by plotting $\ln(C/C_0)$ versus the residence time, as discussed above and shown in Figure 5.2. The rate constants, k_2, k_3 and k_4 were calculated by numerical curve-fitting using nonlinear least-squares method, and listed in Table 5.1. The value of k_1 and k_3 is smaller than k_2, k_4, which means that decomposition of ethanol and acetic acid are rate-controlling steps. These facts confirm the description of the literature (Li et al., 1991) which states that ethanol and acetic acid are main stable intermediates in WO of waste materials.

Carbon fractions for unreacted ethanol and products were provided by substitution of

the rate constants into the analytical solutions of equations (5.6)–(5.10) in Table 5.2. As shown in Figure 5.6, the feature of experimental data at T = 260 °C were captured by this first-order consecutive model. Figure 5.7 show that our results at T = 320 °C also well fitted into the simulation data.

The variation of carbon fractions of acetaldehyde, acetic acid, formic acid, carbon monoxide and carbon dioxide with ethanol conversion are shown in Figure 5.8. In the absence of temperature effect, carbon fraction of acetaldehyde is higher than that of acetic acid in the first half of ethanol conversion and then decreases in the latter half of ethanol conversion. This clearly means acetaldehyde is an intermediate product following ethanol and followed by acetic acid. Therefore, the relation among the network members of ethanol, acetaldehyde and acetic acid is consistent with the experimental data.

5.5 Conclusions

The oxidation of ethanol was studied at 25 MPa over a temperature range of 260–350 °C and residence times from 20.1 to 119.5 s with equivalence ratio of 0.6. The global conversion rate of ethanol in subcritical water was obtained. The kinetic parameters were determined to be $10^{2.9 \pm 0.4}$ s^{-1} for the pre-exponential factor and 53.8 ± 4.6 kJ·mol^{-1} for the activation energy. First-order kinetics was enough to capture the main characteristics of species concentration profiles. Subcritical wet oxidation of ethanol could be described by the consecutive network: $C_2H_5OH \rightarrow CH_3CHO \rightarrow CH_3COOH \rightarrow CO \rightarrow CO_2$.

Chapter 6: Kinetics of ethanol oxidation in high-pressure steam

6.1 Introduction

The reaction rate for subcritical WO of ethanol was measured by Hirosaka et al. (2007) using first-order assumption. They reported the estimation of capacity for ethanol oxidation in subcritical water as a heat source. At the same time, Hirosaka (2008) and Koido (2009) have worked on the numerical simulation of the behaviour of reactive flow in the reactor. These studies have been implemented with a single step reaction rate of reactants considering decomposition of ethanol into acetic acid. At the same time, Koido et al. (2010) elucidated that the subcritical WO of ethanol was well described by the consecutive reaction network: $C_2H_5OH \rightarrow CH_3CHO \rightarrow CH_3COOH \rightarrow CO \rightarrow CO_2$.

However, most of investigations for the oxidation in subcritical water were conducted below the temperature of saturated vapour. The features for the oxidation above the temperature, or HPSO, are almost unknown. In this study, oxidation rate of ethanol in high-pressure steam were experimentally obtained at the pressure of 10 MPa and the temperature ranging from 430 to 490 °C with the fuel equivalence ratio of 0.4. Liquid phase and gas phase products were also analysed qualitatively and quantitatively.

6.2 Experimental apparatus and procedures

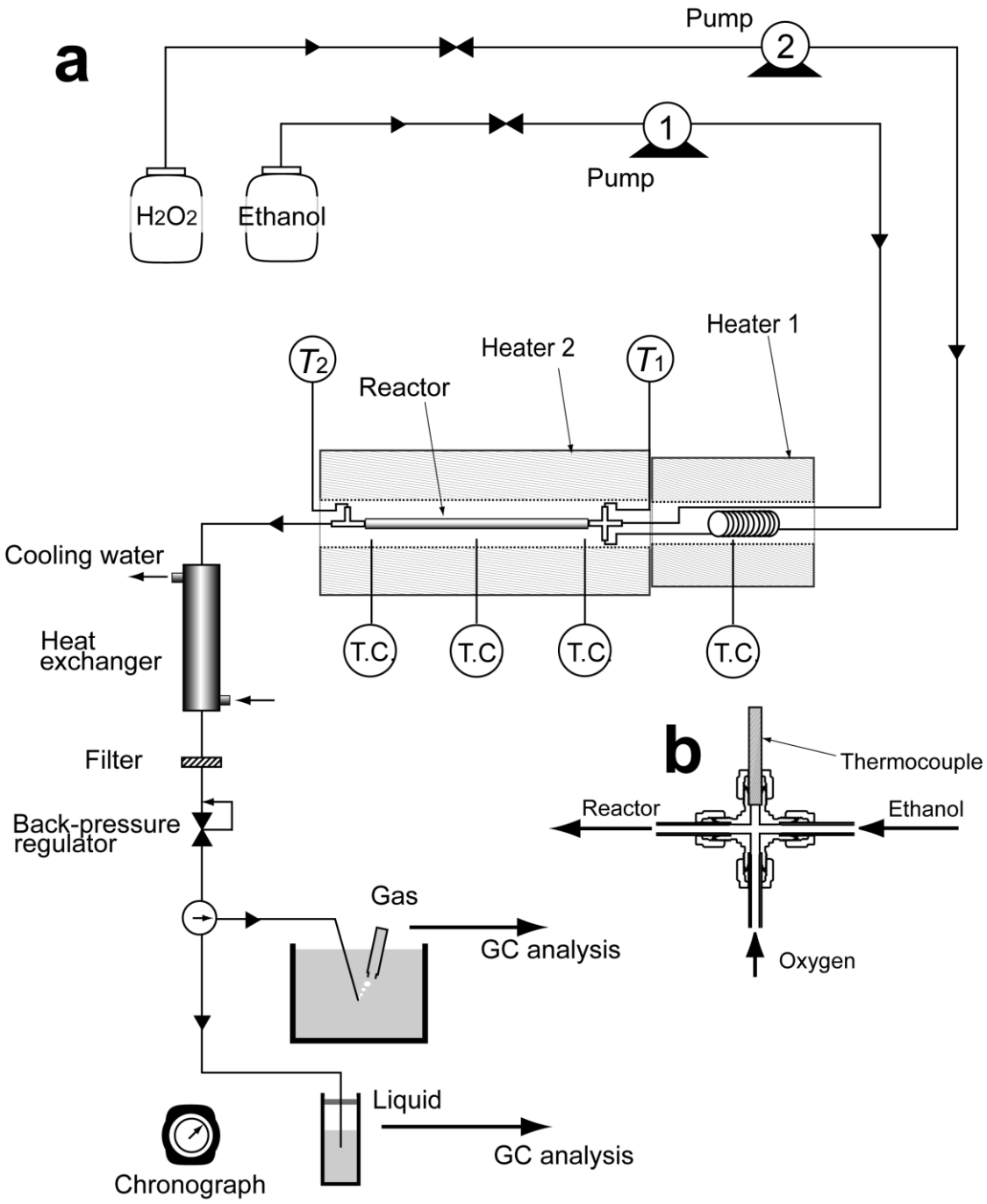

Figure 6.1 Experimental apparatus: (a) whole reactor setup, (b) detail of the mixing cross.

Experiments of the oxidation in high-pressure steam were conducted in a flow type reactor. A schematic illustration of the continuous flow reactor system is shown in Figure 6.1. All tubes from the pumps to the back pressure regulator and the reactor were made of SUS316. The reactor was selected from several straight tubes with different lengths and different diameters in order to control the residence time of reactant: 80 and 130 mm in length with i.d. of 9.5 mm and 90, 150 and 200 mm in length with i.d. of 4.0 mm. The oxidant was prepared by dissolving hydrogen peroxide (H_2O_2) into distilled water in one feed tank. Another feed tank was loaded with ethanol aqueous solution. The two feed streams were separately pressurised by two high-pressure metering pumps and then preheated in an electrical tubular furnace. In order to assure that H_2O_2 is completely decomposed into O_2 and H_2O, the oxidant was preheated through 2.7 m long coiled tube with 1.8 mm i.d. fixed in the tubular furnace "Heater 1" shown in Figure 6.1a. According to the study of Croiset (1997), H_2O_2 could be completely decomposed in the preheating tube for various experimental conditions of this study. Ethanol feed stream was preheated through 2.0 m long coiled tube of 1.8 mm i.d. fixed in the tubular furnace, "Heater 1". After preheating in the "Heater 1", the oxygen aqueous solution was injected into the main flow of ethanol aqueous solution at a tee union fixed in the "Heater 2" (Figure 6.1b) to enhance mixing of two streams.

The temperature at the inlet of reactor, T_1 and that at the outlet of reactor, T_2, were kept equal, that is, the difference between them was lower than 0.1 °C for any cases in our experiments. Mean values of both temperatures were referred to be reaction temperatures, which were 429.9–490.4 °C. After flowing out from the reactor, the effluent was cooled rapidly in a counter-flow heat exchanger and afterwards, the system pressure, 10.1 MPa, was reduced by using a back pressure regulator. The product was then separated into liquid and vapour phases. Gas samples were collected in a water pool as shown in Figure 6.1. The liquid and gas samples were analysed by gas chromatographs.

The flow rates for the reactant and the oxidant were 0.5 or 1.0 ml·min^{-1}. Ethanol and oxygen concentrations at the entrance of the reactor for the experiments were respectively 25 and 187.5 mmol·l^{-1}, 33 and 247.5 mmol·l^{-1}, and 40 and 300 mmol·l^{-1}, while their fuel equivalence ratios were kept $\phi = 0.4$. The concentrations of ethanol were low enough to neglect the calorific value of the oxidation.

6.3 Analytical techniques

Liquid phase samples were analysed by a Hewlett-Packard 5890 gas chromatograph (GC), which was equipped with a flame ionisation detector (FID) and supplied nitrogen as a carrier gas. Separation of the compositions was accomplished using a 30 m × 0.25 mm i.d. × 0.25 μm film thickness Pure–WAX column by GL Sciences Inc. The concentrations of unreacted ethanol, acetaldehyde and acetic acid were determined by the GC–FID.

The gas composition was determined by manually injecting 200 μl vapour sample into two GCs, Shimadzu GC–14B and Yanaco G1880. The GCs are equipped with the two columns packed with Porapak Q and with MS–5A and a thermal conductivity detector (TCD). Helium and argon were employed as the carrier gas for the Shimadzu's and Yanaco's GC, respectively. The gaseous sample was analysed using two columns: the column packed with Porapak Q for detection of carbon dioxide and ethane, and with MS–5A for carbon monoxide, methane and hydrogen.

Residence times were calculated by considering the flow rates of the ethanol and oxidiser into the system. On the basis of the mass balance of the materials at the pump and the plug-flow reactor, an equation for the residence time can be obtained in the simple form: $\tau = V_R(\rho_R / \rho_P)/\dot{v}_P$. In this equation, the residence time, τ, is calculated from both the volume of the reactor, V_R, and the total initial flow rate of the reactant and oxidant at the outlet of the pumps, $\dot{v}_P$. To determine the residence time, it is assumed that the densities of the reactant and oxidant are the same as the densities of water, which are calculated using the Reference Fluid Thermodynamic and Transport Properties Database (REFPROP ver.8) by National Institute of Standards and Technology (NIST) (Lemmon, 2007).

6.4 Results and discussion

6.4.1 First-order oxidation rate of ethanol

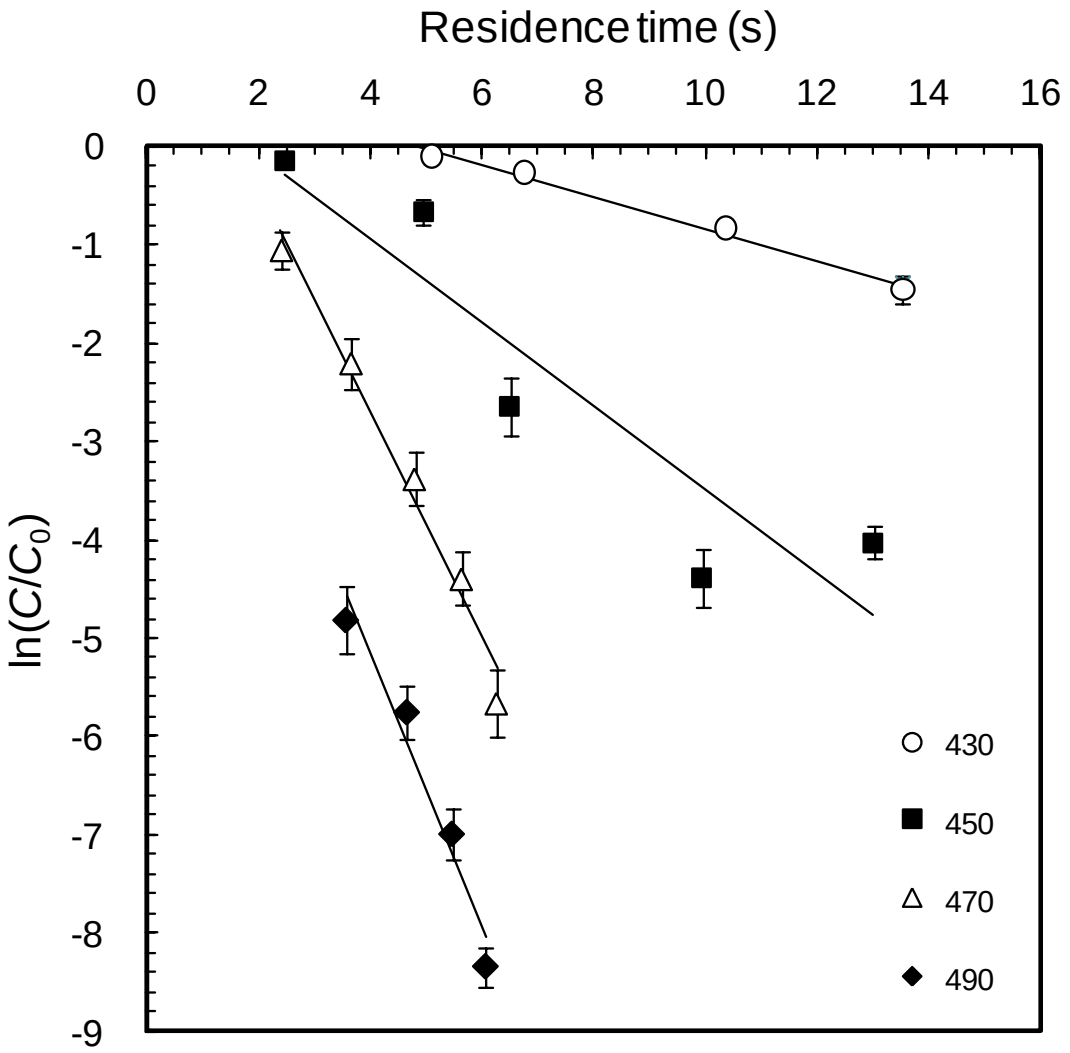

Figure 6.2 Variation of $\ln(C/C_0)$ versus residence time, for the temperature of 430 °C (○), 450 °C (■), 470 °C (△) and 490 °C (◆) at p = 10 MPa.

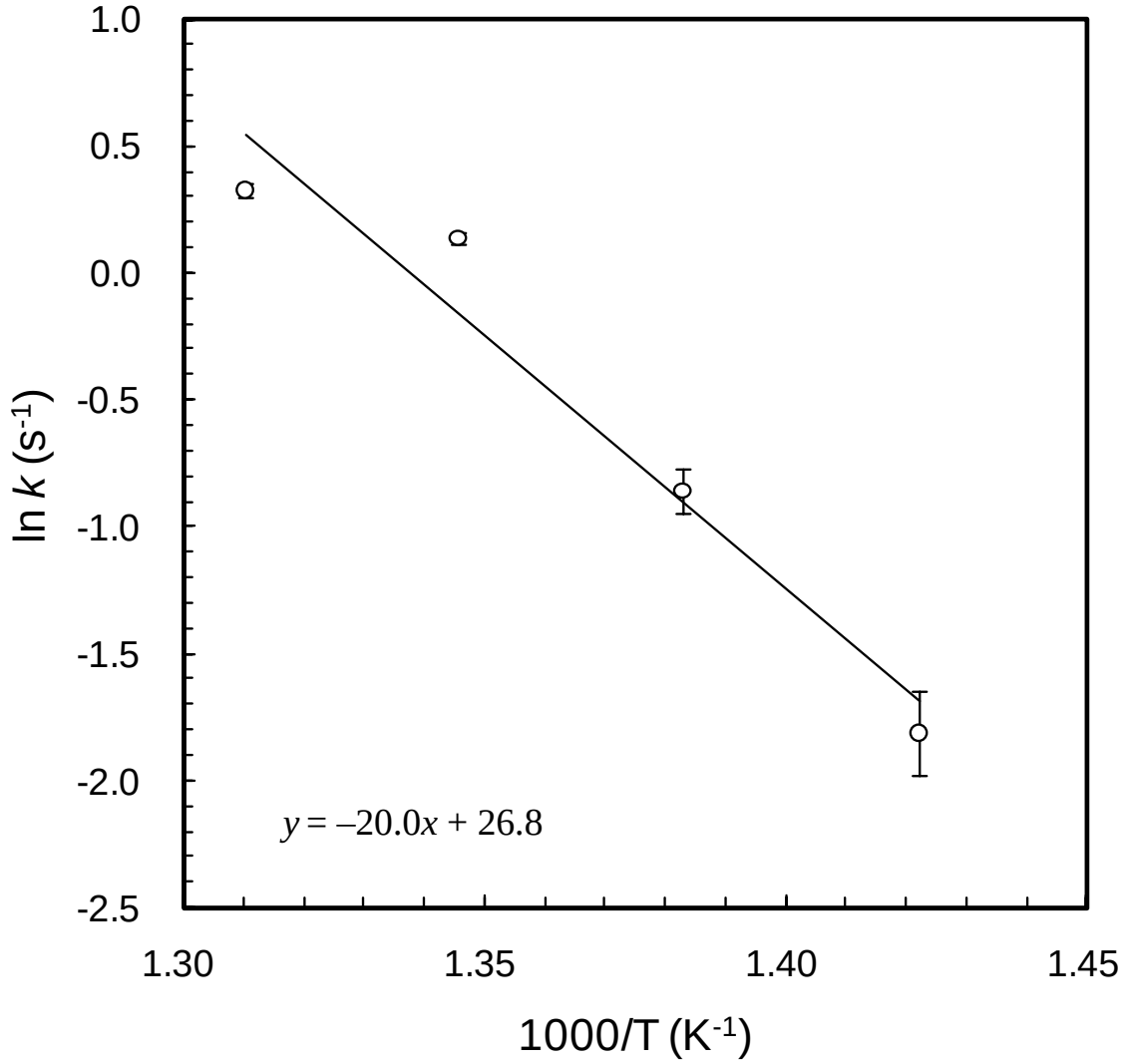

Figure 6.3 Arrhenius plot for the overall conversion rate of ethanol assuming first-order reaction.

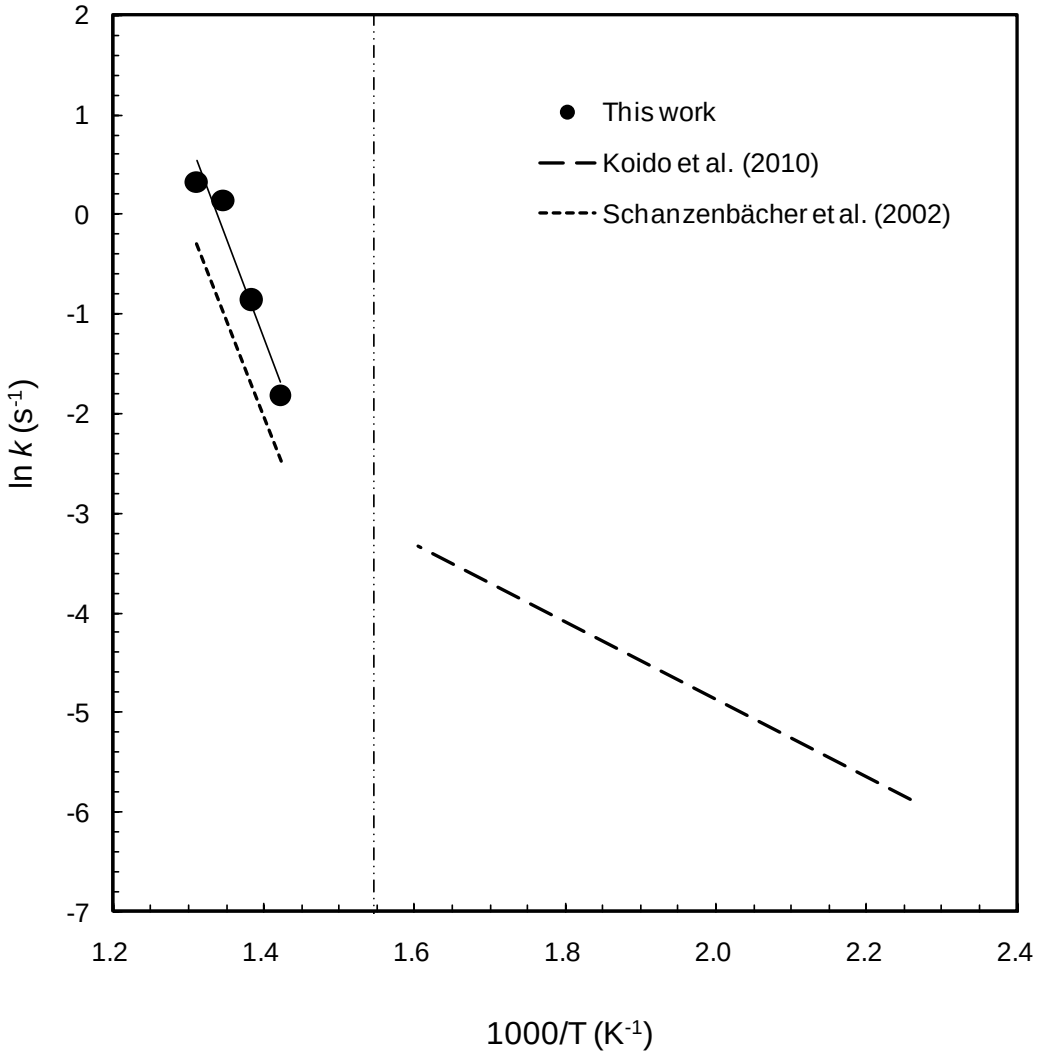

Figure 6.4 Arrhenius plots of conversion rates of ethanol assuming first-order reaction obtained by different experiments: this work at 10 MPa (●), Schanzenbächer et al. (2002) at 24.6 MPa (---), and Koido et al. (2010) at 23.5–25.0 MPa (– –) around the critical temperature.

The oxidation reaction for this work proceeds in the excess amount of steam media. In addition, the oxidant is rich enough to neglect its concentration in the oxidation reaction rate because the fuel equivalence ratio is 0.4. Thus first-order ethanol oxidation rate is assumed and expressed as

$$\frac{\mathrm{d}C}{\mathrm{d}t} = -kC \tag{6.1}$$

where C is the concentration of ethanol and k is the rate constant. This first-order reaction assumption might be fair, because the order of reaction calculated by fitting an analytical solution of n-th order reaction to the experimental data was ranging from around 0.8 to 1.1 for different temperatures.

Figure 6.2 shows variation of $\ln(C/C_0)$ against residence time. Data points for each temperature were approximated by a straight line using the least square method. The lines do not pass through the origin, but seem to intersect the x-axis at positive residence times. The x-intercept for each line provides estimation of the induction period, t_0, and the slope provides estimation of the rate constant, k. Subsequently, the rate constant is plotted against inverse temperature as shown in Figure 6.3. The pre-exponential factor and the activation energy for our experiments at 10.1 MPa and 429.9–490.4 °C are $A = 10^{11.6 \pm 0.4}$ s^{-1} and $E_a = 166.5 \pm 6.1$ kJ·mol^{-1}, respectively. Thus overall first-order reaction rate constant for ethanol oxidation in the high pressure vapour is expressed as:

$$k = 10^{11.6 \pm 0.4} \exp\left(-\frac{166.5 \pm 6.1\,[\mathrm{kJmol^{-1}}]}{RT}\right) \tag{6.2}$$

Kinetic parameters for ethanol oxidation rate in SCW (24.6 MPa, 433–494 °C) were measured by Schanzenbächer et al. (2002). In their research, pre-exponential factor and activation energy were respectively $A = 10^{11.1 \pm 4.5}$ s^{-1} and $E_a = 163.9 \pm 3.3$ kJ·mol^{-1}, which are close to the parameters obtained in our experiment as shown in Figure 6.4. On the other hand, the parameters obtained by Koido et al. [12] for lower temperature WO (23.5–25.0 MPa, 170–350 °C), are $A = 10^{2.7 \pm 0.3}$ s^{-1} and $E_a = 47.2 \pm 5.7$ kJ·mol^{-1}, which are rather smaller values than in SCWO and HPSO.

These results show that ethanol oxidation in high-pressure steam is equivalent to SCWO of ethanol, and that utilisation of the HPSO could overcome the problem of pressure tightness of the reactor in SCWO.

6.4.2 Reaction products

Figures 6.5 and 6.6 respectively show composition of the liquid and gas phase effluents as a function of residence time at T = 470 °C, where [i]/[EtOH]$_0$ is defined as concentration of species i divided by initial concentration of ethanol. Liquid products are identified as acetaldehyde (CH_3CHO) and acetic acid (CH_3COOH), while gas phase products are carbon monoxide, carbon dioxide, methane and ethane. In Figure 6.5, acetaldehyde and acetic acid decrease with the same speed and then approach zero with the residence time. In Figure 6.6, concentration of carbon dioxide monotonically increases with residence time because it is one of the end products of oxidation reaction. Carbon monoxide is the typical intermediate product, because it increases with the decomposition of liquid products and then decrease with the production of carbon dioxide. Methane slightly increases with residence time, though the amount is rather small. Ethane has a negligible amount for all the residence times. Comparing Figures 6.5 and 6.6, it seems that decrease of ethanol causes increase of acetaldehyde and acetic acid and decrease of them produces carbon monoxide, methane and ethane and then carbon dioxide. Based on the principle that reactants with higher oxidation numbers are transformed into products with lower oxidation numbers, ethanol is decomposed into acetaldehyde (CH_3CHO) and acetic acid (CH_3COOH) simultaneously. Thus the reaction network in liquid phase can be expressed as follows:

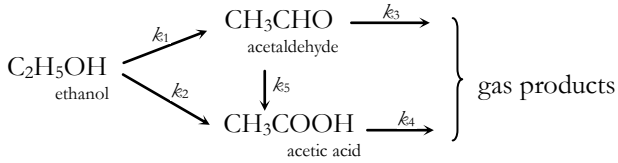

(6.3)

On the basis of the network (6.3), the reaction rate equations and their analytical solutions are given by equations (6.4)–(6.6) in Table 6.1, where [EtOH], [AAL], [AAC] and t_0 are concentration of ethanol, acetaldehyde, acetic acid and induction period, respectively. Analytical solutions were obtained by integrating rate equations with the initial conditions (6.7) on the basis of a technique by Rodiguin and Rodiguina (1964).

The global rate constant for ethanol conversion, $k_1 + k_2$, and t_0, were obtained by plotting constants, k_1, k_2, k_3, k_4 and k_5 were calculated by numerical curve-fitting using nonlinear $\ln(C/C_0)$ versus the residence time, as discussed above and shown in Figure 6.2.

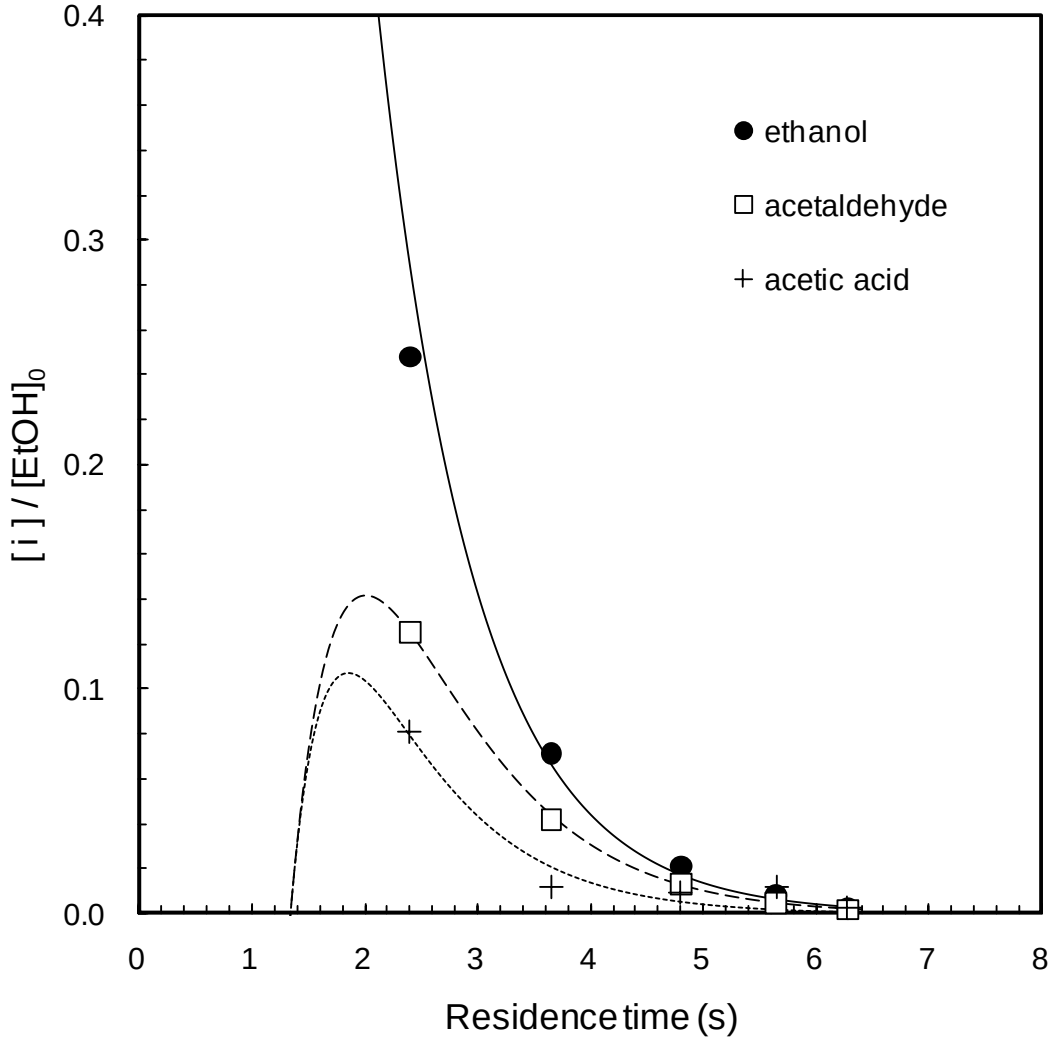

Figure 6.5 Concentration of unreacted ethanol (●) and liquid phase products *i*: acetaldehyde (□) and acetic acid (+), for the experiments at p = 10 MPa, T = 470 °C and C_0 = 40 mmol·l^{-1}. The solid, dashed and dotted curves respectively correspond to analytical solutions of Equations (6.4), (6.5) and (6.6) using $k_1 - k_5$ obtained from numerical fittings to the experimental results.

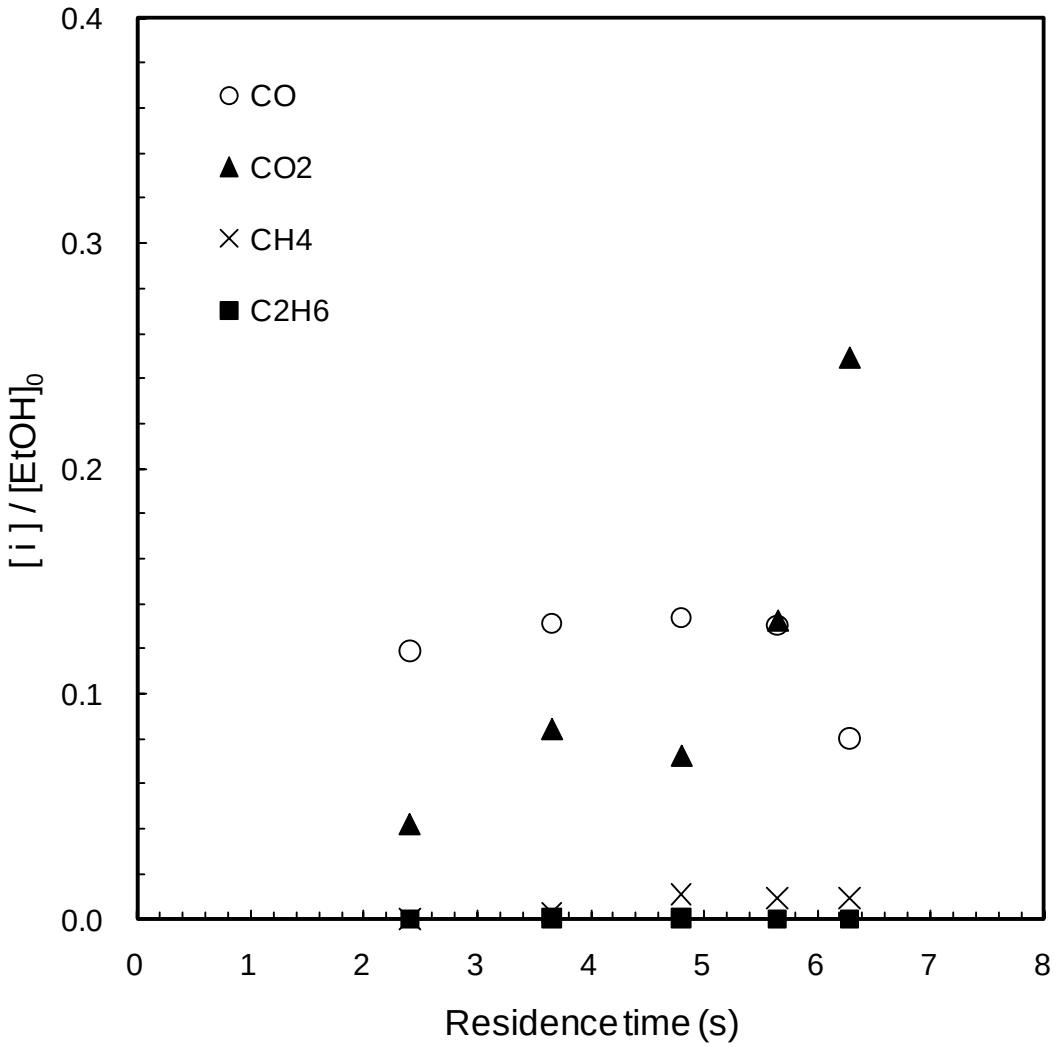

Figure 6.6 Concentration of gas phase products *i*: carbon monoxide (○), carbon dioxide (▲), methane (×) and ethane (■), for the experiments at p = 10 MPa, T = 470 °C and C_0 = 40 mmol·l^{-1}.

Table 6.1 Reaction rate equations and their analytical solutions for the reaction network (6.3). [EtOH], [AAL], [AAC] and t_0 are concentration of ethanol, acetaldehyde, acetic acid and induction period respectively.

eq.	rate equation	analytical solution
6.4	$r_{\mathrm{EtOH}} = \mathrm{d[EtOH]}/\mathrm{d}t$ $= -k_1[\mathrm{EtOH}] - k_2[\mathrm{EtOH}]$	$[\mathrm{EtOH}] = [\mathrm{EtOH}]_0 e^{-(k_1+k_2)(t-\tau_{\mathrm{ind}})}$
6.5	$r_{\mathrm{AAL}} = \mathrm{d[AAL]}/\mathrm{d}t$ $= k_1[\mathrm{EtOH}] - k_3[\mathrm{AAL}] - k_5[\mathrm{AAL}]$	$[\mathrm{AAL}] = [\mathrm{EtOH}]_0 k_1 \ e^{-(k_1+k_2)(t-t_0)}/[(k_3+k_5)-(k_1+k_2)]$ $+e^{-(k_3+k_5)(t-t_0)}/[(k_1+k_2)-(k_3+k_5)]$
6.6	$r_{\mathrm{AAC}} = \mathrm{d[AAC]}/\mathrm{d}t$ $= k_2[\mathrm{EtOH}] - k_4[\mathrm{AAC}] + k_5[\mathrm{AAL}]$	$[\mathrm{AAC}] = [\mathrm{EtOH}]_0 \ e^{-(k_1+k_2)(t-t_0)} k_2[(k_3+k_5)+k_5k_1/k_2-(k_1$ $+k_2)]/[(k_3+k_5)-(k_1+k_2)]/[k_4-(k_1+k_2)]+e^{-(k_3+k_5)(t-t_0)}$ $k_5k_1/[(k_1+k_2)-(k_3+k_5)]/[k_4-(k_3+k_5)]+e^{-k_4(t-t_0)}k_2[$ $(k_3+k_5)+k_5k_1/k_2-k_4]/[(k_1+k_2)-k_4]/[(k_3+k_5)-k_4]$
6.7	at $t = 0$: $[\mathrm{EtOH}] = [\mathrm{EtOH}]_0$ and $[\mathrm{AAL}] = [\mathrm{AAC}] = 0$	

The rate least-squares method. The resulting value of k_5 was almost negligible for each reaction temperature, thus the reaction network (6.3) is a parallel one. As shown in Figure 6.5, the feature of experimental data at T = 470 °C were well reproduced by this first-order parallel reaction model (6.3). Carbon monoxide and carbon dioxide are formed by oxidation of acetaldehyde and acetic acid. The elementary reactions based on the work of Marinov (1999) can be also considered as participating reactions. The mechanism was designed to accommodate the chemistry for atmospheric pressure and high-temperature conditions. Rice and Croiset (2001), however, changed the mechanism and added the other elementary reactions to obtain the kinetic model for SCWO of ethanol. The formation reactions:

$$\begin{aligned} &\mathrm{HCO+M \rightleftharpoons H+CO+M} \\ &\mathrm{HCO+O_2 \rightleftharpoons CO+HO_2} \\ &\mathrm{CH_3CO\ (+M) \rightleftharpoons CH_3+CO\ (+M)} \end{aligned} \tag{6.8}$$

$$\begin{aligned} &\mathrm{HCCO+O_2 \rightleftharpoons CO_2+HCO} \\ &\mathrm{CO+OH \rightleftharpoons CO_2+H} \\ &\mathrm{CO+HO_2 \rightleftharpoons CO_2+OH} \end{aligned} \tag{6.9}$$

are decided as the mechanism of carbon monoxide and carbon dioxide, which is common in the models by Marinov and Rice and Croiset, where M is third body.

On the other hand, methane formation involves several participating reactions such as

$$\begin{aligned} &\mathrm{CH_3+HO_2 \rightleftharpoons CH_4+O_2} \\ &\mathrm{CH_3CHO+CH_3 \rightleftharpoons CH_3CO+CH_4} \end{aligned} \tag{6.10}$$

which are the inherent aspects of Marinov's mechanism. Ethane is formed exclusively by

$$\mathrm{CH_3+CH_3\ (+M) \rightleftharpoons C_2H_6\ (+M)}. \tag{6.11}$$

The methyl radical is a necessary precursor species to methane and ethane formation. The research for hydrothermal gasification (Ishida, 2009) shows that methane originates from water-gas shift reaction, $\mathrm{CO+H_2O \rightarrow CO_2+H_2}$, and methanation reaction, $\mathrm{CO+3H_2 \rightarrow CH_4+H_2O}$. However, no hydrogen was produced in our oxidation experiments. Thus the water-gas shift and methanation reactions did not occur in the reactions of methane

production.

6.5 Conclusions

Ethanol oxidation rate in high-pressure steam at p =10 MPa and T = 430–490 °C were studied under a fuel equivalence ratio of ϕ = 0.4. The reaction rate parameters obtained were $A = 10^{11.6 \pm 0.4}$ s^{-1} and E_a = 166.5 ± 6.1 kJ·mol^{-1} for the first order assumption. This ethanol oxidation rate in high-pressure steam was equivalent to SCWO of ethanol. Qualitative and quantitative analyses of products proved that liquid products were acetaldehyde and acetic acid and gas phase products were carbon monoxide, carbon dioxide, methane and ethane. The parallel reaction network of first order model well described the characteristics of the ethanol decomposition to acetaldehyde and acetic acid. Utilisation of HPSO can overcome the problem of pressure tightness of the reactor in SCWO and be utilised in practical facilities.

Chapter 7: Conclusions

Wet biowastes such as food leftover, animal manure, sewage sludge, are not suitable for incineration, for its moisture content. Biowastes treatments include methane fermentation and hydrothermal process which is viable treatment process. The hydrothermal processes are useful energy conversion technologies for the wet biowaste containing a lot of moisture, such as domestic animal excrement, sewage slug, and organic feedstock. The reaction is accomplished in hot-compressed water near or above the critical point (p = 22.1 MPa and T = 374 °C) with no drying process.

In this chapter, the major conclusions are drawn from the study performed. The implications of this research are also discussed.

- **Numerical experiment for design of reactor used in hydrothermal oxidation**

Premixed hydrothermal combustion of ethanol was numerically studied as a fundamental research to develop an energy conversion system utilising biomass and low quality oil. A simulation code available for oxidation of water solution mixture under sub-/super critical conditions was developed. Lee-Kesler equation was selected as the equation of state. Chemical species of ethanol, oxygen, carbon dioxide and water, were considered as reactants and products of complete reaction. Mixing laws by Chung et al. and Wilke et al. were used for transport properties and that of Plöcker et al. was used for thermal properties and Lee-Kesler equation of state.

Behaviours of ethanol oxidation under sub-/super critical conditions were numerically simulated. For the reaction rate, we selected Schanzenbächer et al.'s expression obtained by the experiment under supercritical condition. Effects of preheat

temperature, heat loss and flow velocity were examined by simulation.

1. The differences of preheat temperatures led to the differences of temperature increase, ΔT, around critical point because of the specific heat peak at the critical point.
2. Larger flow velocity caused slower increase of ethanol conversion and temperature increase. Changes of reaction rate for different flow velocities showed that larger flow velocity caused thicker reaction zone and higher reaction peak than that for smaller one because of the fluid advection.
3. From the calculation with different heat losses (different heat transfer rate coefficients, α), two-step temperature decrease appeared for larger heat loss (α = 2.5×10^4 W m^{-2} K^{-1}) while monotonous temperature decrease appeared for smaller heat loss (α = 2.5×10^3 W m^{-2} K^{-1}).

- **Reaction rate for subcritical WO of ethanol**

Ethanol oxidation in subcritical water was examined at 25 MPa in the temperature range of 260–350 °C with equivalence ratio of 0.6. With oxygen as the oxidiser, the overall first-order decomposition reaction rate were determined to be

$$-\frac{\mathrm{d[EtOH]}}{\mathrm{d}t} = 10^{2.9\pm4.2}\exp\left(\frac{-53.9\pm4.2\ \mathrm{kJ/mol}}{RT}\right)[\mathrm{EtOH}].$$

The products obtained by the hydrothermal oxidation of ethanol were acetaldehyde, acetic acid, carbon monoxide and carbon dioxide. First-order kinetics was enough to capture the main characteristics of species concentration profiles. Consecutive reaction network,

$$C_2H_5OH \rightarrow CH_3CHO \rightarrow CH_3COOH \rightarrow CO \rightarrow CO_2$$

well described the behaviour of components obtained from wet oxidation of ethanol.

- **Reaction rate for HPSO of ethanol**

Ethanol oxidation rate in high pressure steam at the pressure of 10 MPa in the temperature ranging from 430 to 490 °C was studied with the fuel equivalence ratio of 0.4. On the assumption that the reaction order is first order, the reaction rate is

$$-\frac{\mathrm{d[EtOH]}}{\mathrm{d}t} = 10^{11.6\pm0.4}\exp\left(\frac{-166.5 \pm 6.1\ \mathrm{kJ/mol}}{RT}\right)[\mathrm{EtOH}].$$

This ethanol oxidation rate in high-pressure steam was equivalent to that in supercritical water oxidation of ethanol. Liquid products were acetaldehyde and acetic acid and gas phase products are carbon monoxide, carbon dioxide, methane and ethane. A parallel reaction network of first order model

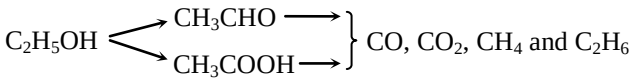

well described the characteristics of the ethanol decomposition to acetaldehyde and acetic acid. Utilisation of the high-pressure steam oxidation can overcome the problem of pressure tightness of the reactor in supercritical water oxidation and be utilised in practical facilities.

Chapter 8: Suggestions for further research

In this chapter, further research needs are identified.

1. Verification of numerical experimental results. Some experiments are needed to examine the possibility of the same trends as the results obtained in Chapter 4 to appear, which is caused by specific heat capacity around critical point.

2. Examination of heat release from real biowastes. The oxidation of real biowastes, e.g. glucose, cellulose and sewage sludge, can generate thermal energy due to dominating exothermic reactions in subcritical water and/or steam.

3. Construction of detailed reaction mechanisms of HPSO. For deeply understanding high-pressure steam oxidation, some important elementary reactions of model compounds need to be identified.

4. Development of hot water boiler. Based on the examination of heat release from biowastes, the hot water boiler system can be developed via hydrothermal oxidation.

References

ANITESCU, G., ZHANG, Z. and TAVLARIDES, L.L. (1999). "A kinetic study of methanol oxidation in supercritical water." *Industrial and Engineering Chemistry Research* **38**, 2231–2237.

ANTAL, JR., M.J., CARLSSON, M., XU, X. and ANDERSON, D.G.M. (1999). "Mechanism and kinetics of the acid catalyzed dehydration of 1- and 2-propanol in hot compressed liquid water." *Industrial and Engineering Chemistry Research* **37**, 3820–3829.

AKIYA, N. and SAVAGE, P.E. (2002). "Roles of water for chemical reactions in high-temperature water." *Chemical Reviews* **102**, 2725–2750.

BAILLOD, C.R., LAMPORTER, R.A. and BARNA, B.A. (1985 March). "Wet oxidation for industrial waste treatment." *Chemical Engineering Progress*, 52–55.

BANDURA, A.V. and LVOV, S.N. (2006). "The ionization constant of water over a wide range of temperatures and densities." *Journal of Physical and Chemical Reference Data* **35**, 15–30.

BARBIER, J., Jr., DELANOE, F., JABOUILLE, F., DUPREZ, D., BLANCHARD, G. and ISNARD, P. (1998). "Total oxidation of acetic acid in aqueous solutions over noble metal catalysts." *Journal of Catalysis* **177**, 378–385.

BENEDICT, M. WEBB, G.B. and RUBIN, L.C. (1940). "An empirical equation for thermodynamic properties of light hydrocarbons and their mixtures." *Journal of Chemical Physics* **8**, 334–345.

BERMEJO, M.D. and COCERO, M.J. (2006). "Supercritical water oxidation: a technical review." *AIChE Journal* **52**, 3933–3951.

BHARGAVA, S.K., TARDIO, J., PRASAD, J., FÖGER, K., AKOLEKAR, D.B., and GROCOTT, S.C. (2006). "Wet oxidation and catalytic wet oxidation." *Industrial and Engineering Chemistry Research* **45**, 1221–1258.

BJERRE, R.V. and SORENSEN, E. (1992). "Thermal decomposition of dilute aqueous formic acid solutions." *Industrial and Engineering Chemistry Research* **31**, 1574–1577.

BROCK, E.E., OSHIMA, Y., SAVAGE, P.E. and BARKER, J.R. (1996). "Kinetics and mechanism of methanol oxidation in supercritical water." *Journal of Physical Chemistry* **100**, 15834–15842.

BROCK, E.E. and SAVAGE, P.E. (1995). "Detailed chemical kinetics model for supercritical water oxidation of C_1 compounds and H_2." *AIChE Journal* **41**, 1874–1888.

CHUNG, T.H., AJLAN, M., LEE, L.L. and STARLING, K.E. (1988). "Generalized multiparameter correlation for nonpolar and polar fluid transport properties." *Industrial and Engineering Chemistry Research* **27**, 671–679.

CROISET, F., RICE, S.F. and HANUSH, R.G. (1997). "Hydrogen peroxide decomposition in supercritical water." *AIChE Journal* **43**, 2343–2352.

DAY, D.C., HUDGINS, R.R. and SILVESTON, P.L. (1973). "Oxidation of propionic acid solutions." *Canadian Journal of Chemical Engineering* **51**, 733–740.

DE LEITENBURG, C., GOI, D., PRIMAVERA, A., TROVARELLI, A. and DOLCETTI, G. (1996). "Wet oxidation of acetic acid catalyzed by doped ceria." *Applied Catalysis B: Environmental* **11**, L29–L35.

DESIMONE, J.M. (2002). "Practical approaches to green solvents." *Science* **297**, 799–803.

DIETRICH, M.J., RANDALL, T.L. and CANNEY, P.J. (1985). "Wet air oxidation of hazardous organics in wastewater." *Environmental Progress* **4**, 171–177.

DINARO, J.L., HOWARD, J.B, GREEN, W.H., TESTER, J.W. and BOZZELLI, J.W. (2000). "Elementary reaction mechanism for benzene oxidation in supercritical water." *Journal of Physical Chemistry* **104**, 10576–10586.

DUTOURNIÉ, P., AYMONIER, C., CANSELL, F. and MERCADIER, J. (2003). "Experiments and simulations of time dependant phenomena in a hydrothermal oxidation tubular reactor." *Industrial and Engineering Chemistry Research* **42**, 4708–4714.

DUTOURNIÉ P. and MERCADIER, J. (2004). "Supercritical waste hydrothermal treatment modelisation of non-stationary phenomena in a reactor." *Journal of Supercritical Fluids* **32**, 153–160.

DUTOURNIÉ P. and MERCADIER, J. (2005). "Unsteady behaviour of hydrothermal oxidation reactors: theoretical and numerical studies near the critical point." *Journal of Supercritical Fluids* **35**, 247–253.

DUTOURNIÉ, P., MERCADIER, J., MATÉOS, D. and CANSELL, F. (2007). "Hydrothermal oxidation treatment reactor: Experimental and simulated study of a non-anticipated phenomenon at the reactor inlet." *Journal of Supercritical Fluids* **42**, 234–240.

EMANUEL, N.M., ZAIKOV, G.E. and MAITUS, Z.K. (1980). "Oxidation of organic compounds. medium effects in radical reactions." Pergamon Press: Oxford, U.K..

EYER, S.L. (2001). "Investigation of catalytic wet oxidation of bayer liquor." Ph.D. thesis, Department of Applied Chemistry, RMIT University, Melbourne, Australia.

FARHATAZIZ, P.C. and ROSS, A.B. (1977). "Selected specific rates of radicals of transients from water in aqueous solutions." National Bureau of Standards, Washington, DC, NSDRS-NBS59.

FERNÁNDEZ, D.P., GOODWIN, A.R.H., LEMMON, E.W., SENGERS, J.M.H.L. and WILLIAMS, R.C. (1997) "A formulation for the static permittivity of water and steam at temperatures from 238 K to 873 K at pressure up to 1200 MPa including derivatives and Debye-Hückel coefficients." *Journal of Physical and Chemical Reference Data* **26**, 1125–1169.

FOUSSARD, J.N., DEBELLEFONTAINE, H. and BESOMBES-VAILHE, J. (1989). "Efficient elimination of organic liquid wastes: wet air oxidation." *Journal of Environmental Engineering* **115**, 367–385.

FURUYA, H., UWABE, R., SUTOH, N., OKUWAKI, A., AMANO, A. and OKABE, T. (1985). "Oxidation of coals in liquid phases. VII. Oxidation of oxygen-containing model compounds of coal by oxygen in concentrated sodium hydroxide solutions." *Bulletin of the Chemical Society of Japan* **58**, 3016–3020.

GLAZE, W.H., LAY, Y. and KANG, J.W. (1995). "Advanced oxidation processes. A kinetic model for the oxidation of 1,2-dibromo-3-chloropropane in water by the combination of hydrogen peroxide and UV radiation." *Industrial and Engineering Chemistry Research* **34**, 2314–2323.

GLOYNA, E.F. and LI, L. (1995). "Supercritical water oxidation research and development update." *Environmental Progress* **14** (3), 182–192.

GOPALAN, S. and SAVAGE, P.E. (1995). "Reaction mechanism for phenol oxidation in supercritical water." *Journal of Physical Chemistry* **98**, 12646–12652.

HASHAIKEH, R., FANG, Z., BUTLER, I.S. and KOZINSKI, J.A. (2005). "Sequential hydrothermal gasification of biomass to hydrogen." *Proceedings of the Combustion Institute*, vol. **30**, pp. 2231–2237.

HAYASHI, R., OHKUMA, K., TONOKURA, K. and OSHIMA, Y. (2007). "Contribution of ionic reaction to sub- and supercritical water oxidation of phenol." *Journal of Chemical Engineering of Japan* **40**, 556–564.

HELLING, R.K. and TESTER, J.W. (1987). "Oxidation kinetics of carbon monoxide in supercritical water." *Energy and Fuels* **1**, 417–423.

HELLING, R.K. and TESTER, J.W. (1988). "Oxidation of simple compound and mixtures in supercritical water: carbon monoxide, ammonia and ethanol." *Environmental Science and Technology* **22**, 1319–1324.

HIROSAKA, K., FUKAYAMA, M., WAKAMATSU, K., ISHIDA, Y., KITAGAWA, K. and HASEGAWA, T. (2007). "Combustion of ethanol by hydrothermal oxidation." *Proceedings of the Combustion Institute*, vol. **31**, pp. 3361–3367.

HIROSAKA, K., KOIDO, K., FUKAYAMA, M., OURYOUJI, K. and HASEGAWA, T. (2008). "Experimental and numerical study of ethanol oxidation in sub-critical water." *Journal of Supercritical Fluids* **44**, 347–355.

HIROSAKA, K. (2008). "Thermal energy production by hydrothermal oxidation." Doctoral Thesis, Department of Aerospace Engineering, Nagoya University, Nagoya, Japan.

HOLLIDAY, R.L., KING, J.W. and LIST, G.R. (1997). "Hydrolysis of vegetable oils in sub and supercritical water." *Industrial and Engineering Chemistry Research* **36**, 932–935.

HOLGATE, H.R., WEBLEY, P.A., TESTER, J.W. and HELLING, R.K. (1992). "Carbon monoxide oxidation in supercritical water: the effects of heat transfer and the water-gas shift reaction on observed kinetics." *Energy and Fuels* **6**, 586–597.

HOLGATE, H.R. and TESTER, J.W. (1993). "Fundamental kinetics and mechanisms of hydrogen oxidation in supercritical water." *Combustion Science and Technology* **88**, 369–397.

HOLGATE, H.R. and TESTER, J.W. (1994). "Oxidation of hydrogen and carbon monoxide in sub- and supercritical water: reaction kinetics, pathways, and water-density effects. 2. Elementary reaction modeling." *Journal of Physical Chemistry* **98**, 810–822.

IAPWS (2007). "Release on the ionization constant of H_2O." *The International Association for the Properties of Water and Steam*, Lucerne, Switzerland.

IAPWS (1997). "Release on the static dielectric constant of ordinary water substance for temperatures from 238 K to 873 K and pressures up to 1000 MPa." *The International Association for the Properties of Water and Steam*, Erlangen, Germany.

IAPWS-IF97 (1997). "Release on the IAPWS industrial formulation 1997 for the thermodynamic properties of water and steam." *The International Association for the Properties of Water and Steam*, Erlangen, Germany.

ICHINOSE, S. and OKUWAKI, A. (1990). "Oxidation of coals in liquid phases. X. Mechanism of the cleavage of benzenecarboxylic acids to oxalic acid and carbon dioxide by the base-catalysed oxygen-oxidation." *Bulletin of the Chemical Society of Japan* **63**, 159–165.

IMAMURA, S., HIRANO, A. and KAWABATA, N. (1982). "The wet oxidation of organic compounds catalyzed by Co-Bi complex oxide." *Bulletin of the Chemical Society of Japan* **55**, 3679–3680.

IMAMURA, S., SAKAI, T. and IKUYAMA, T. (1982). "Wet-oxidation of acetic acid catalyzed by copper salts." *Journal of the Japan Petroleum Institute* **25**, 74–80.

IMAMURA, S. (1999). "Catalytic and noncatalytic wet oxidation." *Industrial and Engineering Chemistry Research* **38**, 1743–1753.

INGALE, M.N., JOSHI, J.B., MAHAJANI, V.V. and GADA, M.K. (1996). "Waste treatment of an aqueous waste stream from a cyclohexane oxidation unit: A case study." *Process Safety and Environmental Protection* **74**, 265–272.

ISHIDA, Y., KUMABE, K., HATA, K., TANIFUJI, K., HASEGAWA, T., KITAGAWA, K., ISU, N. FUNAHASHI, Y. and ASAI, T. (2009). "Selective hydrogen generation from real biomass through hydrothermal reaction at relatively low temperatures." *Biomass and Bioenergy* **33**, 8–13.

ITO, M.M., AKITA, K. and INOUE, H. (1989). "Wet oxidation of oxygen- and nitrogen-containing organic compounds catalyzed by cobalt(III) oxide." *Industrial and Engineering Chemistry Research* **28**, 894–899.

KOIDO, K., HIROSAKA, K., KUBO, T., FUKAYAMA, M., OURYOUJI, K. and HASEGAWA, T. (2006). "Numerical study on hydrothermal oxidation in a tube reactor." *8th International Symposium on Supercritical Fluids*, Kyoto, Japan, p. 120.

KOIDO, K., HIROSAKA, K., KUBO, T., FUKAYAMA, M., OURYOUJI, K. and HASEGAWA, T. (2009). "Numerical study on premixed hydrothermal combustion in tube reactor." *Combustion Theory and Modelling* **13**, 295–318.

KOIDO, K., ISHIDA, Y., KUMABE, K., MATSUMOTO, K. and HASEGAWA, T. (2010) "Kinetics of ethanol oxidation in subcritical water." *Journal of Supercritical Fluids* **55**, 246–251.

LEE, B.I. and KESLER, M.G. (1975). "A generalized thermodynamic correlation based on three-parameter corresponding states." *AIChE Journal* **21**, 510–527.

LEE, D.S. and GLOYNA, E.F. (1992). "Hydrolysis and oxidation of acetamide in supercritical water." *Environmental Science and Technology* **26**, 1587–1593.

LEMMON, E.W., HUBER, M.L. and MCLINDEN, M.O. (2007). "NIST Reference Fluid Thermodynamic and Transport Properties—REFPROP." NIST Standard Reference Database 23—Version 8.0.

LEVEC, J. (1990). "Catalytic oxidation of toxic organics in aqueous solution." *Applied Catalysis* **63**, L1–L5.

LI, L., CHEN, P. and GLOYNA, E.F. (1991). "Generalized kinetic model for wet oxidation of organic compounds." *AIChE Journal* **37**, 1687–1697.

LUCK, F. (1996). "A review of industrial catalytic wet air oxidation processes." *Catalysis Today* **27**, 195–202.

LUCK, F. (1999). "Wet air oxidation: past, present and future." *Catalysis Today* **53**, 81–91.

MANTZAVINOS, D., HELLENBRAND, R., LIVINGSTON, A.G. and METCALFE, I.S. (1997). "Wet oxidation as a pretreatment method for wastewaters contaminated by bioresistant organics." *Water Science and Technology* **36**, 109–116.

MARINOV, N. M. (1999). "A detailed chemical kinetic model for high-temperature ethanol oxidation." *International Journal of Chemical Kinetics* **31**, 183–220.

MARRONE, P.A., HODES, M., SMITH, K.A. and TESTER, J.W. (2004). "Salt precipitation and scale control in supercritical water oxidation—part B: commercial/full-scale applications." *Journal of Supercritical Fluids* **29**, 289–312.

MEYER, J.C., MARRONE, P.A. and TESTER, J.W. (1995). "Acetic acid oxidation and hydrolysis in supercritical water." *AIChE Journal* **41**, 2108–2121.

MISHRA, V.S., MAHAJANI, V. and JOSHI, J. (1995). "Wet air oxidation." *Industrial and Engineering Chemistry Research* **34**, 2–48.

MODELL, M. (1982). "Processing methods for the oxidation of organics in supercritical water." US Patent No. 4338199.

MOORE, W.J. (1972). "Physical chemistry, 5th edition, Longman.

NISHIUMI, H. and SAITO, S. (1975). "An improved generalized BWR equation of state applicable to low reduced temperature." *Journal of Chemical Engineering of Japan* **8**, 356–360.

OKA, K., AMANO, K. and ENBUTSU, I. (2000). "Development of a method of analysis for flow, heat and chemical reactions in supercritical fluid." *Transactions of the Japan Society of Mechanical Engineers B* (in Japanese) **66** (651), 2823–2830.

PATTERSON, D.A., METCALFE, I.S., XIONG, F. and LIVINGSTON, A.G. (2001). "Wet oxidation of linear alkylbenzene sulfonate 2. Effect of pH." *Industrial and Engineering Chemistry Research* **40**, 5517–5525.

PENG, D.Y. and ROBINSON, D.B. (1976). "A new two-constant equation of state." *Industrial and Engineering Chemistry Fundamentals* **15**, 59–64.

PLÖCKER, U., KNAPP, H. and PRAUSNITZ, J.M. (1978). "Calculation of high-pressure vapor-liquid equilibria from a corresponding-states correlation with emphasis on

asymmetric mixtures." *Industrial and Engineering Chemistry Process Design and Development* **17**, 324–332.

RICE, S.F., HUNTER, T.B., RYDEN, A.C. and HANUSH, R.G. (1996). "Raman spectroscopic measurement of oxidation in supercritical water. 1. Conversion of methanol to formaldehyde." *Industrial and Engineering Chemistry Research* **35**, 2161–2171.

RICE, S.F. and STEEPER, R.R. (1998). "Oxidation rates of common organic compounds in supercritical water." *Journal of Hazardous Materials* **59**, 261–278.

RICE, S.F. and CROISET, E. (2001). "Oxidation of simple alcohols in supercritical water. III. Formation of intermediates from ethanol." *Industrial and Engineering Chemistry Research* **40**, 86–93.

RIVAS, F.J., KOLACZKOWSKI, S.T., BELTRAN, F.J. and MCLURGH, D.B. (1998). "Development of a model for the wet air oxidation of phenol based on a free radical mechanism." *Chemical Engineering Science* **53**, 2575–2586.

ROBERT, R., BARBATI, S., RICQ, N. and AMBROSIO, M. (2002). "Intermediates in wet oxidation of cellulose: identification of hydroxyl radical and characterisation of hydrogen peroxide." *Water Research* **36**, 4821–4829.

RODIGUIN, N.M. and RODIGUINA, E.N. (1964). "Consecutive chemical reactions. Mathematical analysis and development." Van Nostrand, Princeton, NJ.

SCHANZENBÄCHER, J., TAYLOR, J.D. and TESTER, J.W. (2002). "Ethanol oxidation and hydrolysis rates in supercritical water." *Journal of Supercritical Fluids* **22**, 139–147.

SHAW, R.W., BRILL, T.B., CLIFFORD, A.A., ECKERT, C.A. and FRANCK, E.U. (1991). "Supercritical water, a medium for chemistry." *Chemical and Engineering News* **69**, 26–39.

SHENDE, R.V. and MAHAJANI, V.V. (1997). "Kinetics of wet oxidation of formic acid and acetic acid." *Industrial and Engineering Chemistry Research* **36**, 4809–4814.

SHENDE, R.V. and LEVEC, J. (1999). "Wet oxidation kinetics of refractory low molecular mass carboxylic acids." *Industrial and Engineering Chemistry Research* **38**, 3830–3837.

SPAN, R. and WAGNER, W. (1996). "A new equation of state for carbon dioxide covering the fluid region from the triple-point temperature to 1100 K at pressures up to 800 MPa." *Journal of Physical and Chemical Reference Data* **25**, 1509–1596.

SOAVE, G. (1972). "Equilibrium constants from a modified Redlich–Kwong equation of state." *Chemical Engineering Science* **27**, 1197–1203.

TAYLOR, J.D., STEINFELD, J.I. and TESTER, J.W. (2001). "Experimental measurement of the rate of methyl tert-butyl ether hydrolysis in sub- and supercritical water." *Industrial and Engineering Chemistry Research* **40**, 67–74.

THOMASON, T. and MODELL, M. (1984). "Supercritical water destruction of aqueous wastes." *Hazardous Waste* **1**, 453–466.

THORNTON, T.D. and SAVAGE, P.E. (1992). "Kinetics of phenol oxidation in supercritical water." *AIChE Journal* **38**, 321–327.

TROMANS, D. (1998). "Temperature and pressure dependent solubility of oxygen in water: a thermodynamic analysis." *Hydrometallurgy* **48**, 327– 342.

TYN, M.N. and CALUS, W.F. (1975). "Estimating liquid molal volume." *Processings* **21**, 16–17.

VIELCAZALS, S., MERCADIER, J., MARIAS, F., MATÉOS, D., BOTTREAU, M., CANSELL, F. and MARRAUD, C. (2006). "Modeling and simulation of hydrothermal oxidation of organic compounds." *AIChE Journal* **52**, 818–825.

WAGNER, W. and KRUSE, A. (1998). "Properties of Water and Steam, Springer." Berlin.

WAKABAYASHI, T. and OKUWAKI, A. (1988). "Oxidation of coals in liquid phases. Kinetics of the base-catalyzed oxidation of acetate ion by oxygen at elevated temperatures." *Bulletin of the Chemical Society of Japan* **61**, 4329–4334.

WEBLEY, P.A. and TESTER, J.W. (1989). "Fundamental kinetics of methanol oxidation in supercritical water." *Supercritical Fluid Science and Technology*, ACS Symposium Series Vol. 406, Chapter 17, 259–275

WEBLEY, P.A., HOLGATE, H.R., STEVENSON, D.M. and TESTER, J.W. (1990). "Oxidation kinetics of model compounds of metabolic waste in supercritical water." SAE Technical Paper Series #901333, 20th Intersociety Conference on Environmental Systems, Williamsburg.

WEBLEY, P.A. and TESTER, J.W. (1991). "Fundamental kinetics of methane oxidation in supercritical water." *Energy and Fuels* **5**, 411–419.

WIGHTMAN, T.J. (1981). "Studies in supercritical wet air oxidation." Master Thesis, Department of Chemical Engineering, University of California at Berkeley.

WILKE, C.R. and CHUNG, P. (1955). "Correlation of diffusion coefficients in dilute solutions." *AIChE Journal* **1**, 264–270.

XU, X., MATSUMURA, Y., STENBERG, J. and ANTAL, JR., M.J. (1996). "Carbon-catalyzed gasification of organic feedstocks in supercritical water." *Industrial and Engineering Chemistry Research* **35**, 2522–2530.

YAMAMOTO, S., TORATANI, M. and SASAO, Y. (2005). "Preconditioning method applied to near-critical carbon-dioxide flows in micro-channel." *JSME International Journal B* **48** (3), 532–539.

ZIMMERMAN, F.J. (1950). "Waste disposal." US Patent No. 2665249.

ZIMMERMAN, F.J. (1958). "New waste disposal process." *Chemical Engineering* **25** (August), 117–120.

Appendix-A: Lee-Kesler equation and methodology for estimating properties around the critical point

A.1 Lee-Kesler equation of state

Lee-Kesler equation (A.1) calculates the compressibility factor (and derived quantities) for the fluid of interest

$$Z = Z^{(0)} + \frac{\omega}{\omega^{(r)}}\left(Z^{(r)} - Z^{(0)}\right), \tag{A.1}$$

where superscripts (0) and (*r*) are respectively a simple fluid, such as argon or methane and a reference fluid, chosen to be n-octane. Acentric factor ω is defined by the following equation:

$$\omega = -\log(p^{sat}/p_c)\big|_{T_r=0.7} - 1.0\,. \tag{A.2}$$

The acentric factors are calculated for a simple fluid (0) to be zero and for reference fluid (*r*) 0.3978. The values of $Z^{(0)}$ and $Z^{(r)}$ are calculated by following equation

$$\begin{aligned} Z^{(i)} = \frac{p_r V_r^{(i)}}{T_r} = 1 + \frac{B}{V_r^{(i)}} + \frac{C}{(V_r^{(i)})^2} + \frac{D}{(V_r^{(i)})^5} \\ + \frac{c_4}{T_r^3 (V_r^{(i)})^2}\left(\beta + \frac{\gamma}{(V_r^{(i)})^2}\right)\exp\left(-\frac{\gamma}{(V_r^{(i)})^2}\right) \end{aligned} \tag{A.3}$$

With

Table A1. Constants for the Lee-Kesler equation.

constant	simple fluids	reference fluids	constant	simple fluids	reference fluids
b_1	0.118119	0.2026579	c_3	0.0	0.016901
b_2	0.265728	0.331511	c_4	0.042724	0.041577
b_3	0.15479	0.027655	$d_1 \times 10^4$	0.155428	0.48736
b_4	0.030323	0.203488	$d_2 \times 10^4$	0.623689	0.0740336
c_1	0.023674	0.0313385	β	0.65392	1.226
c_2	0.018698	0.0503618	γ	0.060167	0.03754

$\omega^{(r)} = 0.3978$

$$B = b_1 - b_2/T_r - b_3/T_r^{\,2} - b_4/T_r^{\,3}$$

$$C = c_1 - c_2/T_r + c_3/T_r^{\,2}$$

$$D = d_1 + d_2/T_r$$

There are two universal sets of constants for b_1, b_2, b_3, b_4, c_1, c_2, c_3, c_4, d_1, d_2, β, and γ, one for the simple fluid, and one for the reference fluid. They are given in Table A1.

A.2 Thermochemical properties

Specific heat at constant pressure of ideal gas is calculated by:

$$C_p^{id} = a + bT + cT^2 + dT^3 . \tag{A.4}$$

Coefficients of equation (A.4) for each substance are summarised in Table A2. The difference of isobaric specific heat between ideal gas and real gas (liquid) was estimated by:

$$\frac{C_p - C_p^{id}}{R} = \frac{C_v - C_v^{id}}{R} - 1 - T_r \left(\frac{\partial p_r}{\partial T_r} \right)_{V_r}^2 \Bigg/ \left(\frac{\partial p_r}{\partial V_r} \right)_{T_r} . \tag{A.5}$$

Table A2. Constants for Equation (A.4) with respect to each substance.

substance	a	b	c	d
C_2H_5OH	9.015	2.141×10^{-1}	-8.391×10^{-5}	1.373×10^{-8}
CO_2	19.80	7.344×10^{-2}	-5.602×10^{-5}	1.715×10^{-8}
H_2O	32.24	1.924×10^{-3}	1.056×10^{-5}	-3.597×10^{-9}
O_2	28.11	-3.680×10^{-6}	1.746×10^{-5}	-1.065×10^{-8}

The each term for equation (A.5) are expressed as following equations for the first term,

$$\frac{C_v - C_v^{id}}{R} = \frac{2(b_3 + 3b_4 / T_r)}{T_r^2 V_r} - \frac{3c_3}{T_r^3 V_r^2} - 6E \tag{A.6}$$

with

$$E = \frac{c_4}{2T_r^3\gamma}\left\{\beta + 1 - \left(\beta + 1 + \frac{\gamma}{V_r^2}\right)\exp\left(-\frac{\gamma}{V_r^2}\right)\right\},$$

for the third term,

$$\left(\frac{\partial p_r}{\partial T_r}\right)_{V_r} = \frac{1}{V_r}\left\{1 + \frac{b_1 + b_3 / T_r^2 + 2b_4 / T_r^3}{V_r} + \frac{c_1 - 2c_3 / T_r^3}{2V_r^2} + \frac{d_1}{5V_r^5} - \frac{2c_4}{T_r^3 V_r^2}\left[\left(\beta + \frac{\gamma}{V_r^2}\right)\exp\left(-\frac{\gamma}{V_r^2}\right)\right]\right\} \tag{A.7}$$

and

$$\left(\frac{\partial p_r}{\partial V_r}\right)_{T_r} = -\frac{T_r}{V_r^2}\left[1 + \frac{2B}{V_r} + \frac{3C}{V_r^2} + \frac{6D}{V_r^5} + \frac{c_4}{T_r^3 V_r^2}\left\{3\beta + \left(5 - 2\beta - \frac{2\gamma}{V_r^2}\right)\frac{\gamma}{V_r^2}\right\}\exp\left(-\frac{\gamma}{V_r^2}\right)\right]. \tag{A.8}$$

The constants such as B, C, D, b_1, b_3, b_4, c_1, c_3, c_4, d_1, β, and γ have already described in preceding section (see section A.1). Table A3 presents the procedure for calculation of the thermodynamic quantities from known values of temperature and pressure.

Table A3. Calculation procedure for Z, $\Delta C_p / R$ and $\Delta h / RT_c$.

Step	From	Calculate
1	T, p, T_c, p_c	T_r, p_r
2	T_r, p_r, eq. (A1.3) with constants "simple fluid"	$V_r^{(0)}$, $Z^{(0)}$, $(\Delta C_p/R)^{(0)}$, $(\Delta h/RT_c)^{(0)}$
3	T_r, p_r, eq. (A1.3) with constants "reference fluid"	$V_r^{(r)}$, $Z^{(r)}$, $(\Delta C_p/R)^{(r)}$, $(\Delta h/RT_c)^{(r)}$
4	$\Im = \Im^{(0)} + \omega/\omega^{(r)} \cdot (\Im^{(r)} - \Im^{(0)})$ $\Im^{(0)} = Z^{(0)}$, $(\Delta C_p/R)^{(0)}$, etc. $\Im^{(r)} = Z^{(r)}$, $(\Delta C_p/R)^{(r)}$, etc.	$\Im = Z$, $\Delta C_p/R$, $\Delta h/RT_c$

A.3 Transport properties

Viscosity and thermal conductivity are estimated by the equation obtained by Chung et al. (1988). Diffusion coefficient is estimated by the equations obtained by Wilke and Chang (1955).

A.3.1 Viscosity

Viscosity is estimated by following equations that were empirically extended to dense fluids. The units of each term should be treated carefully. All units are described in original paper (Chung et al., 1988).

$$\eta = \eta_\kappa + \eta_{\mathrm{p}} \tag{A.9}$$

where $\eta_\kappa = \eta_0(1/G_2 + A_6 Y)$; $\eta_{\mathrm{p}} = \{36.344\times10^{-6}(M_r T_c)^{1/2}/V_c^{2/3}\}A_7 Y^2 G_2 \exp(A_8 + A_9/T^* + A_{10}/T^{*2})$; $Y = \rho V_c/6$; $T^* = 1.2593T/T_c$; $G_1 = (1.0-0.5Y)/(1-Y)^3$; and $G_2 = \{A_1[1-\exp(-A_4 Y)]/Y + A_2 G_1 \exp(A_5 Y) + A_3 G_1\}/(A_1 A_4 + A_2 + A_3)$. The Chapman-Enskog theory for the dilute gas viscosity is written as

$$\eta_0 = (4.0785 \times 10^{-5}) \frac{(MT)^{1/2}}{V_c^{2/3} \Omega^*} F_c \tag{A.10}$$

which is expressed by empirical equation:

$$\Omega^* = \left(\frac{A}{T^{*B}} \right) + \frac{C}{\exp(DT^*)} + \frac{E}{\exp(FT^*)} + GT^{*B} \sin(ST^{*W} - H) \tag{A.11}$$

where $A = 1.16145$, $B = 0.14874$, $C = 0.52487$, $D = 0.77320$, $E = 2.16178$, $F = 2.43787$, $G = -6.435 \times 10^{-4}$, $H = 7.27371$, $S = 18.0323$, and $W = -0.76830$. The factor F_c has been empirically found to be

$$F_c = 1 - 0.2756\omega + 0.059035\mu_r^4 + \kappa \tag{A.12}$$

where ω is the acentric factor and κ is a correction factor for hydrogen-bonding effect of association substances. The term μ_r is a dimensionless dipole moment:

$$\mu_r = 131.3\mu / (V_c T_c)^{1/2} \tag{A.13}$$

The constants A_1–A_{10} are linear functions of ω, μ_r, and κ, fitted as follows:

$$A_i = a_0(i) + a_1(i)\omega + a_2(i)\mu_r^4 + a_3(i)\kappa \qquad i = 1 - 10 \tag{A.14}$$

Table A4. Constants used for the generalised viscosity correlation.

i	$a_0(i)$	$a_2(i)$	$a_3(i)$	$a_4(i)$
1	6.32402	50.41190	−51.68010	11189.02000
2	0.12102×10^{-2}	-0.11536×10^{-2}	-0.62571×10^{-2}	0.37283×10^{-1}
3	5.28346	254.20900	−168.48100	3898.27000
4	6.62263	38.09570	−8.46414	31.41780
5	19.74540	7.63034	−14.35440	31.52670
6	−1.89992	−12.53670	4.98529	−18.15070
7	24.27450	3.44945	−11.29130	69.34660
8	0.79716	1.11764	0.12348×10^{-1}	−4.11661
9	−0.23816	0.67695×10^{-1}	−0.81630	4.02528
10	0.68629×10^{-1}	0.34793	0.59256	0.72663

where a_0, a_1, a_2, and a_3 are given in Table A4. $\kappa = 0.075908$ for water and O_2, 0.174823 for ethanol, and 0.0 for CO_2.

A.3.2 Thermal conductivity

Thermal conductivity is estimated by following equations. The units of each term should be treated carefully. All units are described in original paper (Chung et al., 1988).

$$\lambda = \lambda_k + \lambda_p \tag{A.15}$$

with $\lambda_k = \lambda_0(1/H_2 + B_6 Y)$; $\lambda_p = \{3.309\times10^{-4}(T_c/M_r)^{1/2}/V_c^{2/3}\}B_7 Y^2 H_2 T_r^2$; $Y = \rho V_c/6$; $G_1 = (1.0-0.5Y)/(1-Y)^3$; and $H_2 = \{B_1[1-\exp(-B_4 Y)]/Y + B_2 G_1 \exp(B_5 Y) + B_3 G_1\}/(B_1 B_4 + B_2 + B_3)$. The thermal conductivity for dilute gases is written as

$$\lambda_0 = 7.452(\eta_0/M)\Psi \tag{A.16}$$

where $\Psi = 1+\alpha\{[0.215+0.28288\alpha-1.061\beta+0.26665Z]/[0.6366+\beta Z+1.061\times\alpha\beta]\}$; $\alpha = (C_V/R)-(3/2)$; $\beta = 0.7862-0.7109\omega+1.3168\omega^2$; and $Z = 2.0+10.5T_r^2$. The constants B_1–B_7 are functions of ω, μ_r, and κ as shown below:

$$B_i = b_0(i)+b_1(i)\omega+b_2(i)\mu_r^4+b_3(i)\kappa, \qquad i = 1-7 \tag{A.17}$$

with b_0, b_1, b_2, and b_3 given in Table A5.

Table A5. Constants used for the generalised correlation for thermal conductivity.

i	$b_0(i)$	$b_2(i)$	$b_3(i)$	$b_4(i)$
1	2.41657	0.74824	−0.91858	121.72100
2	−0.50924	−1.50936	−49.99120	69.98340
3	6.61069	5.62073	64.75990	27.03890
4	14.54250	−8.91387	−5.63794	74.34350
5	0.79274	0.82019	−0.69369	6.31734
6	−5.86340	12.80050	9.58926	−65.52920
7	81.17100	114.15800	−60.84100	466.77500

A.4 Mixing rule

Mixing rule for Lee-Kesler EOS and transport properties are described here.

A.4.1 Mixing rule for Lee-Kesler EOS

The mixing rules proposed by Plöcker et al. (1978) are

$$T_{cm} = \frac{1}{V_{cm}^{0.25}} \sum\sum X_i X_j V_{cij}^{0.25} T_{cij} \tag{A.18}$$

$$V_{cm} = \sum\sum X_i X_j V_{cij} \tag{A.19}$$

$$p_{cm} = \frac{0.2905 - 0.085\omega_m \; RT_{cm}}{V_{cm}} \tag{A.20}$$

$$\omega_m = \sum X_i \omega_i \tag{A.21}$$

where the cross coefficients are given by

$$T_{cij} = \sqrt{T_{ci} T_{cj}} \tag{A.22}$$

and

$$V_{cij} = \frac{1}{8}(V_{ci}^{1/3} + V_{cj}^{1/3})^3. \tag{A.23}$$

A.4.1 Mixing rule for transport properties

$$\sigma_m^3 = \sum\sum X_i X_j \sigma_{ij}^3 \tag{A.24}$$

$$\varepsilon_m / k = [\sum\sum X_i X_j (\varepsilon_{ij} / k) \sigma_{ij}^3] / \sigma_m^3 \tag{A.25}$$

$$V_{cm} = (\sigma_m / 0.809)^3 \tag{A.26}$$

$$T_{cm} = 1.2593 \varepsilon_m / k \tag{A.27}$$

$$\omega_{\mathrm{m}} = [\sum\sum X_i X_j \omega_{ij} \sigma_{ij}^3] / \sigma_{\mathrm{m}}^3 \tag{A.28}$$

$$M_{\mathrm{m}} = \{[\sum\sum X_i X_j (\varepsilon_{ij}/k)\sigma_{ij}^2 M_{ij}^{1/2}]/[(\varepsilon_{\mathrm{m}}/k)\sigma_{\mathrm{m}}^2]\}^2 \tag{A.29}$$

$$\mu_{\mathrm{m}}^4 = \{\sum\sum X_i X_j (\mu_i^2 \mu_j^2)/[(\varepsilon_{ij}/k)\sigma_{ij}^3]\}\sigma_{\mathrm{m}}^3 (\varepsilon_{\mathrm{m}}/k) \tag{A.30}$$

$$\kappa_{\mathrm{m}} = \sum\sum X_i X_j \kappa_{ij} \tag{A.31}$$

$$\mu_{r\mathrm{m}} = 131.3\mu_{\mathrm{m}} / (v_{c\mathrm{m}} T_{c\mathrm{m}})^{1/2} \tag{A.32}$$

where the binary parameters are given by the combining rules,

$$\sigma_{ij} = (\sigma_i \sigma_j)^{1/2} \tag{A.33}$$

$$\varepsilon_{ij}/k = [(\varepsilon_i/k)(\varepsilon_j/k)]^{1/2} \tag{A.34}$$

$$\omega_{ij} = \tfrac{1}{2}(\omega_i + \omega_j) \tag{A.35}$$

$$M_{ij} = 2M_i M_j / (M_i + M_j) \tag{A.36}$$

$$\kappa_{ij} = (\kappa_i \kappa_j)^{1/2} \tag{A.37}$$

with

$$\sigma_i = 0.809 V_c^{1/3} \tag{A.38}$$

$$\varepsilon_i/k = T_{ci}/1.2593\,. \tag{A.39}$$